5-3-2019

Impacts Analysis of Cross-Coupling Droop Terms on Power Systems with Converter-Based Distributed Energy Resources

Thaer Qunais

Impacts analysis of cross-coupling droop terms on power systems with converter-based distributed energy resources

By

Thaer Qunais

A Dissertation
Submitted to the Faculty of
Mississippi State University
in Partial Fulfillment of the Requirements
for the Degree of Doctor of Philosophy
in Electrical and Computer Engineering
in the Department of Electrical and Computer Engineering

Mississippi State, Mississippi

May 2019

Impacts analysis of cross-coupling droop terms on power systems with converter-based distributed energy resources

By

Thaer Qunais

Approved:

Masoud Karimi-Ghartemani
(Major Professor)

Yong Fu
(Committee Member)

Joni Kluss
(Committee Member)

Seungdeog Choi
(Committee Member)

James E. Fowler
(Graduate Coordinator)

Jason M. Keith
Dean
Bagley College of Engineering

Name: Thaer Qunais

Date of Degree: May 03, 2019

Institution: Mississippi State University

Major Field: Electrical and Computer Engineering

Major Professor: Masoud Karimi-Ghartemani

Title of Study: Impacts analysis of cross-coupling droop terms on power systems with converter-based distributed energy resources

Pages of Study: 108

Candidate for Degree of Doctor of Philosophy

Microgrid (MG) concept has been emerged to enable integration of renewable energy sources and storage devices using power electronic converters. An MG can be grid connected to exchange power with the main grid, isolated that is completely separated from the grid, or islanded that is temporarily separated from the grid. The P-f and Q-V drooping approach is commonly used to control and achieve power sharing among the generators. This study presents an approach for systematically modeling a class of microgrid (MG) systems. The derived model 1) accommodates grid-connected and islanded operation of the MG simultaneously, and 2) allows modeling of converter-based as well as directly-interfaced resources. The originally nonlinear model is then converted to a linear model whose eigenvalues determine local stability of the MG.

The model is used to analyze the impacts of adding cross-coupling droop terms (P-V and Q-f) on an MG's performance. Various performance aspects such as stability, stability robustness, transmission power loss, voltage profile, and power sharing are considered.

The conclusions are as follows. (1) Addition of a small portion of cross-coupling will reduce the losses without compromising other aspects in a grid-connected MG. Larger cross-coupling terms will compromise the system stability. (2) Large cross-coupling terms can be added to reduce the power loss and to improve the system stability in an isolated MG. Simulation and experimental results are presented to verify the derivations.

Key words: Droop Controls, Microgrid, Cross-Coupling Droop Terms, Transmission Losses, Distributed Generation

DEDICATION

To my mom Yusra, and my dad Issam, my beloved wife Yasmin, my supporting brothers Laith, Mohammad, and Omar, and my dear sister Besan.

ACKNOWLEDGEMENTS

First of all, I would like to praise Allah for guiding me on this road to fulfill my PhD. I would like to give thanks and appreciation to all those who have helped me and supported me in the completion of this step.

To begin with, I would like to express my immense gratitude and dedication to my advisor Dr. Masoud Karimi for his unconditional support and guidance during my PhD study and research. I would like to thank my committee members, Dr. Yong Fu, Dr. Joni Kluss, and Dr. Seungdeog Choi for their feedback to help strengthen my research.

I would like to give special thanks to my parents for always putting me first and allowing me to pursue my education and for their constant encouragement and prayers.

To my beloved wife Yasmin who has made countless sacrifices to help me get to this point in my life. Thank you for all the late nights and early mornings. But most of all, thank you for your unconditional love and being my best friend.

In addition, I would like to thank my friends Salem Batiyah, Mohammad Mousa, Maziar Babaei, and Omar Ibrahim for their continuous support and our effective discussions.

I would like to commend the Department of Electrical and Computer Engineering, Mississippi State University and its staff for giving me opportunities and making me feel welcomed during the course of my PhD.

TABLE OF CONTENTS

LIST OF TABLES

LIST OF FIGURES

CHAPTER I

INTRODUCTION

1.1 State of Modern Electric Power System

The electric power industry in the United States (US) is undergoing major changes. The previous utility industry had a structure of large vertically integrated monopolies until the last decade of the twentieth century. This structure is being shifted toward a more horizontal structure where utilities are classified into power generation, transmission, and distribution as separate business facilities [14]. In 1992, the US Congress passed the Energy Policy Act which allowed the deregulation of power industry and introduced the open electricity market [1, 55]. Thanks to this evolution in electric industry, it has made it easier for new players to enter the market, and it is now possible for almost anybody to produce electricity and export it to the power system. In addition, consumers will have the option from which generator they purchase power. Enabling the introduction of new electricity generation technologies is one of the main reasons for the deregulation of the electricity market. This competitive market together with a diversified and increased generation capacity will result in reduced energy prices.

The main reason for introducing new types of generation is related to environment. Electricity generation is one of the main sources of greenhouse gas emissions in the world. Power plants that are based on fossil fuels, such as coal, gas, and oil, or materials made

from fossil fuels such as hydrocarbon gas liquids (HGL), contribute to about of total U.S. energy-related carbon dioxide [10]. The conventional power generation can impact the environment in other ways which include the need of huge water resources to produce steam, and provide cooling, release of pollutants into water bodies, and land use for power generation, and transmission and distribution lines [12].

Another reason for introducing new generation is that the margin between the highest demand and the potential available production is very small. This is clearly observed in fast-growing economies such as Brazil, South Africa, and India. The margin is also getting tight for some parts of North America and Europe [3]. Building large conventional power plants is becoming less of an option due to political and environmental reasons. Moreover, large investments are required and it can take ten years or longer to complete.

Sustainability is another reason that has encouraged to decrease the dependency on fossil fuel-based electricity and to seek for alternatives. Although large conventional power plants are mainly based on fossil fuel due to economic reasons, it is unsustainable because of its limited reserve. Since supplies are limited and cannot be replaced in a short time, changing from conventional production based on fossil fuels to renewable sources, such as bio-fuels, solar and wind is a promising solution. Consequently, integration of renewable energy resources has been growing rapidly worldwide over the past years, driven by technology progress, sharp cost reductions, and policy support in the form of incentives [25]. For instance, of electricity generation in Denmark is expected to come from renewables by 2022. China already surpassed its 2020 solar photo-voltaic (PV) target, and the International Energy Agency (IEA) expects China to exceed its wind target in 2019 [24].

The integration of distributed energy resources (DERs) into the electric power system will introduce new types of phenomena which require new types of solutions. The main changes that will be taking place are:

1. Large generating units connected to the transmission system are replaced by small units connected at low voltage or medium voltage of the grid through power electronics converters.

2. The vertically integrated utility (with generation, transmission, and distribution monopolized) is divided such that the generation market is open to competition.

In summary, distribution grids are being transformed from passive to active networks, in the sense that decision-making and control are distributed, and power flows are bidirectional. Therefore, power grid is becoming more complex and is more difficult to manage and control. However, experts think that there are no invincible technical challenges that can prevent the grid restructuring, but the economic and regulatory frameworks are critical to this achievement [25].

The realization of active distribution networks by incorporating DERs requires the implementation of essentially new system concepts. A control and management architecture is required in order to facilitate full integration of distributed generation into the system. One promising way to realize the emerging potential of microgeneration is to take a systematic approach that views a set of generation, storage, and associated loads as a subsystem or a microgrid [19–21, 31]. Microgrids dominantly include power electronic

converter-based units in their structure. This research identifies and investigates a fundamental control aspect related to such units.

1.2 Problem Statement and Literature Review

Environmental, economic, and political issues have increased interest in clean and renewable energy generation. The microgrid (MG) concept facilitates the integration of renewable energy resources (RES). Moreover, it improves the reliability of distribution systems, reduces emissions, and potentially lowers the cost of energy [32, 45]. An MG generally consists of distributed generators (DGs), energy storage systems (ESS), and loads. Distributed energy resource (DER) is used to specify all these types of energy systems. A DER may be interfaced to the grid using a power electronic converter, such as PV, and storage systems, or can be directly coupled, such as diesel generators.

To reach the intended objectives of the MG concept, effective tools for their design, analysis and operation are required. Efficient mathematical models are required to reach these goals. Mathematical modeling of the MG is a challenge due to the following conditions [2, 40, 54]: 1) different modes of operation including grid-connected and standalone, 2) different types of resources in terms of converter-based or directly-interfaced, and 3) different control schemes adopted by converter-based DERs. Some existing models treat the renewable generators as current sources such as the WECC generic models for PV systems [13]. The voltage and frequency ride-through responses require more detailed models and cannot be accurately studied using such models.

Partial small signal models of the DERs for specific working conditions are reported in the literature. A small-signal model for a system of parallel-connected inverters is presented in [9] which neglects the inner control loops, lines, and loads dynamics. In [62], the models of the network lines and loads are ignored too. Detailed state space representation of multi-inverter MGs are reported in [33,42,43,46,48]. These models include the dynamics of all inverters, controllers, filters, and network components. However, the dynamic models in all [9, 33, 42, 43, 46, 48, 62] are developed for stability analysis of autonomous MGs and they do not consider the grid-connected operation mode. A small-signal model of a single grid-connected inverter is derived in [15,56] where the grid is represented as a stiff ac bus, and the simplified model ignores the filter and other network dynamics. A more detailed small-signal model is presented in [18,49] for the purposes of stability analysis and controller design of MGs in islanded and grid-connected modes. The modeling approach handles the two operational modes separately where every mode has its own mathematical model. Moreover, the main grid is represented as an ideal voltage source neglecting its dynamics.

This work develops an approach to systematically model a class of multi-source MG structures. The developed model is detailed (including current and voltage dynamics) and can accommodate both the grid-connected and islanded modes of operation. Furthermore, the dynamic model is applicable to MG systems that contain conventional (rotating machines) and electronically-interfaced DERs. The model is first developed by taking the system nonlinearities in consideration. Subsequently, a linear version of the model is also developed for eigenvalue and stability analysis of the MG.

The proposed model is then employed to investigate the impacts of cross-coupling droop terms on the stability and other properties of the MG. The and drooping is commonly used to control conventional generators where the real power is drooped versus the frequency (or rotor speed) and the reactive power is drooped versus the voltage magnitude [6,38,44,63]. This method is developed based on the fact that in a synchronous generator (SG), the real power is in direct relationship with rotor speed and the rotor speed is directly coupled with the frequency. In other words, if more real power is drawn from an SG, its speed will drop. Moreover, when more reactive power is drawn from it, its voltage magnitude will drop. The governor and automatic voltage regulator (AVR) control systems modify and linearize these two natural characteristics of the SG into the linear and droops expressed by

(1.1)

where and are the frequency and amplitude of the output voltage, and are their nominal (or rated) values, and are the output real and reactive powers, and are the set-points of active and reactive powers, and and are the frequency and voltage droop coefficients, respectively. The and droop characteristics are shown graphically in Fig. 1.1.

Problem Statement: In DER applications, where non-synchronous generating units are used, is the same and drooping approach the best option? what are the possible alternatives?

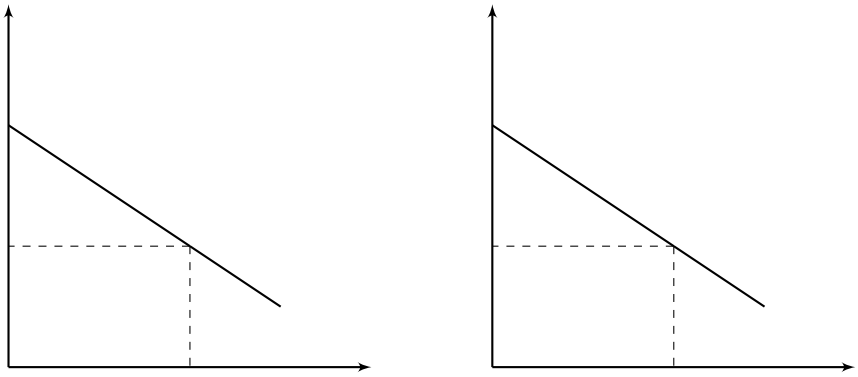

Figure 1.1: Conventional frequency and voltage droop characteristics

In conventional power system, power system stabilizer (PSS) adds a feedback term from the active power loop to the AVR which modulates the terminal voltage of the generator. The PSS is used to improve local stability margins of the SG by damping the generator oscillations [30,41,59]. This seems to be the only case that a coupling term from the frequency loop is used in the voltage or AVR loop.

In the literature, a number of methods are proposed to improve the performance of the droop controllers used in MGs [8, 16, 17, 22, 60]. In one category, a virtual impedance is chosen to reduce the impacts of mismatching in the feeder lines and also to alter the output impedances of inverters in control system. Therefore, the global reactive power sharing accuracy and the local transient performances of the inverter can be improved. However, the proper design and implementation of the virtual impedance to avoid stability issues or high-frequency noise amplifications is a challenge in this approach [39, 57].

The virtual power decoupling control is one of the methods used to improve the performance of the droop controller. An orthogonal linear rotational transformation matrix

is used to decouple the active and reactive power flows by rotating the power vector. The transformed real and reactive powers, also called virtual powers, are used instead of actual real and reactive powers. In [4], the decoupled power control method is applied for parallel connected inverters operating in both islanded and grid-connected modes. However, the line $-$ ratio needs to be known to determine the transformation angle. Moreover, in the grid-connected mode, the grid is modeled by an infinite bus which is very limiting.

A method of estimating the grid impedance is proposed in [56] and the angle of the grid impedance is used as the transformation angle to decouple the active and reactive power flow controls. In [28], the line parameters are assumed to be available, and the rotational transformation matrix takes into account the capacitive nature of the medium length transmission lines. An online impedance estimation algorithm of both the transmission line and the load is proposed in [53]. The system equivalent impedance is then used in the power transformation matrix. The limitations of [28, 53, 56] are that only a simplified MG with a single DER connected to grid is considered, and the grid is modeled by an infinite bus, thus ignoring its dynamics.

The virtual power-based droop control assuming that the line impedance information is known is proposed in [5]. The decoupled power control method is combined with an arctan droop scheme in [50] where an arctan-based function replaces the constant droop coefficients. Utilizing the arctan gradient algorithm offers a dynamic droop adjustment throughout the power range. Therefore, it is proven to improve system stability. Moreover, the arctan function is bounded (has desirable horizontal asymptotes) which can ensure a natural bounding of the operating frequency. However, the line parameters must

be available to build the power conversion matrix. Instead of assuming that the distribution line impedance is known and using it to transform the power vector, [58] derives an optimal value of the transformation angle that results in highest stability margins. A real and reactive power control based on the virtual voltage and frequency concepts is proposed in [36, 37] where the voltage and frequency are transformed to a virtual frame rather than transforming the power vector. In all [36, 37, 58], a transformation angle of is recommended to improve system stability. The shortcoming of [5,36,37,50,58] is that an isolated MG with only one DER is considered except for [50] and [5] where the study system is a two-DER isolated MG. The grid-connected mode of operation is not taken into account in [5, 36, 37, 50, 58].

A and drooping approach is used in [64, 67, 68]. This is expressed by

(1.2)

This approach is proved to be more stable than the conventional approach of (1.1) for a wider range of filter and line impedances in an isolated MG. However, this extreme shift of drooping principles is not compatible with the working principles of the existing grid, i.e. (1.1), and will not allow cohesive integration of DERs into the existing grid. In other words, when connected to the grid or in order to achieve seamless transition between grid-connected and islanded operations, an MG must respect the grid's working principles. The drooping approach in (1.2) is also used in [65] for a system that consists of a single-phase grid-connected inverter. The grid is modeled by an ideal voltage source neglecting all its

dynamics. Therefore, this will result in a less accurate model of the system and does not allow understanding of the interactions between the DERs and the main grid.

1.3 Research Objectives

The main objective of this research is to identify and quantify the impacts of cross-coupling droop terms (formulated by in (1.3)) on the MG performance in both isolated and grid-connected modes of operation. We approach this objective by

1. Identifying multiple performance indices that can represent the impacts. Various performance aspects are considered which include stability, stability robustness, voltage profile, power sharing, and transmission loss.

2. Evaluating the performance indices versus for both modes of operation.

3. Formulating trade-offs that can lead to optimized level of cross-coupling terms.

1.4 Research Approach

The question of finding a trade-off between (1.1) and (1.2) is studied systematically in this work. To this aim, a generalized drooping mechanism with cross-coupling terms is considered according to

(1.3)

where is an angle in the range of to . For , (1.3) reduces to (1.1) and for it is reduced to the other extreme that is (1.2). Several system performance aspects including stability, stability robustness, transmission power loss, voltage profile, and power

sharing in both an autonomous and grid-connected microgrid settings are studied for all values of .

The single-line diagram of the MG under study that comprises of number of inverters is shown in Fig. 1.2. Each inverter is connected to a local load. Transmission lines connect the inverters to a point of common coupling (PCC) where a common load resides.

In the studied system, the inverters are controlled using a virtual synchronous machine (VSM) approach such as synchronverter [66] or the universal controller of [26]. We adopt and improve the VSM of [26]. The proposed improved VSM (iVSM) is shown in Fig. 1.3. The modifications are as follows. (1) The internal frequency variable is used in the droop law to avoid measurement of output frequency. (2) The inverter output voltage magnitude is calculated as $\sqrt{-}$.

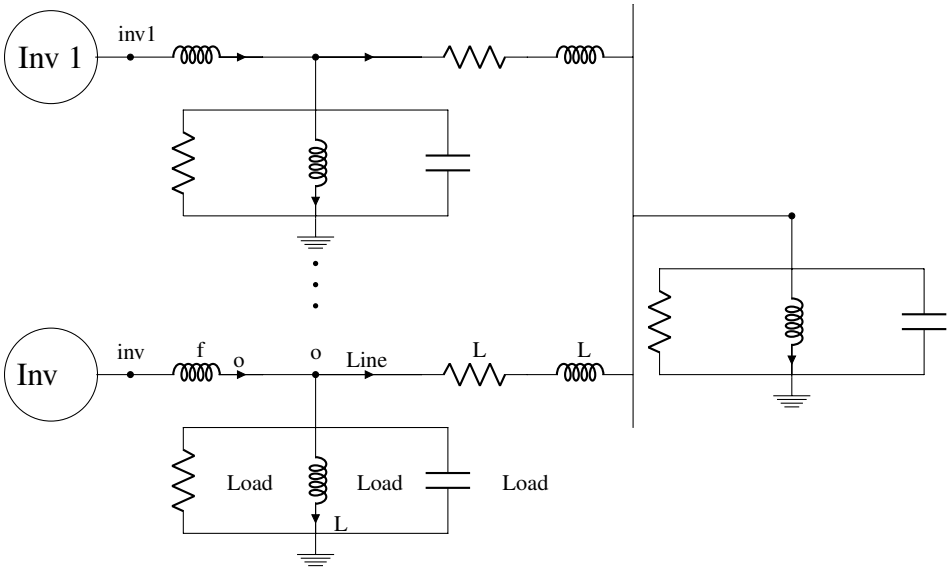

Figure 1.2: Proposed microgrid structure

The rotation transformation matrix shown in Fig. 1.3 implements the generalized droops with cross-coupling terms of (1.3). The transformed real and reactive powers denoted by and are defined as

(1.4)

In steady-state, ref and ref and

ref ref

Solving (1.4) for and yields equation (1.3), where and in (1.3) are given by

(1.5)

A full -based dynamic model of the study system of Fig. 1.2 is developed in Chapter II.

The adoption of control system from among VSMs has the following advantages: 1) The developed dynamic model for this system is valid for both the grid-connected and islanded modes. Specifically, one DG unit can be selected to act as the grid by simply modifying its controller parameters to make it emulate the operation of a large synchronous generator. 2) Representing the grid as a large SG and including its governor and exciter systems, rather than modeling the grid as an ideal voltage source, would result in a more accurate model of the entire system. This will more accurately represent the interactions between the DERs and the main grid.

The work done in this study proves the following facts.

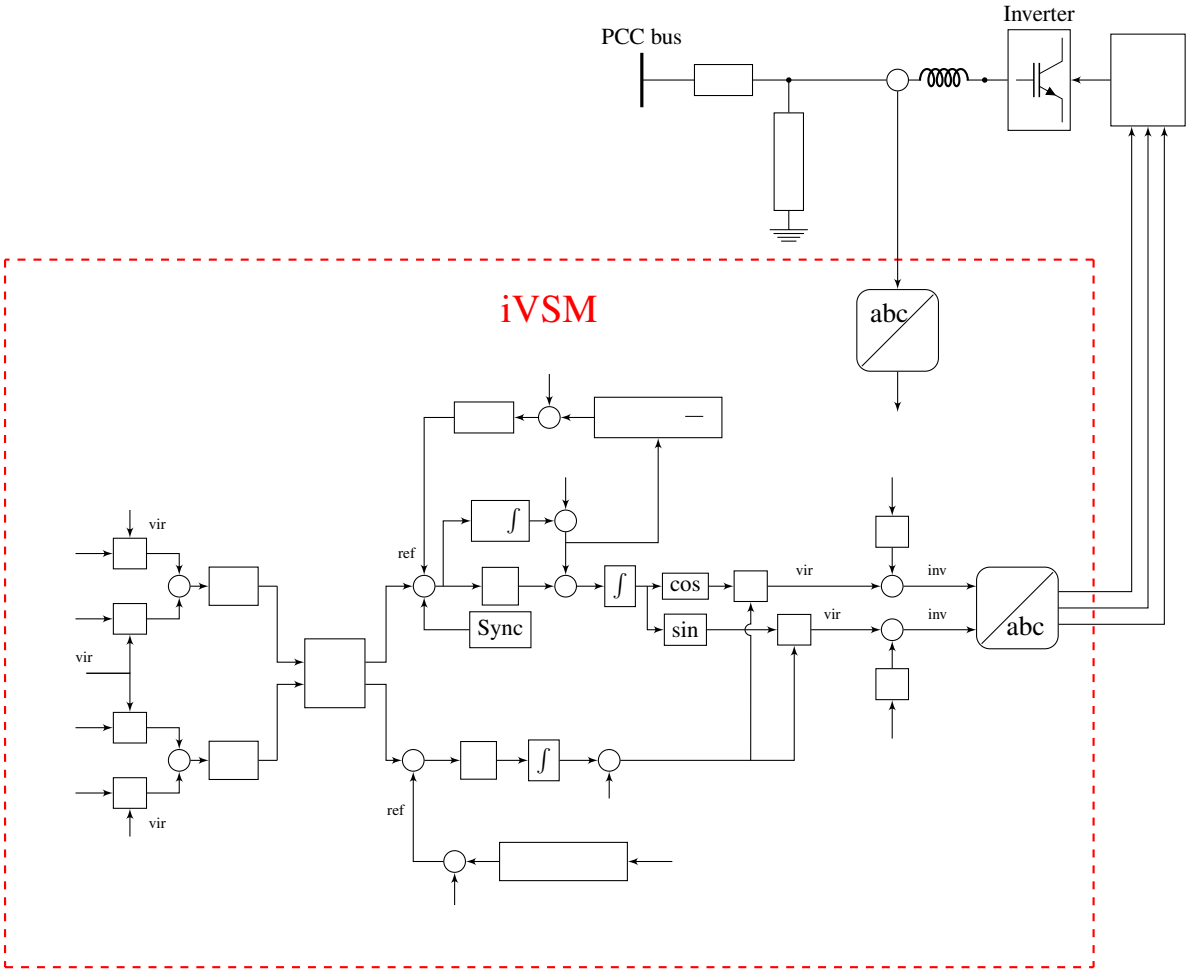

Figure 1.3: Structure of iVSM

1. A grid-connected MG will have the highest level of system stability if its DG units adopt the conventional droop method, i.e. .

2. In a grid-connected MG, including a small amount of cross-coupling, e.g. , can significantly improve the system efficiency without noticeably compromising the stability.

3. In an isolated MG, the portion of the cross-coupling terms can be increased all the way to the extreme point, i.e. . This will both reduce the transmission loss and improve the system stability. However, such a setting is not desirable for grid-connected operation.

Global conclusion is that a modest selection of cross-coupling terms, e.g.

, will establish a desirable trade-off between the system stability (in both grid-connected and islanded modes) and efficiency. For an extended period of operation in islanded mode, the cross-coupling terms may be increased to improve both the stability and efficiency.

1.5 Contributions

The contributions of the research work presented in this dissertation can be summarized as follows.

1. Development of a detailed systematic mathematical model for a proposed multi-inverter MG structure that uses a universal controller to control the operation of its three-phase inverters in both modes of operation.

2. Development of a linearized systematic model for the proposed MG at the equilibrium point for the purposes of small-signal stability study.

3. Analyze the impacts of adding cross-coupling droop terms on the MG's performance. Several performance aspects such as stability, stability robustness, transmission power loss, voltage profile, and power sharing are considered.

4. Evaluate the MG performance in both autonomous and grid-connected modes of operation and during transition between them using simulations.

5. Investigate the impacts of adding cross-coupling droop terms on MG's performance in both operational modes for different lines characteristics. We use the derived mathematical model in conjunction with extensive simulations for the study MG system to obtain the results and formulate the trade-offs.

6. Perform real-time simulations in Real-Time Digital Simulator (RTDS) to confirm the results that are achieved. Laboratory experiment is also conducted to further validate the analysis.

7. Derive general guidelines as how to set different levels of cross-coupling terms in the study system. The variations in the MG size and in the lines characteristics are considered in setting the general rules. To this aim, a multi-variable nonlinear problem is formulated. Particle swarm optimization (PSO) is used to solve this optimization problem by obtaining the optimal transformation angles that should be used in the iVSM controller of each DG unit.

CHAPTER II

MATHEMATICAL MODEL

2.1 System Modeling in State-Space Form

A complete dynamic model is developed for the MG shown in Fig. 1.2. Such a model is required for stability analysis of the system. The model includes: 1) the dynamics of the converter-based DERs and their controllers 2) and the network lines and loads dynamics. The model can be used for both grid-connected and standalone operations. Furthermore, the dynamic model is applicable to MG systems that contain conventional (rotating machines) and electronically-interfaced DERs. The MG has multiple subsystems that are modeled separately and then integrated. The - transformation is defined by

– (2.1)

and the - transformation [61] is defined by

dq (2.2)

where is the inverter virtual voltage angle. Modeling of different subsystems is discussed in the following.

2.1.1 Inverter and Controller

The iVSM structure applied to the three-phase inverters in the MG setting is illustrated in Fig. 1.3. The dynamics of the iVSM are given by

$$\begin{matrix} \text{ref} \\ \text{ref} \\ \text{ref} \end{matrix} \tag{2.3}$$

where the power references $_{\text{ref}}$ and $_{\text{ref}}$ are set using the droop characteristics given by

$$\text{ref} \quad \frac{c}{c} \quad — \\ \text{ref} \quad \text{o} \tag{2.4}$$

where , , $_{\text{NL}}$ is the no-load frequency, $_{\text{NL}}$ is the no-load voltage, and are real positive constants, is the cut-off frequency of the low-pass filter, is the controller internal frequency variable, is the controller internal angle variable, is the inverter virtual voltage magnitude, and is the inverter output voltage magnitude. Note that the presence of LPF is not necessary but it is used for generality in order to enable modeling of governor slow dynamics in SG. The set-points $_{\text{NL}}$ and $_{\text{NL}}$ are adjusted by a low-bandwidth secondary controller to maintain the voltage and frequency at the PCC close to 120 V and 60 Hz, respectively. The block diagram of the secondary controller is shown in Fig. 2.1.

The transformed virtual active power and reactive power are denoted by and , respectively, and calculated as

$$\begin{bmatrix} \\ \end{bmatrix} \quad \begin{bmatrix} \\ \end{bmatrix} \quad \begin{bmatrix} \\ \end{bmatrix} \begin{bmatrix} \\ \end{bmatrix} \tag{2.5}$$

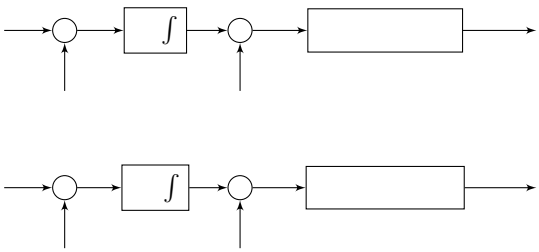

Figure 2.1: Block diagram of voltage and frequency secondary controller

The virtual inverter voltage is and which in reference frame will be and . The expressions of real and reactive powers and in the frame at the terminals are presented as

$$\begin{matrix} - & \text{od} & \text{d} & & \text{oq} & \text{q} \\ - & \text{od} & \text{q} & & \text{oq} & \text{d} \end{matrix} \tag{2.6}$$

The iVSM dynamics are then written as

$$\text{ref} \tag{2.7}$$

$$\text{ref}$$

The reference power dynamics can be presented as follows

$$\text{ref} \quad \left(\quad \text{NL} \quad — \quad \right) \tag{2.8}$$

2.1.2 Output L filter, Line, and Load

The differential equations describing the filter dynamics are

$$\begin{matrix} \text{od} & \overline{\text{f}} & \text{d} & \text{od} & \overline{\text{f}} & \text{od} & \text{oq} \\ \text{oq} & \overline{\text{f}} & \text{q} & \text{oq} & \overline{\text{f}} & \text{oq} & \text{od} \end{matrix} \tag{2.9}$$

A parallel RLC is used to model the load which leads to the state equations of

$$\begin{array}{llllll} \text{Ld} & \frac{}{\text{Load}} & \text{od} & \text{Lq} & & \\ \text{Lq} & \frac{}{\text{Load}} & \text{oq} & \text{Ld} & & \\ \text{od} & \frac{}{\text{Load}} & \text{od} & \text{Ld} & \text{Lined} & \frac{\text{od}}{\text{Load}\quad\text{Load}} \quad \text{oq} \\ \text{oq} & \frac{}{\text{Load}} & \text{oq} & \text{Lq} & \text{Lineq} & \frac{\text{oq}}{\text{Load}\quad\text{Load}} \quad \text{od} \end{array} \tag{2.10}$$

The distribution line is a series RL with the state equations of

$$\begin{array}{llllll} \text{Lined} & \frac{}{\text{L}} & \text{od} & \text{pccd} & \frac{\text{L}}{\text{L}} & \text{Lined} \quad \text{Lineq} \\ \text{Lineq} & \frac{}{\text{L}} & \text{oq} & \text{pccq} & \frac{\text{L}}{\text{L}} & \text{Lineq} \quad \text{Lined} \end{array} \tag{2.11}$$

2.1.3 Integrating Different DERs

The angle of the first inverter is used as the common reference. The state equations of all individual inverters can be translated to this common frame with the help of the transformation technique defined in (2.12) [48].

$$i \tag{2.12}$$

In (2.12), is the angle of the reference frame of th inverter with respect to the common reference frame. The variables , are defined in the common reference frame, and , are defined in the local frame of reference. For instance, in an MG with two DGs, the phase angle deviations of the reference frames with respect to the common reference frame are given as . The transformation is illustrated graphically in Fig. 2.2.

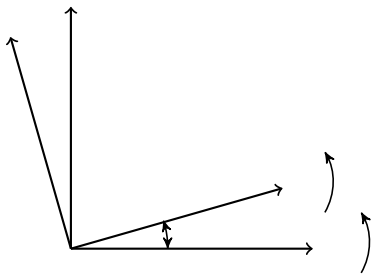

Figure 2.2: Reference Frame Transformation

It is noteworthy to notice that a real pole exists at zero due to the zero state variable in this model as shown in Fig. 3.1. The virtual -axis voltage of the th inverter in the common reference frame can be expressed as . The variables of inverter 2 in its local reference frame can be translated to the common reference frame as

$$\text{dq2} \qquad ^{2} \qquad ^{2} \qquad ^{1} \tag{2.13}$$

A complete state-space model of each inverter can be obtained by combining the dynamic models of the iVSM, output L filter, line, and load. The state equations governing the full islanded microgrid system on a common reference frame can be obtained by combining the models of the individual inverters on a common reference frame together with the dynamic model of the common load connected to the PCC which is presented as

$$\begin{aligned}
&\text{Ldpcc} \quad \frac{}{\text{pcc}} \quad \text{pccd} \qquad \text{Lqpcc} \\
&\text{Lqpcc} \quad \frac{}{\text{pcc}} \quad \text{pccq} \qquad \text{Ldpcc} \\
&\text{pccd} \quad \frac{}{\text{pcc}} \sum \text{Line} \qquad \text{Ldpcc} \quad \frac{\text{pccd}}{\text{pcc} \quad \text{pcc}} \qquad \text{pccq} \\
&\text{pccq} \quad \frac{}{\text{pcc}} \sum \text{Line} \qquad \text{Lqpcc} \quad \frac{\text{pccq}}{\text{pcc} \quad \text{pcc}} \qquad \text{pccd}
\end{aligned} \tag{2.14}$$

2.1.4 Complete Nonlinear Model of MG

Define the state vector of the th DER as

$$\begin{matrix} 1 & 2 & 3 & 4 & 5 & 6 & 7 & 8 & 9 & 10 & 11 & 12 \\ od & oq & Ld & Lq & od & oq & Line\ d & Line\ q & d & & & ref \end{matrix} \tag{2.15}$$

for . Also define the common load state vector as

$$pcc \quad pcc_1 \quad pcc_2 \quad pcc_3 \quad pcc_4 \quad Ldpcc \quad Lqpcc \quad pccd \quad pccq \tag{2.16}$$

The state vector of the entire system is defined as

(2.17)

Then, the complete state-space model of the system that contains -number of generators (inverters or SGs) can be obtained and expressed in a compact form as

$$\begin{cases} & pcc \\ & pcc \\ \vdots & \\ & pcc \\ pcc \quad n+1 & pcc \quad pcc \end{cases} \tag{2.18}$$

where each , has 12 elements and $_{pcc}$ has 4 elements. Thus, the vector functions and are 12-dimensional and 4-dimensional, respectively. Their expressions can be derived from (2.7)-(2.11), and (2.14). They are expressed as

$$\overline{f_i}\ d\ od\ \frac{i}{f_i}\ od\ \overline{f_i}\ 9\ 5\ \frac{i}{f_i}\ 1$$

$$\overline{f_i}\ q\ oq\ \frac{i}{f_i}\ oq\ \overline{f_i}\ 9\ 12\ 6\ \frac{i}{f_i}\ 2$$

$$\overline{Load_i}\ od\ \overline{Load_i}\ 5$$

$$\overline{Load_i}\ oq\ \overline{Load_i}\ 6$$

$$\overline{Load_i}\ od\ Ld\ Line\ \frac{od_i}{Load_i\ Load_i}$$

$$\overline{Load_i}\ 1\ 3\ 7\ \overline{Load_i\ Load_i}\ 5$$

$$\overline{Load_i}\ oq\ Lq\ Line\ \frac{oq_i}{Load_i\ Load_i}$$

$$\overline{Load_i}\ 2\ 4\ 8\ \overline{Load_i\ Load_i}\ 6$$

$$\overline{L_i}\ od\ \frac{L_i}{L_i}\ Line\ \overline{L_i}\ 5\ \frac{L_i}{L_i}\ 7$$

$$\overline{L_i}\ oq\ \frac{L_i}{L_i}\ Line\ \overline{L_i}\ 6\ \frac{L_i}{L_i}\ 8$$

$$\left[\ NL\ \sqrt{od\ \ oq}\ -\ od\ d\ \ oq\ q\ \ od\ q\ \ oq\ d\ \right]$$

$$\left[\ NL\ \sqrt{5\ \ 6}\ -\ 1\ 9\right.$$

$$\left.2\ 9\ \ 12\ \ 1\ 9\ \ 12\ \ 2\ 9\ \right]$$

$$\left[\ ref\ -\ od\ d\ \ oq\ q\ \ od\ q\ \ oq\ d\ \right]$$

$$\left[\ 11\ -\ 1\ 9\ \ 2\ 9\ \ 12\ \ 1\ 9\ \ 12\ \ 2\ 9\ \right]$$

$$\left(\ NL\ \frac{-i}{}\ ref\ \right)\ \left(\ NL\ \frac{i_{10}}{}\ 11\right)$$

$$\left[\ ref\ -\ od\ d\ \ oq\ q\ \ od\ q\ \ oq\ d\ \right]$$

$$10\ \left[\ 11\ -\ 1\ 9\ \ 2\ 9\ \ 12\right.$$

$$\left.1\ 9\ \ 12\ \ 2\ 9\ \right] \tag{2.19}$$

$$
\begin{aligned}
&\text{pcc} \quad \overline{\text{pcc}}\ \text{pccd} \quad \overline{\text{pcc}}\ \text{pcc}_3 \\
&\text{pcc} \quad \overline{\text{pcc}}\ \text{pccq} \quad \overline{\text{pcc}}\ \text{pcc}_4 \\
&\text{pcc} \quad \overline{\text{pcc}} \sum \text{Line} \quad \text{Ldpcc} \quad \frac{\text{pccd}}{\text{pcc}\ \text{pcc}} \\
&\quad \overline{\text{pcc}} \sum {}_{7} \quad \text{pcc}_1 \quad \overline{\text{pcc}\ \text{pcc}}\ \text{pcc}_3 \\
&\text{pcc} \quad \overline{\text{pcc}} \sum \text{Line} \quad \text{Lqpcc} \quad \frac{\text{pccq}}{\text{pcc}\ \text{pcc}} \\
&\quad \overline{\text{pcc}} \sum {}_{8} \quad \text{pcc}_2 \quad \overline{\text{pcc}\ \text{pcc}}\ \text{pcc}_4
\end{aligned}
\tag{2.20}
$$

The scalar function is defined as

$$
\text{ref1} \tag{2.21}
$$

$$
{}_{10} \qquad {}_{11} \quad - \qquad {}_{1}\ {}_{9} \qquad {}_{2}\ {}_{9}
$$

The constant matrices , , , and are given by

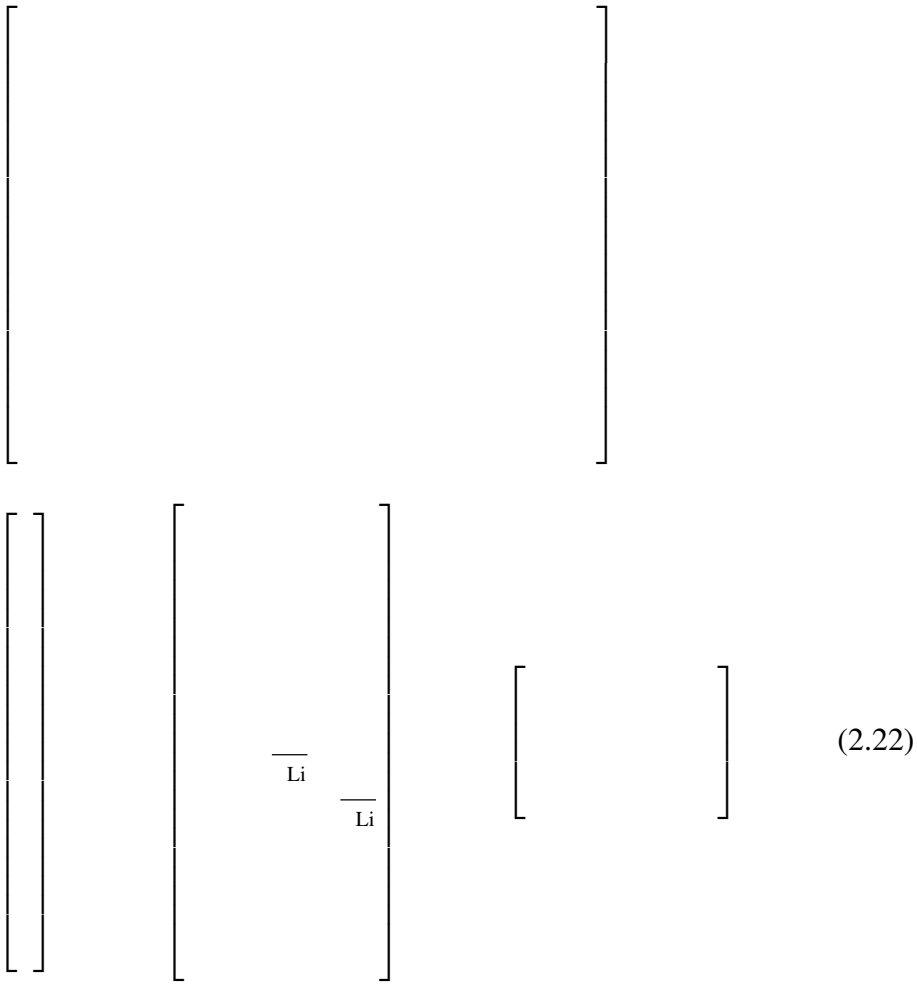

(2.22)

2.2 Linearized Model

The dynamical model in (2.18) is nonlinear. A linearized model can be calculated at the equilibrium point. This leads to

(2.23)

where is the combined small-signal state vector and is the Jacobian matrix that can be expressed as

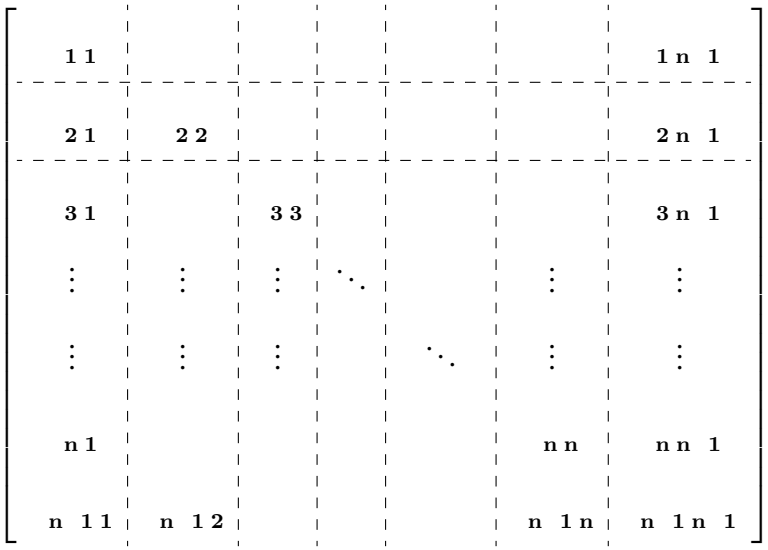

(2.24)

where

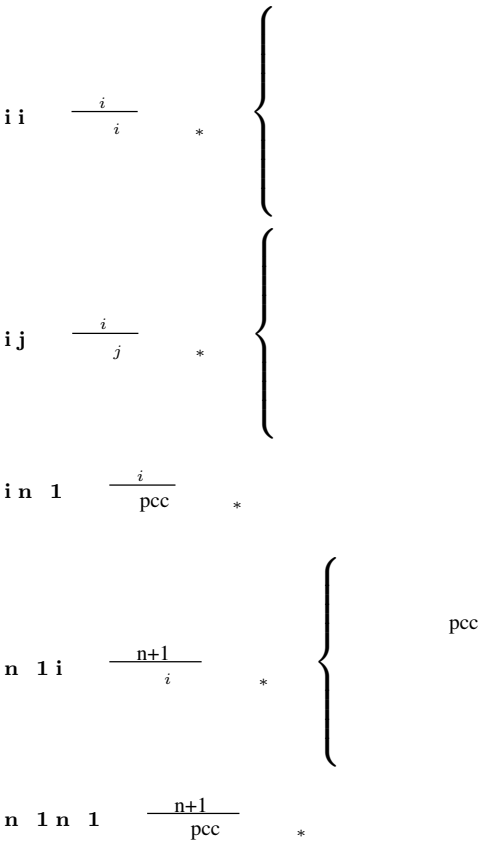

(2.25)

Where , denotes the equilibrium point of (2.18), and , , and are given by

$$\begin{bmatrix} & & \\ & \overline{\text{pcc}} & \\ & & \overline{\text{pcc}} \end{bmatrix} \quad \begin{bmatrix} & \overline{\text{pcc}} & \\ \overline{\text{pcc}} & & \overline{\text{pcc}} \\ & \overline{\text{pcc}} & \end{bmatrix}$$

$$\overline{\quad} \quad \text{d1} \quad \overline{\quad} \quad \text{d1} \quad \overline{\quad} \quad \text{od1} \quad \text{oq1}$$

(2.26)

The elements of the matrix $\frac{i}{i}$ $_*$ are given by

$$\frac{i}{\text{f}i} \quad \overline{\text{f}i} \quad \frac{i^*}{\text{f}i} \quad \frac{\overset{*}{\text{d}i}}{\text{f}i \quad i^{*\,2}}$$

$$\overline{\text{Load}i} \qquad\qquad \overline{\text{Load}i}$$

$$\overline{\text{Load}i \quad \text{Load}i} \quad \overline{\text{L}i} \quad \frac{\text{L}i}{\text{L}i}$$

$$\overline{\quad} \quad \text{d}$$

$$- \quad \text{d} \quad \frac{q \quad v \quad \text{od}i^*}{\sqrt{\overset{*2}{\text{od}i} \quad \overset{*2}{\text{oq}i}}} \quad \frac{q \quad v \quad \text{oq}i^*}{\sqrt{\overset{*2}{\text{od}i} \quad \overset{*2}{\text{oq}i}}}$$

$$\overline{\quad} \quad \text{od} \quad \text{oq} \quad \text{od} \quad \text{oq} \quad - \quad \text{d} \quad \frac{\overset{*}{\text{oq}i} \quad \overset{*}{\text{od}i}}{\overset{*}{i}^{\,2}}$$

$$\overline{\quad} \quad \text{d} \quad \overline{\quad} \quad \text{d}$$

$$\overline{\quad} \quad \text{od} \quad \text{oq} \quad \text{od} \quad \text{oq}$$

(2.27)

The remaining entries of the matrix that do not appear in (2.27) are all zeros. Matlab is used to calculate the system equilibrium point by setting the nonlinear differential equations in (2.18) to zero as . The Matlab code is given in Appendix A.1.

2.3 Summary

This chapter presents an approach for systematically modeling a class of microgrid (MG) systems. The derived model 1) accommodates grid-connected and islanded operation of the MG simultaneously, and 2) allows modeling of converter-based as well as directly-interfaced resources. Full modeling of virtual synchronous machines and actual synchronous generators is addressed. The model is first developed by taking the system nonlinearities in consideration. Subsequently, a linear version of the model is also developed for eigenvalue and stability analysis of the MG.

CHAPTER III

DEFINITION OF PERFORMANCE INDICES

Several performance indices are defined in this chapter in order to quantify the impacts of cross-coupling terms. Various performance aspects including system stability, robustness, power loss, power sharing, and voltage profile are considered. The developed MG model in chapter 2 together with the performance indices will be used for assessing stability margins and the other performance aspects of the MG.

3.1 Stability Indices

For every transformation angle , the operating point of the system is obtained and used to determine the eigenvalues of the state space matrix in (2.23).

To investigate the relative stability of the system, the dominant poles are divided into two groups. A group of the high-frequency dominant poles and a group of the low-frequency dominant poles. The eigenvalue spectrum showing the dominant poles and their classification is depicted in Fig. 3.1 for a two-inverter situation. Only two poles are considered in every group (critical poles). One pole that has the minimum damping ratio and another pole that has the shortest distance to the -axis as they are the most influential on system stability and damping. The minimum damping ratio $_{min}$ and the shortest distance are found at every value of the angle .

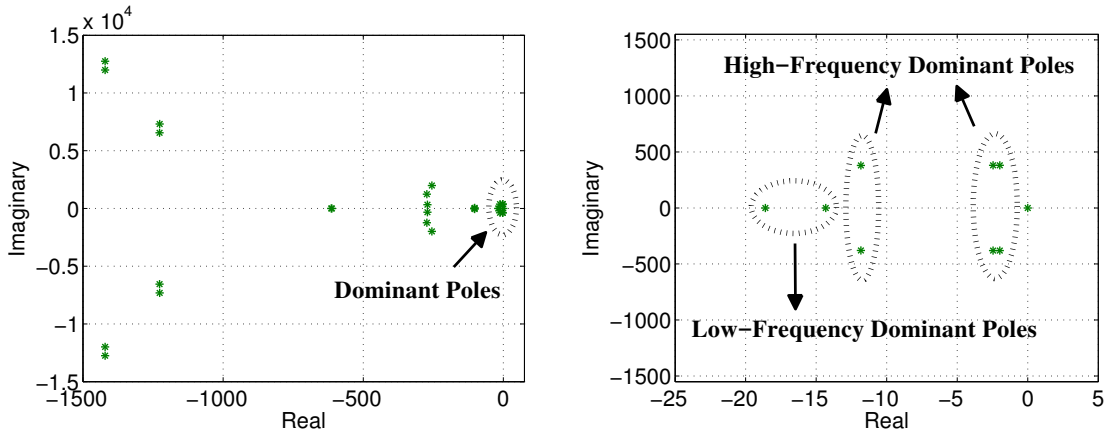

(a) Eigenvalue spectrum

(b) Classification of dominant poles

Figure 3.1: Islanded MG with two DG units operating at

Two stability indices are then defined for each group by (3.1). The first index considers the damping ratio of the critical poles and it is called *damping improvement index* (DII). The second index accounts for the critical poles distance to the imaginary axis and it is called *distance stability improvement index* (DSII). The improvement in stability and damping is quantified with respect to the conventional droop method ( ).

$$\begin{aligned} \text{DII} \quad & \frac{\min \qquad \min}{\min} \\ \text{DSII} \quad & \frac{\min \qquad \min}{\min} \end{aligned} \tag{3.1}$$

It is noteworthy that positive values of DII and DSII at any given angle indicate that the damping ratio and the distance to the -axis of the critical poles are both larger than those at . In other words, using this given results in a more stable system than using . On the contrary, negative DII and DSII at a specific angle means that the damping ratio and the distance to the -axis of the critical poles are both smaller than

those at . This implies that the system stability degrades if this angle is used rather than using .

3.2 Voltage Regulation Index

It is desired that the voltage magnitude of critical buses in an MG remain close to the nominal voltage. Therefore, the effect of cross-coupling droop terms on the voltage profile of the system needs to be quantified. The voltage deviation of the overall system as a function of the rotation angle is quantified by using the *voltage regulation error index* (VREI)

$$\text{VREI} \quad \frac{-\sum}{} \tag{3.2}$$

where is the MG nominal voltage, and represents the number of buses in the MG which are the local loads' buses and the PCC bus.

3.3 Power Loss Improvement Index

The efficiency of the system is investigated for different values of transformation angle . The amount of total power losses $_{\text{loss}}$ in transmission lines as the angle is varied from to is determined. The real power loss in the th line can be calculated as $_{\text{Line}}$. The total transmission loss of a system containing lines is $\sum$. The impact of cross-coupling droop terms on system efficiency is quantified by introducing the *power loss improvement index* (PLII) defined by

$$\text{PLII} \quad \frac{}{} \tag{3.3}$$

It is noted that a positive value of PLII at a specific angle indicates that the transmission losses are less than those at . For example, a PLII of 50% at means that the lines losses at are half the amount of losses at . On the other hand, a negative PLII at a given angle means that the losses are higher than those at . For instance, a PLII of 200% at means that the lines losses at are three times the amount of losses at .

3.4 Power Sharing Indices

The impact of the rotation angle on real and reactive powers sharing is quantified by defining the *active and reactive power sharing error indices* PSEI and QSEI as

$$\text{PSEI} \quad \frac{-\sum}{\text{trans.}} \qquad \text{QSEI} \quad \frac{-\sum}{\text{trans.}} \tag{3.4}$$

where is the number of inverters, $_{\text{trans.}}$ is the total transmitted apparent power to the common load, and are the output active power and reactive power of each inverter, respectively, and and are the ideal active and reactive power shares of each inverter.

3.5 Sensitivity Index

The sensitivity of the entire system to uncertainties in physical parameters is also investigated for different values of the transformation angle . The interface filter inductance is an example of an uncertain physical parameter. The *sensitivity index* (SI) is defined as

$$\text{SI} \quad -\sum \frac{\text{i,1} \qquad \text{i,2}}{\text{i,1}} \tag{3.5}$$

where is the number of the dominant poles that move to the right when the physical parameter is changed, and $_{i,1}$ and $_{i,2}$ are the real parts of those poles at the initial and final values of that parameter, respectively.

3.6 Summary

Multiple performance indices are identified in this chapter in order to assess the impacts of cross-coupling droop terms on the study MG's performance. Different performance perspectives including system stability, robustness, power loss, power sharing, and voltage profile are investigated. The stability and power loss indices are defined in such a way to reflect performance improvement with respect to the conventional droop method while the other indices quantify the deviation from the desired values.

CHAPTER IV

PERFORMANCE EVALUATION

A dynamic model of the study system is derived in chapter 2. The proposed model is applicable to grid-connected and standalone MG systems that contain synchronous generators and inverter-based resources. After that, a set of performance indices are defined in chapter 3 to quantify the impacts of cross-coupling droop terms. This chapter employs the proposed model along with the indices to evaluate the performance of the study system. Two cases of standalone and grid-connected MGs are studied separately in the following two sections.

4.1 Scenario I: Standalone Mode

The autonomous 208 V/60 Hz three-phase microgrid shown in Fig. 1.2 used here that comprises two inverters at 2 kVA that are implemented using voltage-source converter (VSC) topology at 500 V DC side, 10 kHz switching frequency, and the interface filter inductance of mH. Each inverter supplies a local load of 400 W, 300 Var. Inverter 1 and inverter 2 are connected to the PCC by 2 km and 1 km-long transmission lines, respectively. The line resistance and reactance are R_L km, X_L km [34]. A 2.2 kVA, 0.82 PF lagging common load is connected to the PCC bus.

The iVSM of Fig. 1.3 with the following parameters is used for the inverters: ,
, , , V, ,
, , (kg.m , s),
, . Details about the
design algorithm for the controller parameters are given in [26].

The transformation angle for both inverters is equal and varied over a range of (
). The predefined indices are determined at every value of . The impacts of cross-coupling droop terms on system performance are quantified by plotting these indices versus
.

The stability indices graphs for the high-frequency critical dominant (HFCD) poles and low-frequency critical dominant (LFCD) poles are shown in Fig. 4.1. The following observations are made from this figure.

1) The DII and DSII of the HFCD poles have positive values, and they increase significantly as the angle is reduced. Maximum DII and DSII are achieved when the DG units operate at where the DII and DSII are almost 60%.

2) The DII and DSII of the LFCD poles remain relatively close to zero when varies from 0 to 90 degrees. It can be concluded that the system stability and damping are mostly determined by the HFCD poles and they are improved because their DII and DSII increase significantly when decreases.

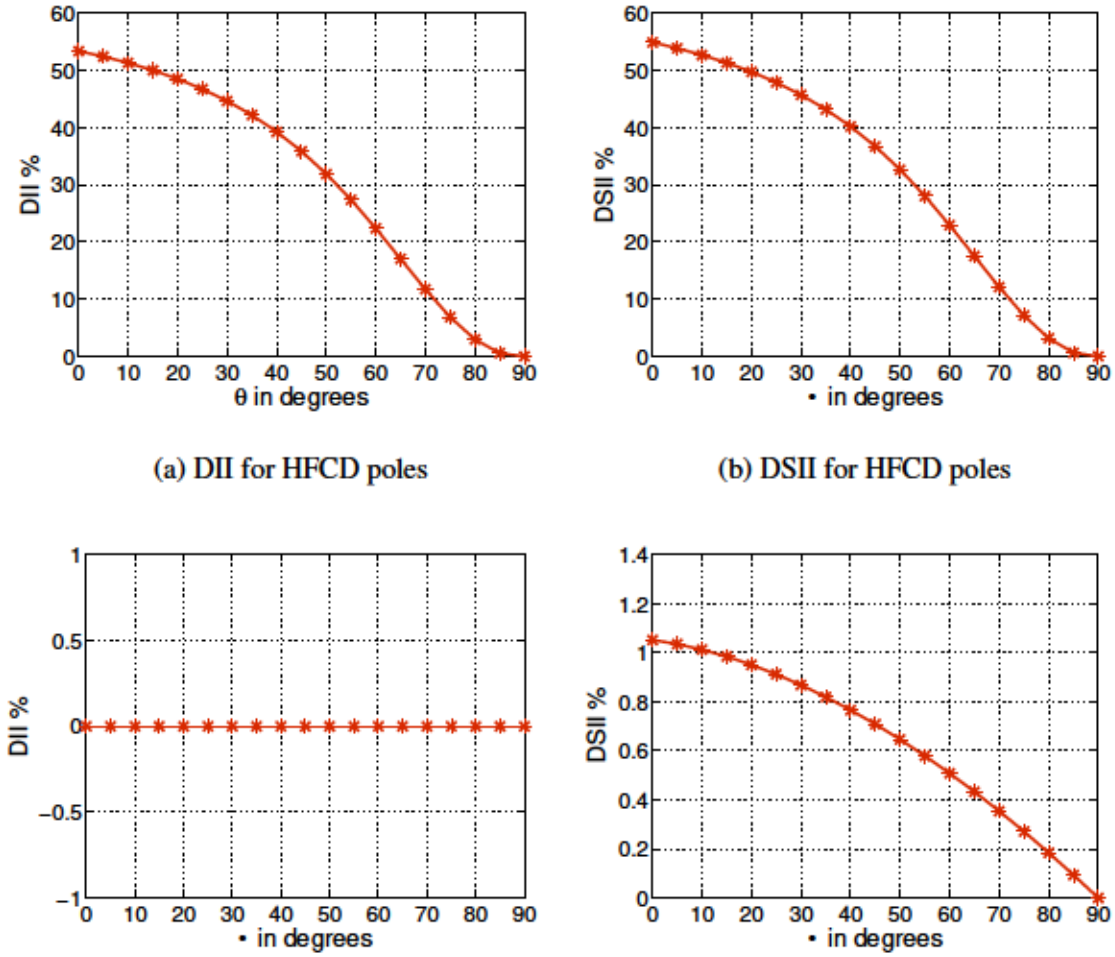

(a) DII for HFCD poles

(b) DSII for HFCD poles

(c) DII for LFCD poles

(d) DSII for LFCD poles

Figure 4.1: Stability indices - Standalone Mode

The VREI versus θ is illustrated in Fig. 4.2 (a) where the output voltages of both inverters and the point of common coupling voltage (v_{o1}, v_{o2}, v_{pcc}) are considered. It can be noted that the the value of θ does not have an impact on the voltage profile of the system where the whole range of VREI change is less than 0.2%.

The plot of PLII in percentage versus θ is shown in Fig. 4.2 (b) which indicates that the system efficiency improves as the angle θ decreases all the way to about 50°. Beyond

, the system efficiency continues to improve slightly as drops to at which the PLII is maximum. Then, the PLII decreases for smaller than until it reaches about 8% when .

The graph of PSEI and QSEI as a function of the angle are shown in Fig. 4.2 (c). As can be seen, the real power is shared equally when the DG units operate using the conventional droop controller ( ) while the maximum QSEI implies that there is maximum error in reactive power sharing. In contrast, if the DG units use the reverse droop controller, the reactive power will be shared equally while the real power will not be distributed accurately. As decreases from 90 , the reactive power sharing improves and the real power sharing degrades.

To examine the impact of cross-coupling droop terms on controller sensitivity, the inductance of the interface filter is changed from mH to mH for each value of the angle and the SI given in (3.5) is depicted in Fig. 4.2 (d). It can be observed that the system is much robust with respect to this change in angle although a slight decrease in sensitivity is observed at smaller values of . The controller sensitivity to line impedance changes is also investigated. The graphs of SI versus the angle when lines ratio changes from 7.7 to 0.8 and when the length of line 1 is increased from 0.1 km to 2 km are shown in Fig. 4.3. This concludes that the system is very robust to line impedance changes.

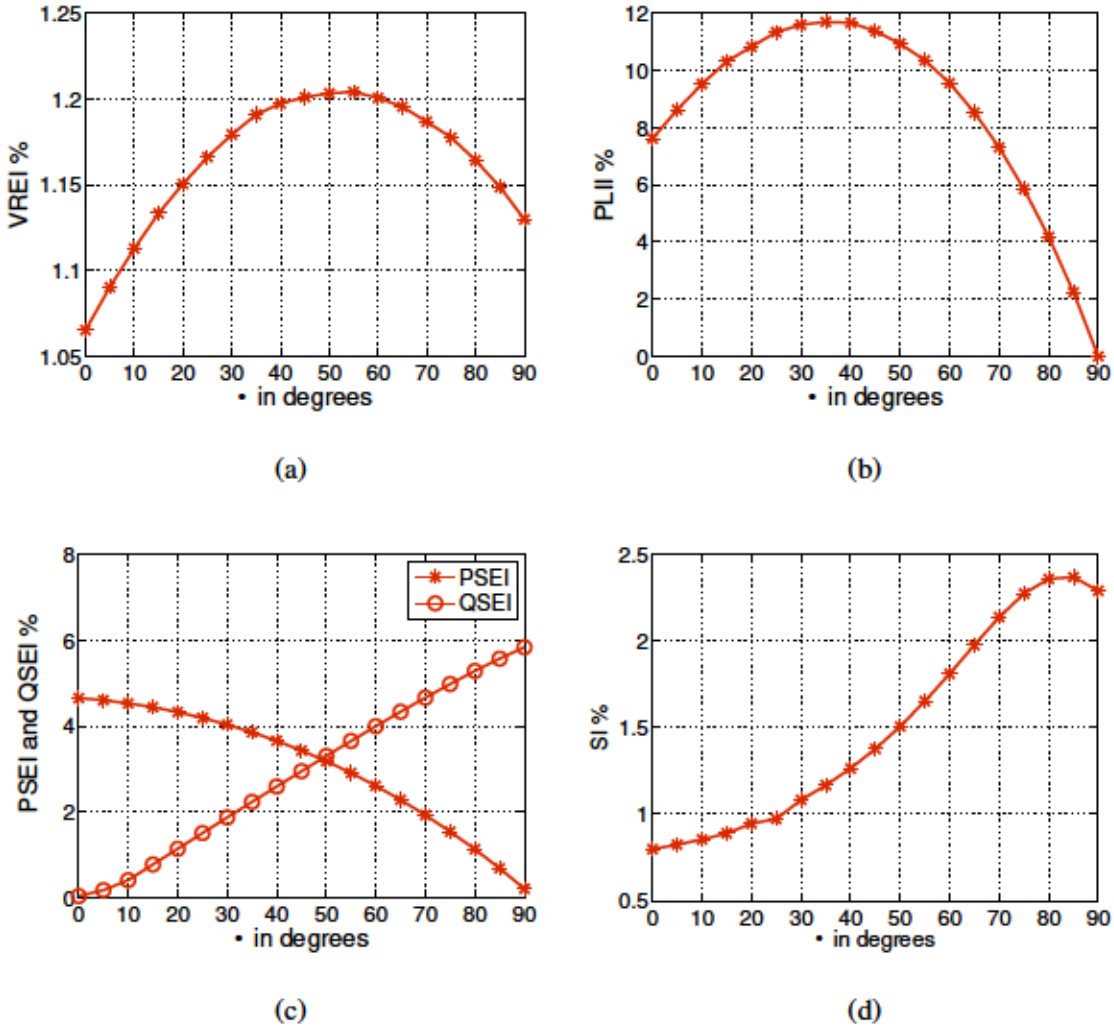

Figure 4.2: (a) VREI (b) PLII (c) PSEI and QSEI (d) SI - Standalone Mode

4.2 Scenario II: Grid-Connected Mode

4.2.1 Double-Inverter Microgrid

In this study, we consider three generators where one of them is selected to model the main grid while the other two are selected to operate as converter-based DERs to represent a grid-connected MG with two sources.

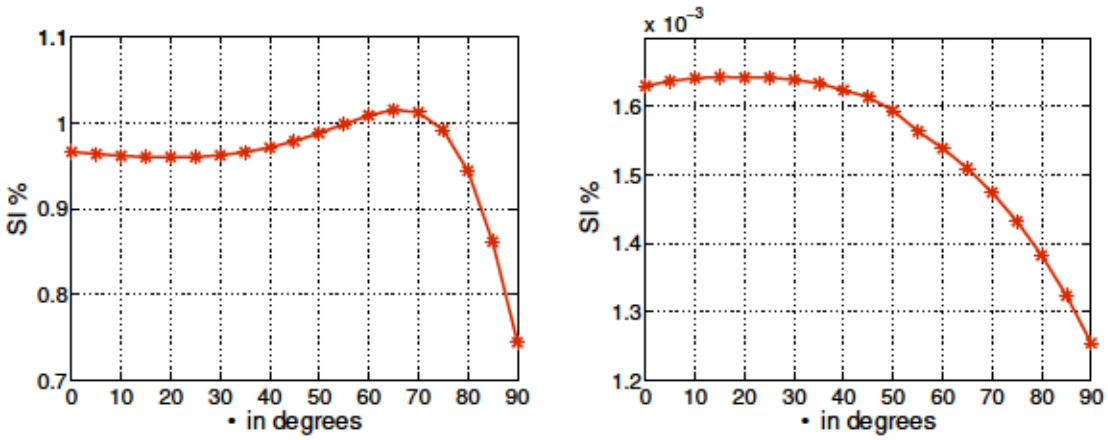

(a) R/X changes from 7.7 to 0.8

(b) Line 1 length increases from 0.1 km to 2 km

Figure 4.3: SI - Standalone Mode

The inverters' power and control parameters are the same as used in standalone mode, Section 4.1. They are connected to the PCC by 1 km and 0.5 km-long transmission lines, respectively, where a 2.2 kVA, 0.82 PF lagging common load resides. The synchronous generator (modeling the grid) is rated at $S_1 = 20$ kVA and its control parameters are $\alpha_1 = 3$, $V_g = 120\sqrt{2}$ V, $Z_{\text{base}} = \frac{(V_g/\sqrt{2})^2}{(S_1/3)} = 2.16\ \Omega$, $k_1 = (1/3)(2\alpha_1 Z_{\text{base}}) = 4.32$, $k_{q1} = k_1/V_g = 0.0255$, $k_{p1} = k_1/V_g^2 = 1.5 \times 10^{-4}$, $H = 5$ s, $J = (HS_1)/(0.5\omega^2) = 1.4072$ kg.m^2, $k_{\omega 1} = 1/(J\omega) = 0.0019$, $k_{f1} = S_1/\Delta f = 20000/2 = 1 \times 10^4$, $k_{v1} = S_1/\Delta V = 20000/12\sqrt{2} = 1.1785 \times 10^3$. The synchronous reactance and the armature resistance of the SG are selected at 1 pu and 0.02 pu, respectively, leading to $L_g = Z_{\text{base}}/\omega = 5.7$ mH and $R_g = 0.02 Z_{\text{base}} = 0.0432\ \Omega$.

The transformation angle θ of DG-1 is set to 90° to emulate the grid, whereas the angle of inverters is equal and are changed from 0° to 90° in this study. The cut-off frequency of the governor low-pass filter is selected at $\omega_c = 2\pi f_c = 2\pi \times 1$ rad/s for the SG. This

parameter is selected at 100 Hz in the converter-based DERs. The local load supplied by the grid is 12 kW, 9 kVar. Line 1 that connects the MG to the main grid is 2 km long, see Fig. 1.2.

The stability indices for the HFCD and LFCD poles as a function of the angle are shown in Fig. 4.4. It is observed that, contrary to the standalone case, the DII and DSII decrease as decreases from . This means that the system stability and damping degrade. The system at is the least stable. This represents the reverse droop controller that acts opposite to the conventional droop principle used in the main grid.

The graph of VREI as a function of is illustrated in Fig. 4.5 (a) for the entire four bus voltages. This confirms that the inverters do not have a noticeable impact on the voltage profile in this grid-connected scenario.

The plot of PLII versus is illustrated in Fig. 4.5 (b). It shows that the PLII increases up to about 60% when decreases from 90 to 75 degrees. It then decreases to zero when is further decreased to about 50 degrees. For smaller than 50 degrees, the PLII keeps decreasing to negative numbers sharply which means that the amount of transmission losses increases. When the MG operates based on the reverse droop principle ( ), the transmission losses are maximum value at around nine times the amount of losses when it operates at conventional droop angle of 90 degrees. The graph of PSEI and QSEI for this scenario are shown in Fig. 4.5 (c). Similar observations as those for the PSEI and QSEI of the autonomous MG can be made. The impact of cross coupling droop terms on controller sensitivity is also investigated, the inductance of the interface filter is changed from mH to mH for each value of the angle and the SI is illustrated in Fig. 4.5 (d). It

can be noted that the system is much robust with respect to this change in angle although sensitivity slightly decreases as θ decreases from $90°$ to $65°$. The SI is almost flat for $25° < \theta < 65°$, then it slightly increases as θ continues to decrease down to $0°$.

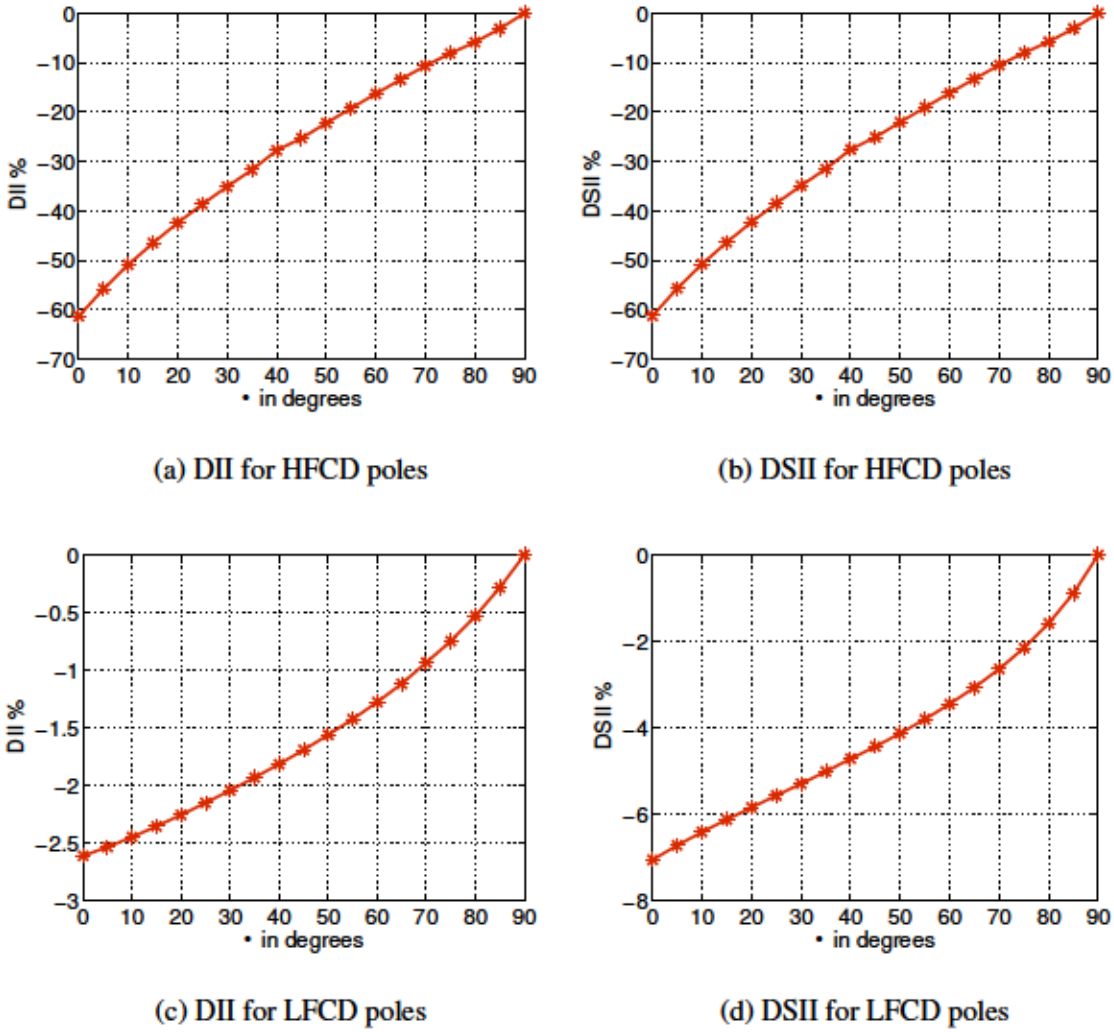

(a) DII for HFCD poles

(b) DSII for HFCD poles

(c) DII for LFCD poles

(d) DSII for LFCD poles

Figure 4.4: Stability indices - Grid-Connected Mode (Double-inverter microgrid)

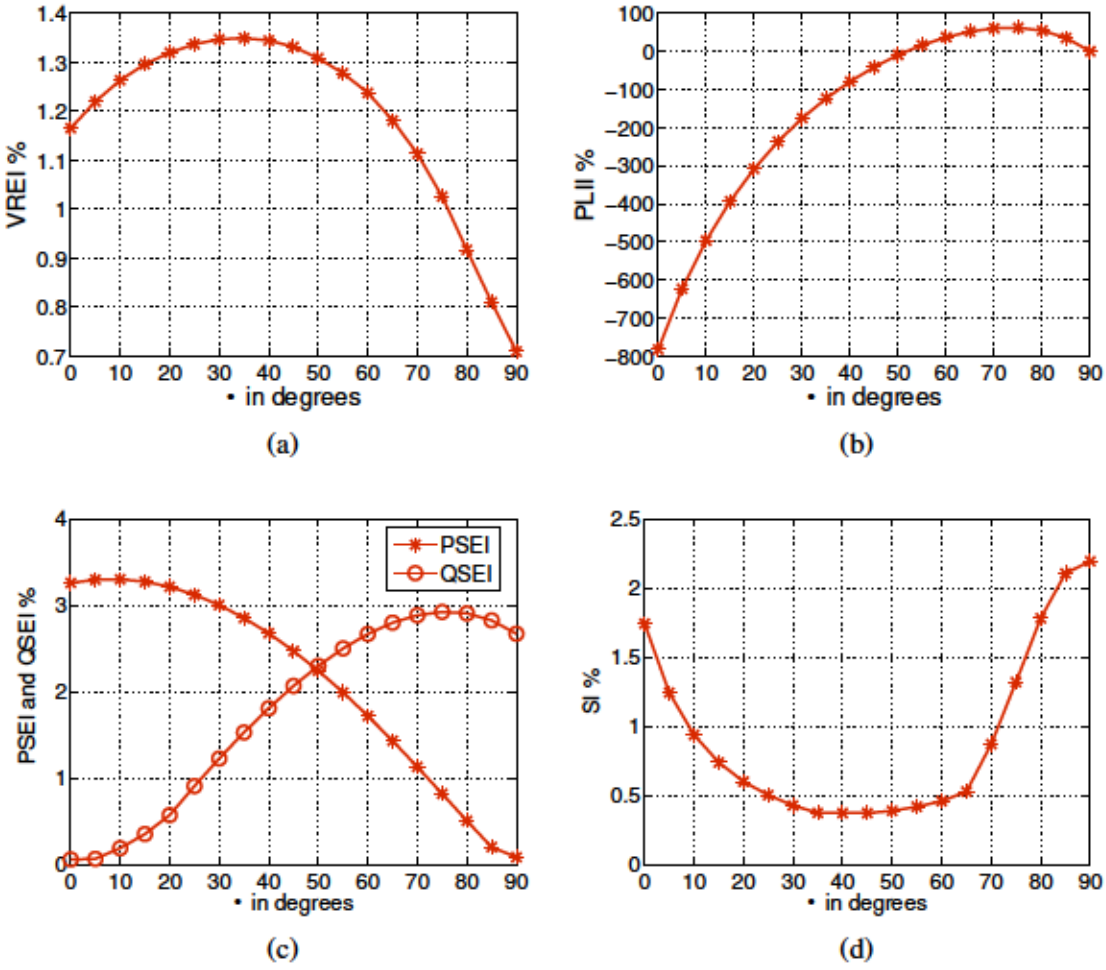

Figure 4.5: (a) VREI (b) PLII (c) PSEI and QSEI (d) SI - Grid-Connected Mode (Double-inverter microgrid)

4.2.2 Single-Inverter Microgrid

In this study, we consider two generators where one of them is selected to model the main grid while the other one is selected to operate as converter-based DER to represent a grid-connected MG with a single source. The synchronous generator (modeling the grid) and the inverter's power and control parameters, the common and local loads are all the same as used in grid-connected mode, Section 4.2.1. The inverter is connected to the PCC

by 1 km-long transmission line. Line 1 that connects the MG to the main grid is 2 km long. The transformation angle of DG-1 is set to to emulate the grid, whereas the angle of inverter is changed from to .

The stability indices for the HFCD and LFCD poles as a function of the angle are shown in Fig. 4.6. It is noted that the DII and DSII decrease as decreases from . This means that the system stability and damping degrade. The system at is the least stable.

The graph of VREI as a function of is illustrated in Fig. 4.7 (a) for the entire three bus voltages. This shows that the amount of cross-coupling droop terms do not have a significant influence on the system voltage profile where the whole range of VREI variation is about 0.3%.

The plot of PLII versus is illustrated in Fig. 4.7 (b). It shows that the PLII increases up to about 50% when decreases from 90 to 70 degrees. It then decreases to zero when is further decreased to about 45 degrees. For smaller than 45 degrees, the PLII keeps decreasing to negative numbers sharply which means that the amount of transmission losses increases. When the MG operates based on the reverse droop principle ( ), the transmission losses are maximum value at around four times the amount of losses when it operates at conventional droop angle of 90 degrees. It is observed that the curves of stability indices and PLII have the same pattern of the corresponding curves in the two grid-connected inverters scenario. However, the voltage profiles of the two systems are not the same due to the difference in generation-load characteristics.

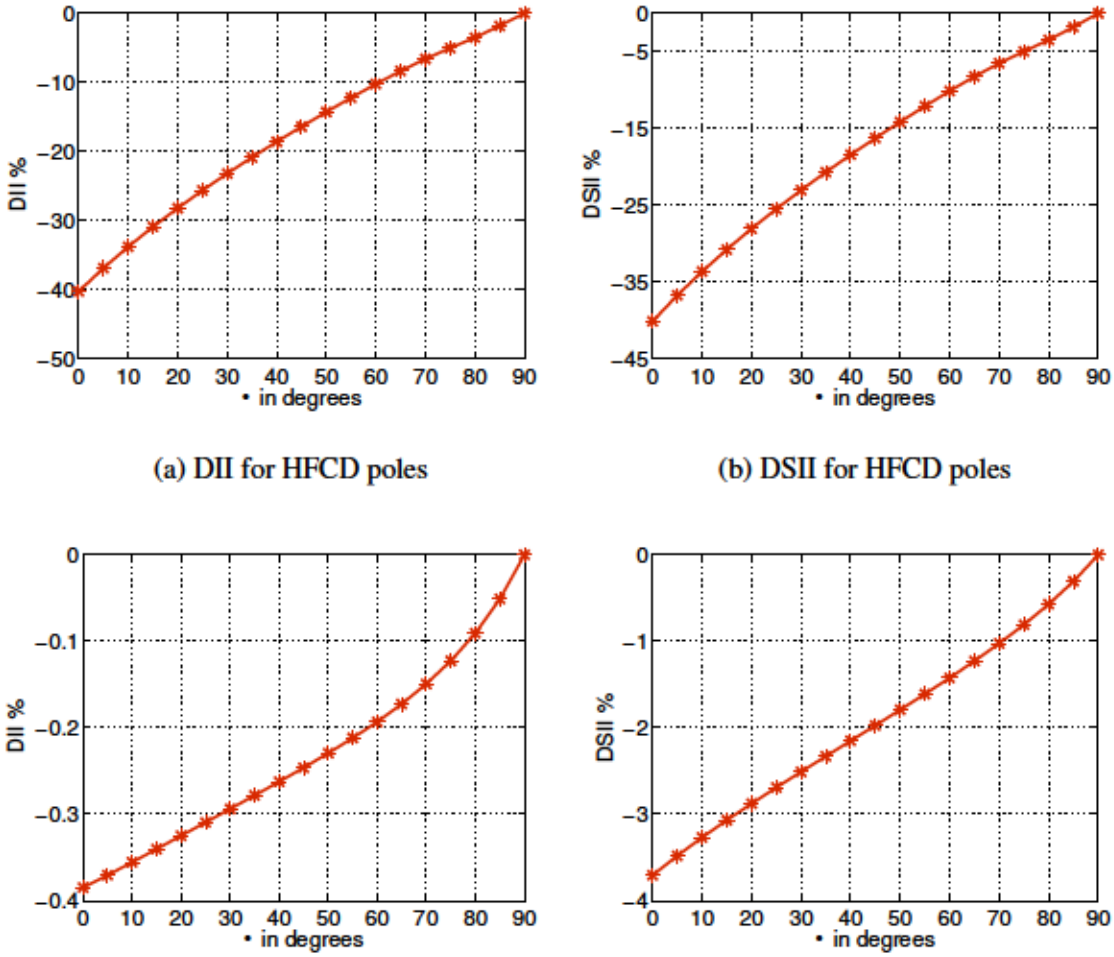

(a) DII for HFCD poles

(b) DSII for HFCD poles

(c) DII for LFCD poles

(d) DSII for LFCD poles

Figure 4.6: Stability indices - Grid-Connected Mode (Single-inverter microgrid)

4.3 Performance Evaluation Under Different R/X Line Ratio

The lines R/X-ratio of about 7.7 has been used in the analysis of the study system according to the practical data of some distribution cables. However, the performance of the standalone and grid-connected MGs considering different values of lines R/X-ratio is investigated as follows.

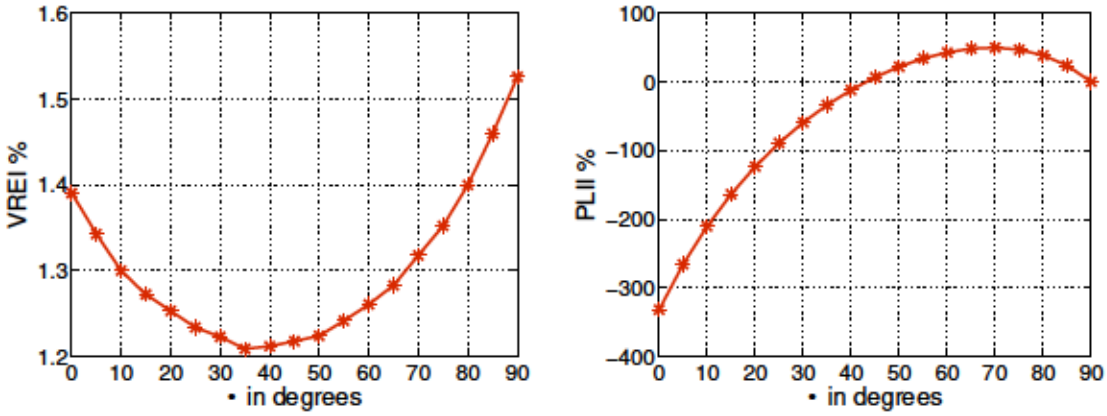

(a) (b)

Figure 4.7: (a) VREI (b) PLII - Grid-Connected Mode (Single-inverter microgrid)

4.3.1 Scenario I: Standalone Mode

The islanded MG considered in Section 4.1 is analyzed for two other cases of R/X-ratio equal to 4 and 0.8. The graphs of all performance indices versus the angle θ are shown in Figs. 4.8 - 4.11. It can be observed that similar conclusions are obtained regardless of the R/X line ratio.

4.3.2 Scenario II: Grid-Connected Mode

The analysis of the grid-connected MG in Section 4.2 is validated for two other cases of R/X-ratio equal to 4 and 0.8. The plots of all performance indices as a function of the angle θ are illustrated in Figs. 4.12 - 4.15. These results confirm that the conclusions are still valid for different R/X line ratios. It is worth noting that the system loses stability for θ below 15° when the line R/X-ratio is equal to 0.8.

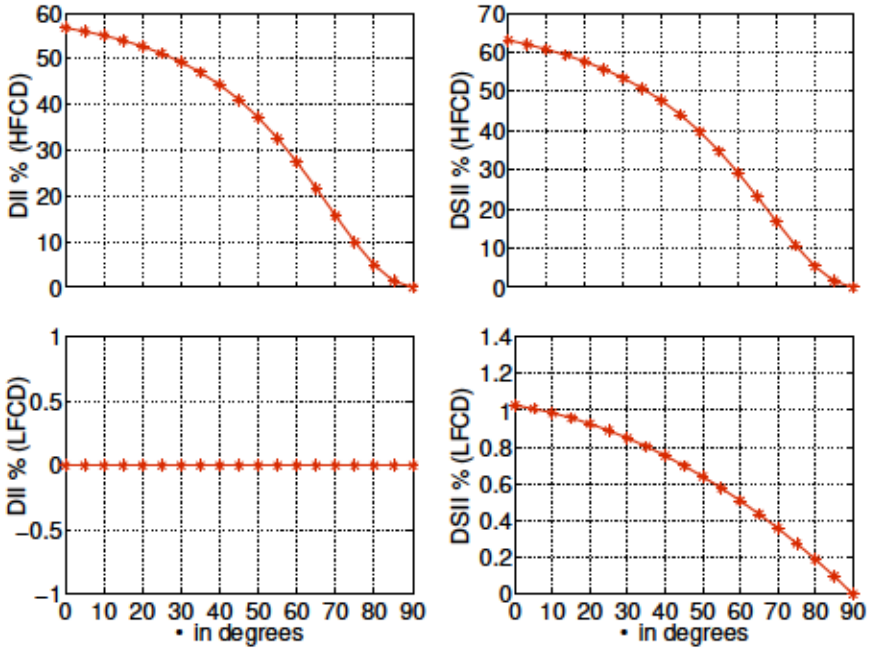

Figure 4.8: Stability indices for $R/X = 4$ line ratio - Standalone Mode

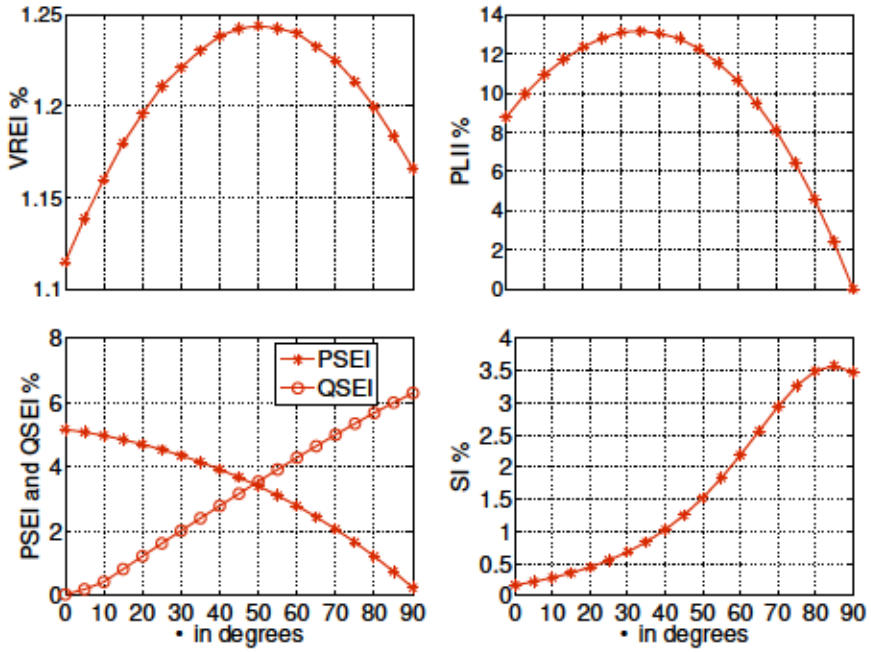

Figure 4.9: VREI, PLII, PSEI/QSEI, and SI for $R/X = 4$ line ratio - Standalone Mode

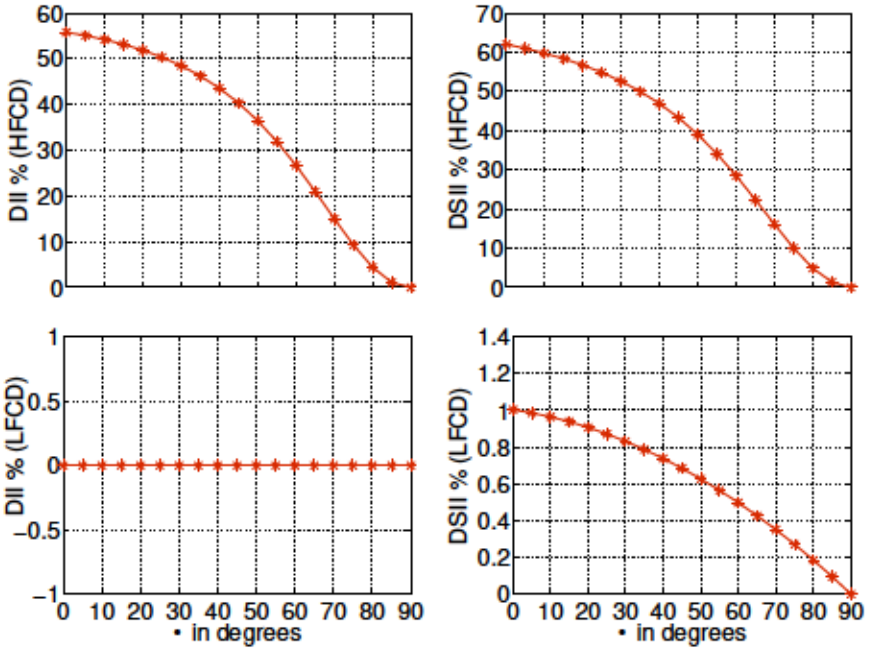

Figure 4.10: Stability indices for $R/X = 0.8$ line ratio - Standalone Mode

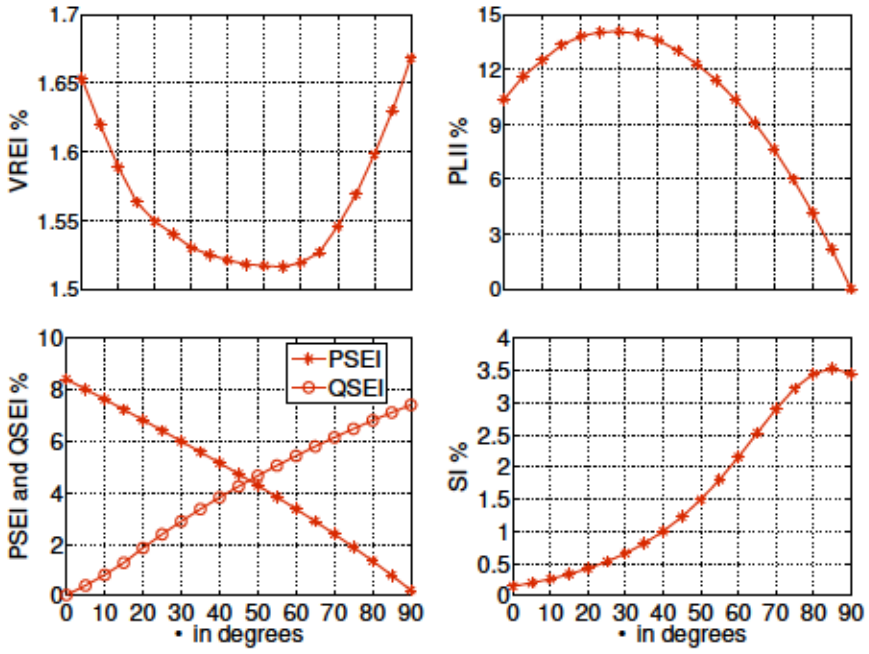

Figure 4.11: VREI, PLII, PSEI/QSEI, and SI for $R/X = 0.8$ line ratio - Standalone Mode

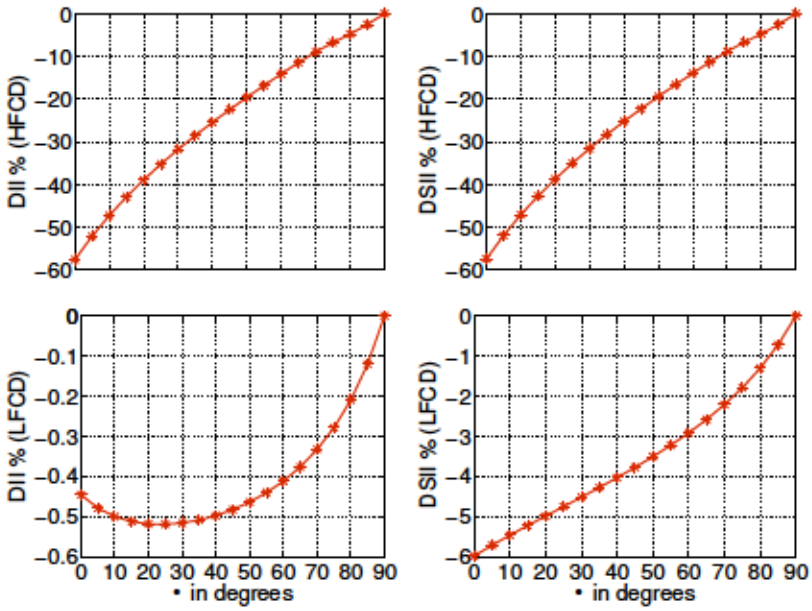

Figure 4.12: Stability indices for $R/X = 4$ line ratio - Grid-connected Mode

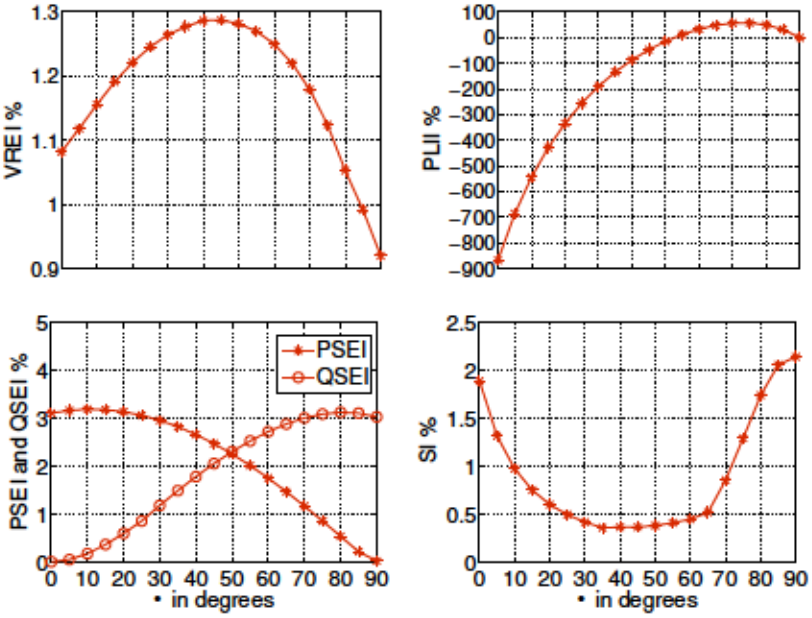

Figure 4.13: VREI, PLII, PSEI/QSEI, and SI for $R/X = 4$ line ratio - Grid-connected Mode

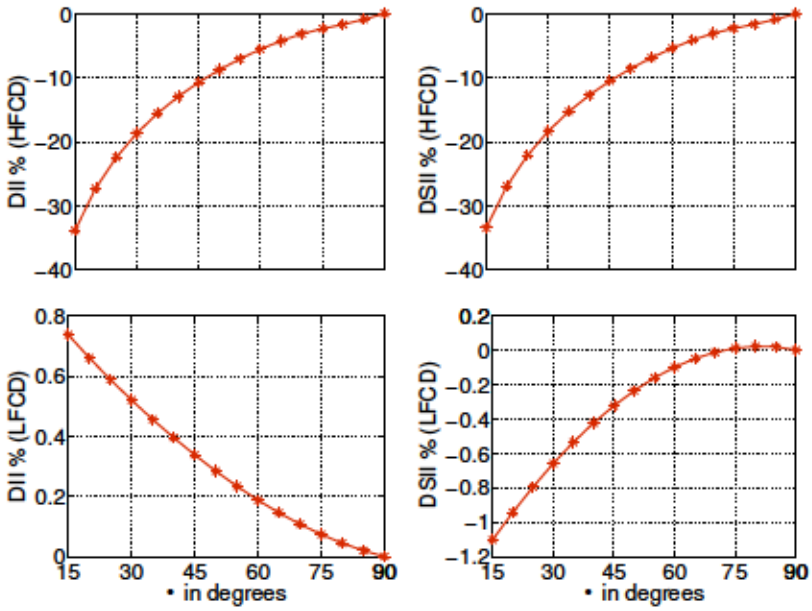

Figure 4.14: Stability indices for $R/X = 0.8$ line ratio - Grid-connected Mode

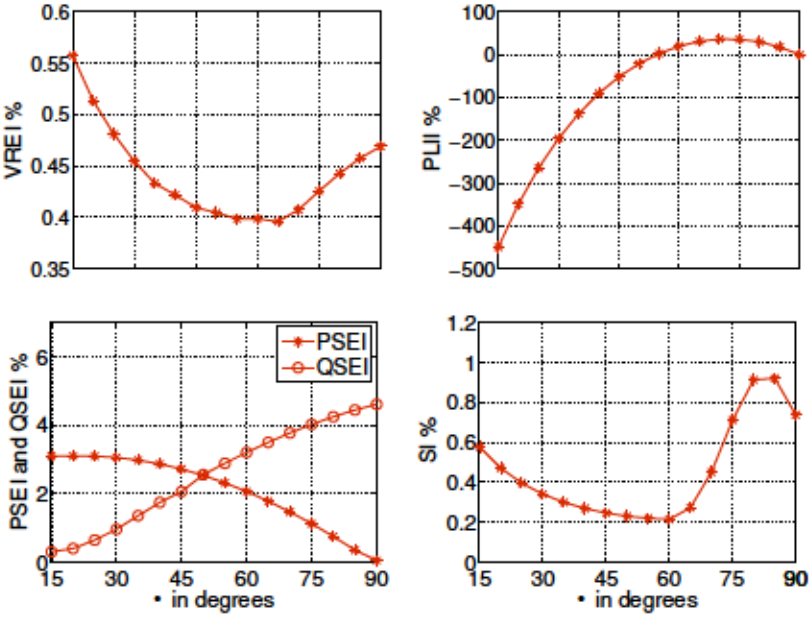

Figure 4.15: VREI, PLII, PSEI/QSEI, and SI for $R/X = 0.8$ line ratio - Grid-connected Mode

4.4 Summary

The developed model of the study MG system in conjunction with the predefined indices are used in this chapter to evaluate the system performance. The rotation angles that specify the level of cross-coupling drooping terms are changed equally from to in all inverters. The predefined indices are determined at every value of , and the impacts of cross-coupling droop terms on system performance are quantified by plotting these indices versus . The conclusions of this study for both islanded and grid-connected MGs are summarized in Table 4.1. Note that the sensitivity is measured with respect to the filter inductance uncertainties and line impedance uncertainties.

Table 4.1: Summary of cross-coupling droop terms impacts on system performance: decreasing from 90

Mode	Stability	Voltage profile	Efficiency	Power sharing	Sensitivity
Standalone	Improves.	Slightly influenced.	Improves.	sharing degrades. sharing improves.	Relatively unchanged.
Grid-connected	Degrades.	Slightly influenced.	Improves for just below ( ) and degrades for smaller values of	sharing degrades. sharing improves.	Relatively unchanged.

CHAPTER V

RESULTS

A detailed mathematical model of the study system in the reference frame is developed in chapter 2. The proposed model is then employed to investigate the impacts of cross coupling droop terms on the stability and other properties of the MG. To this aim, several performance indices are defined in chapter 3. The study system performance in both modes of operation is evaluated by plotting the performance indices as a function of the transformation angle in chapter 4. Detailed results of the study system in both operational modes and during transition between them are provided in this chapter in order to verify the conclusions derived in chapter 4. The results include computer simulations conducted in PSIM power simulation software in addition to real-time simulations performed in Real-Time Digital Simulator (RTDS) and experimental results obtained from a laboratory experimental set-up.

Real-time digital simulator (RTDS) is a combination of computer hardware and software designed for simulating power system electromagnetic transients [29]. The RTDS hardware is composed of individual racks of digital signal processors connected to each other using a common backplane. The digital signal processors share the computational burden to solve the system equations.

RSCAD software is a graphical user interface (GUI) that is used by RTDS. It consists of individual modules that allow the user to perform all the needed steps to prepare and run simulations. The RSCAD's libraries contain all the fundamental elements of an electrical power system. The user can build a schematic diagram of the system to be simulated in the RSCAD/Draft module where comprehensive libraries of power system, control, and protection component models exist. When the system diagram is completed it can be compiled for the RTDS simulator. The compile process generates the code for the simulator hardware and checks the circuit for errors before it can be run in the RunTime environment.

The RSCAD/RunTime module allows the user to control and interact with the real time simulations. The RunTime module provides meters and plots that allow the user to monitor the system response. Sliders can also be used to change the input values, and switches can be added to control the breakers if they are needed in the circuit.

The contents of this chapter are summarized as follows.

Both computer and real-time simulations of the autonomous MG considered in Section 4.1 are conducted in order to confirm the previous conclusions.

The impacts analysis of cross coupling droop terms on the performance of double-inverter and single-inverter MGs is verified by PSIM results. The effect of increasing the droop coefficients of the DG units on the stability of the double-inverter MG is also investigated.

The study system performance during transition from islanded mode to grid-connected mode is examined. Computer and real-time simulations are carried out to study the influence of cross coupling droop amount on MG performance during transition.

Experimental results are provided to confirm the derived conclusions by implementing a two-machine MG in laboratory.

To further validate the study results, a modified IEEE 13-bus system is considered as a case study. Detailed simulations of the test system are performed in all modes of operation.

5.1 Scenario I: Standalone Mode

Simulations of the islanded MG studied in Section 4.1 are presented to verify the analysis of the impacts of cross-coupling droop terms on its performance. Simulations are conducted in PSIM power simulation software [47] to validate the previous analysis. The common load is increased from 1.2 kW, 0.8 kVar to 2 kW, 1.5 kVar at s. The system voltage profile is shown in Fig. 5.1. It can be observed that the amount of cross-coupling does not affect the voltage magnitudes where the system voltage profile at is similar to that at . The output real power of DG-2 is illustrated in Fig. 5.2. It is noted from both the start-up transient and the post-disturbance transient that the system damping is significantly improved when which perfectly agrees with the analysis.

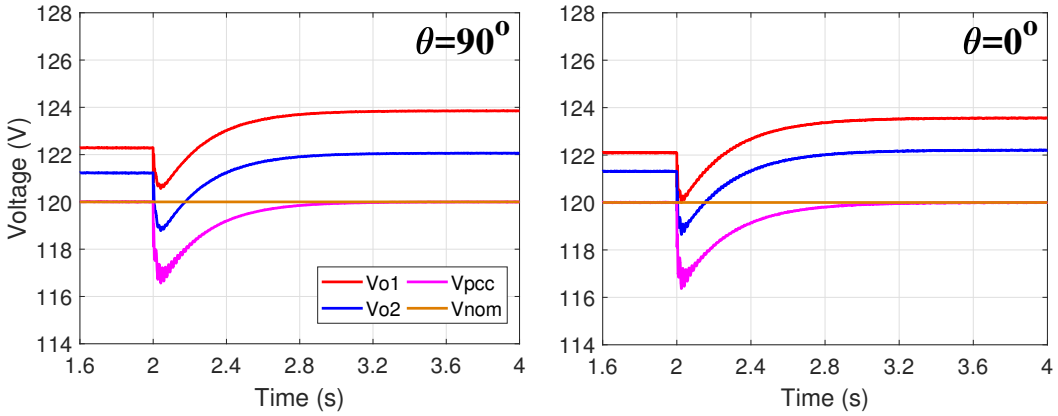

Figure 5.1: Voltage amplitudes - Standalone Mode

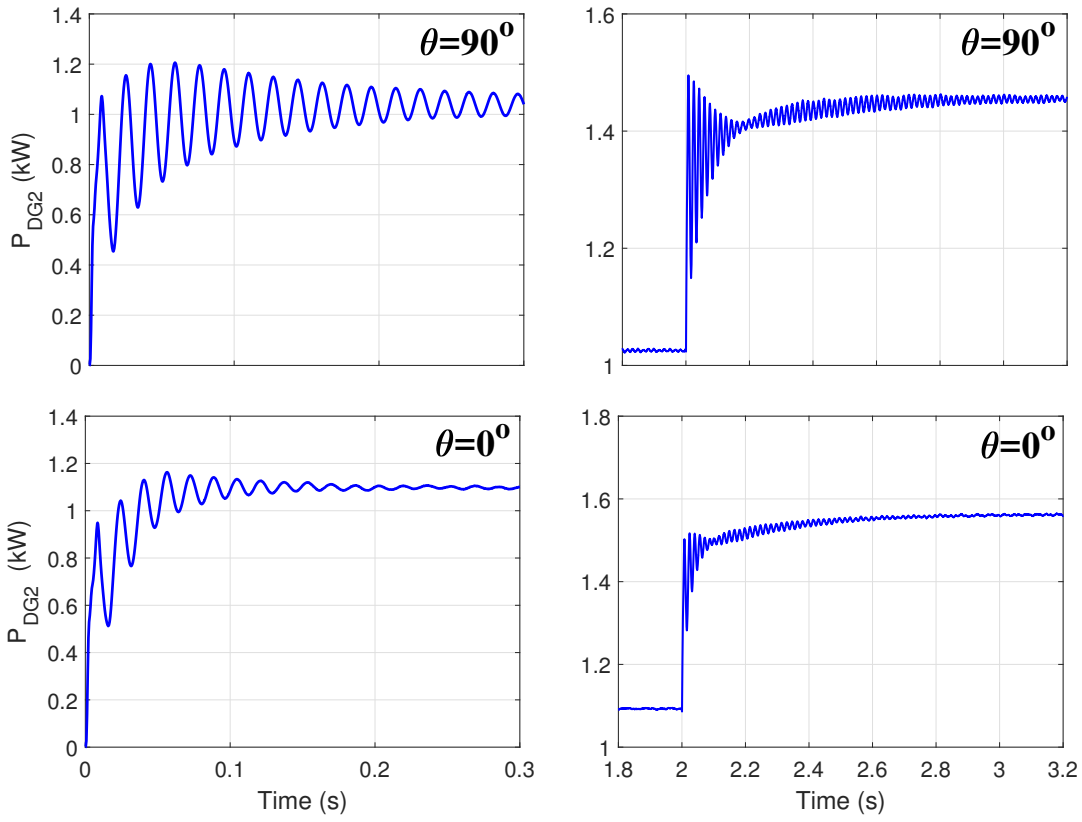

Figure 5.2: Output real power of DG-2 - Standalone Mode

Real-time simulation of the system is performed using Real-Time Digital Simulator (RTDS) to further verify the analysis. The real time voltage amplitudes of the load buses and the output real power of DG-2 for are shown in Figs. 5.3 and 5.4, respectively, when the common load increases. It is noted that the real-time results agree with the computer simulation results shown in Figs. 5.1 and 5.2.

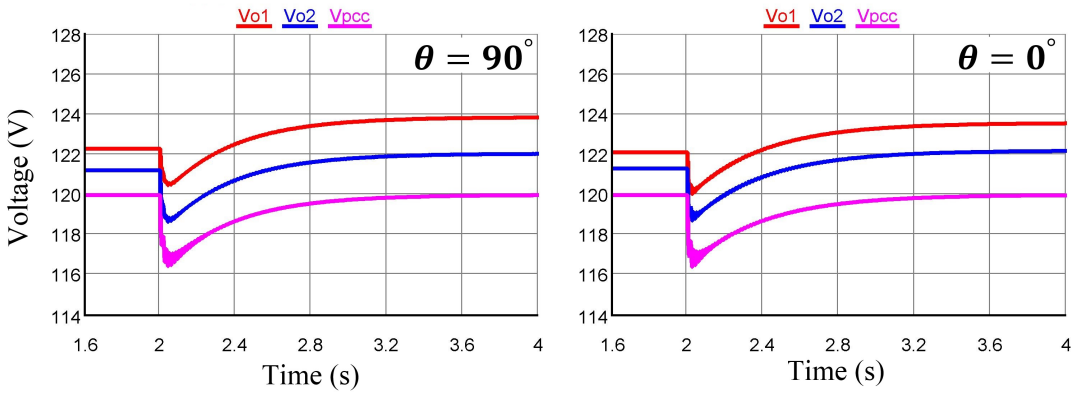

Figure 5.3: Real-time voltage amplitude - Standalone Mode

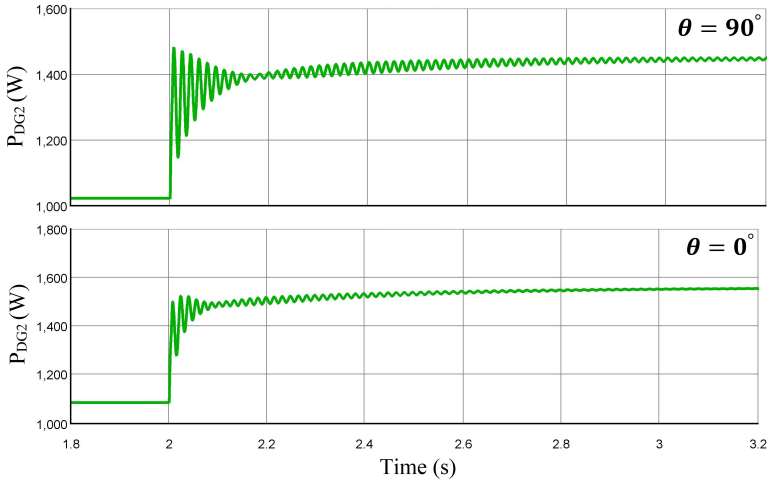

Figure 5.4: Real-time output power of DG-2 - Standalone Mode

5.2 Scenario II: Grid-Connected Mode

5.2.1 Double-Inverter Microgrid

Simulations are carried out to verify the aforementioned analysis of impacts of cross-coupling droop terms on performance of the double-inverter grid-connected system considered in Section 4.2. At s, the common load connected at the PCC is increased from 1.8 kW, 1.25 kVar to 4 kW, 2.5 kVar. The d-axis current of the grid when the DG units operate at is illustrated in Fig. 5.5. It can be seen that the system is less damped when which is consistent with the previous analysis.

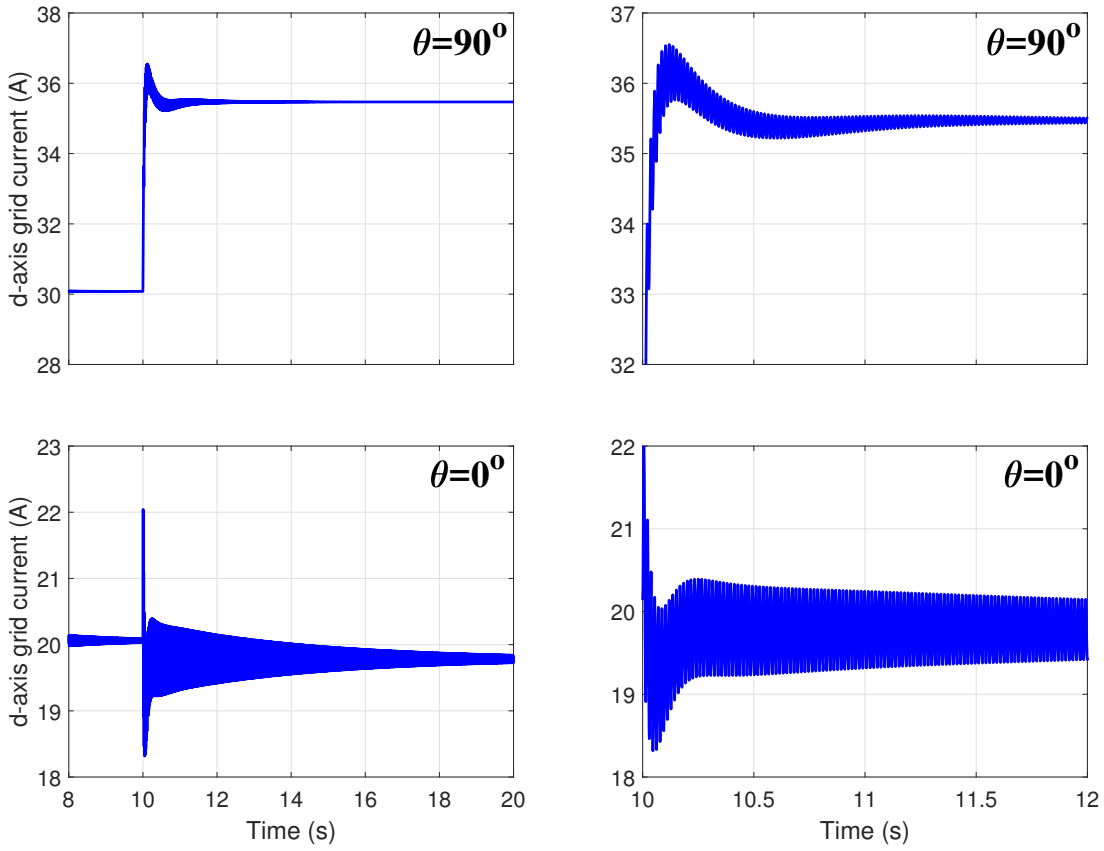

Figure 5.5: Common load increases at s. (Left) d-axis current of grid. (Right) Zoomed-in view of d-axis current of grid.

The impact of increasing the droop coefficients and of the DG units on system stability for different values of is also investigated. Fig. 5.6 shows the eigenvalue trace for when the droop coefficients are increased starting from , . As can be seen, when the value of increases, higher values of droop coefficients can be selected before system becomes unstable.

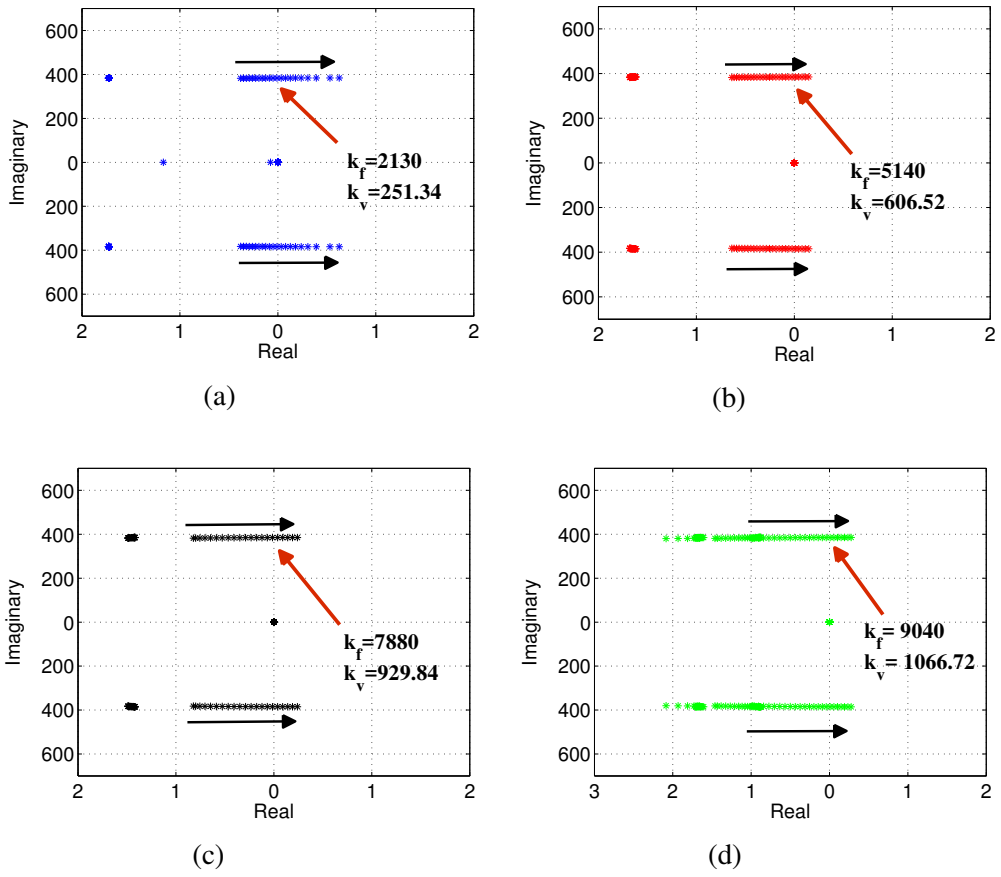

Figure 5.6: Eigenvalue spectrum when the DG units droop coefficients and are increased- Grid-Connected Mode (Double-inverter microgrid).

Simulations are conducted to validate this result where the droop coefficients and are increased by six times at s at each value of . It is observed from Fig. 5.7 that the system becomes unstable when and maintains stability when which shows agreement with the eigenvalue spectrum in Fig. 5.6.

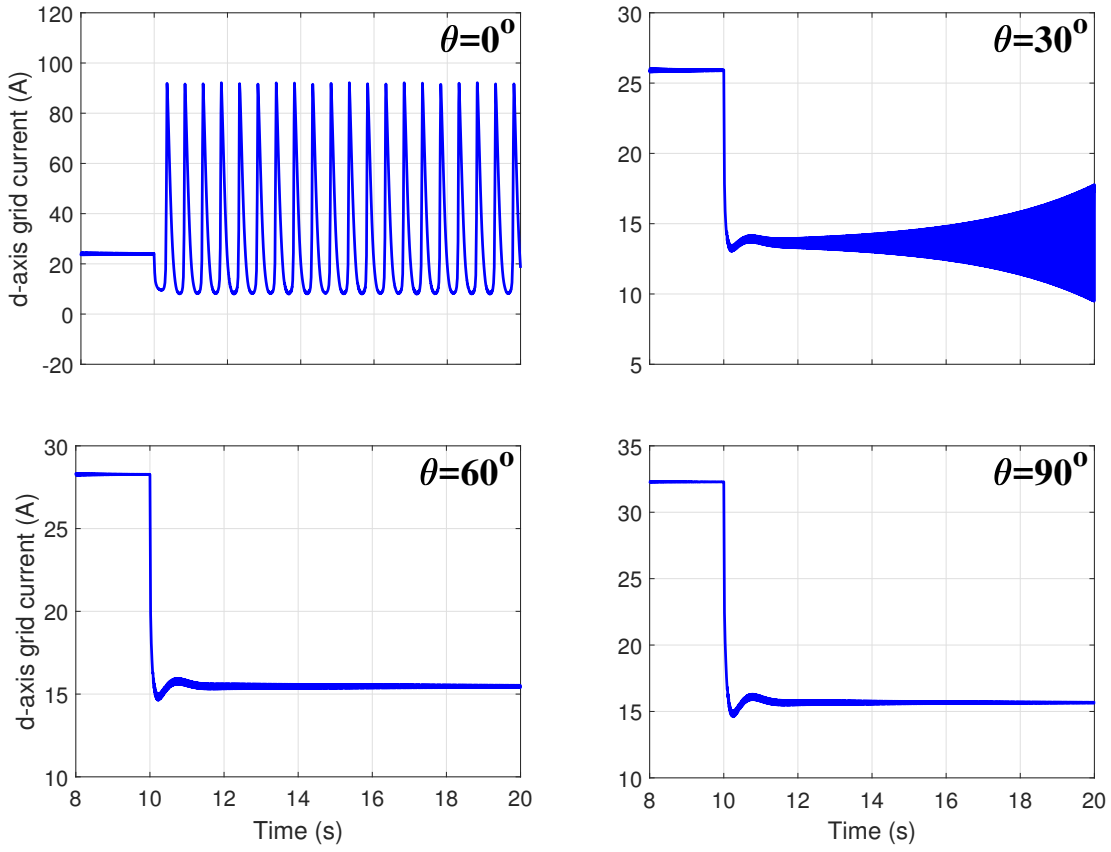

Figure 5.7: d-axis current of grid when the DG units droop coefficients and are increased by six times at s - Grid-Connected Mode (Double-inverter microgrid).

5.2.2 Single-Inverter Microgrid

Simulations are performed to validate the previous analysis of impacts of cross-coupling droop terms on performance of single-inverter grid-connected system studied in Section 4.2. At s, the common load connected at the PCC is increased from 1.8 kW, 1.25 kVar to 4 kW, 2.5 kVar. The d-axis current of the grid when the DG unit operate at is shown in Fig. 5.8. It can be seen that the system is less damped when which is consistent with the previous analysis.

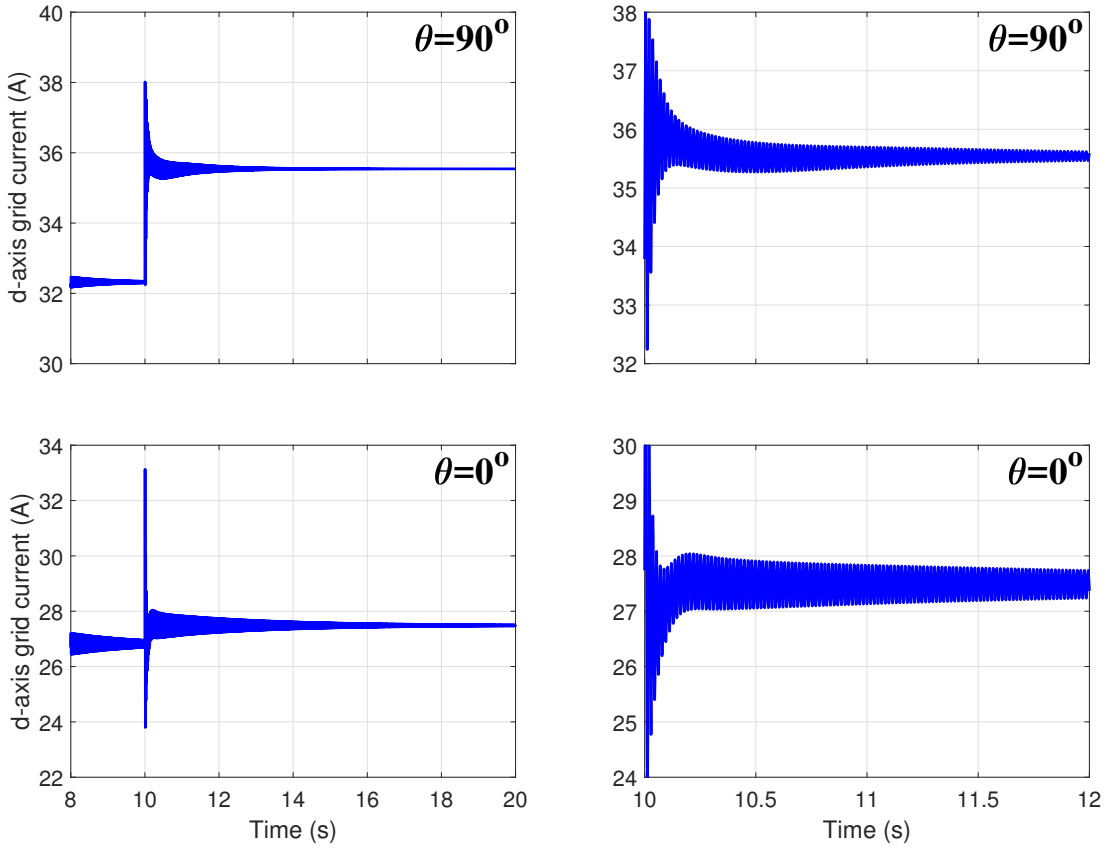

Figure 5.8: Common load increases at s. (Left) d-axis current of grid. (Right) Zoomed-in view of d-axis current of grid.

5.3 Scenario III: Transition Mode

According to the plots of the performance indices in both modes of operation, a mild amount of cross-coupling can be included if seamless transition and efficient operation in both modes are desired. To verify this conclusion, the transformation angle of is selected to add a modest level of cross-coupling, while is adopted to include a large amount of cross-coupling. The output real power of the main grid, the output currents of DG-2 and DG-3, and the voltage magnitudes for both values of when the grid connects at s are depicted in Figs. 5.9, 5.10 and 5.11, respectively. It is observed that transitions from standalone to grid-connected mode is done more smoothly with smaller transients when small amount of cross-coupling is added.

Real-time simulation is also carried out to confirm this conclusion. The output real power of the main grid, the output currents of DG-2 and DG-3, and the voltage magnitudes for are shown in Figs. 5.12, 5.13, and 5.14, respectively.

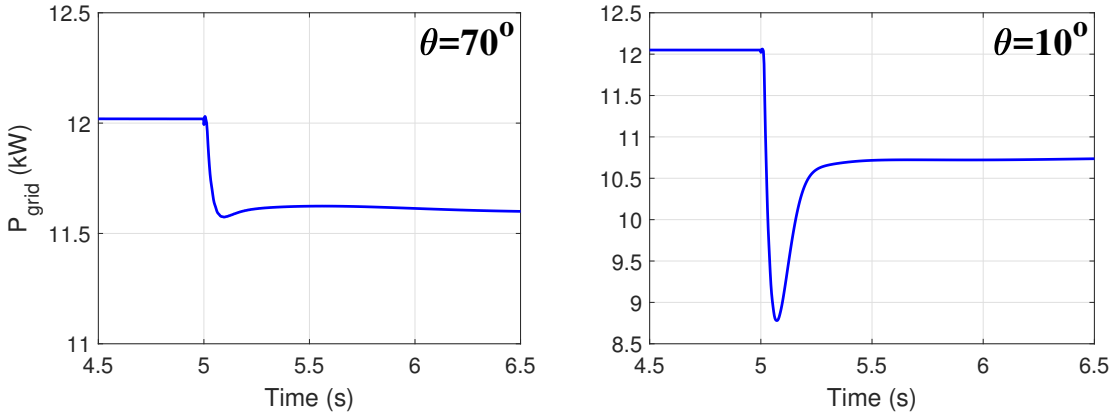

Figure 5.9: Output real power of the grid - Transition Mode

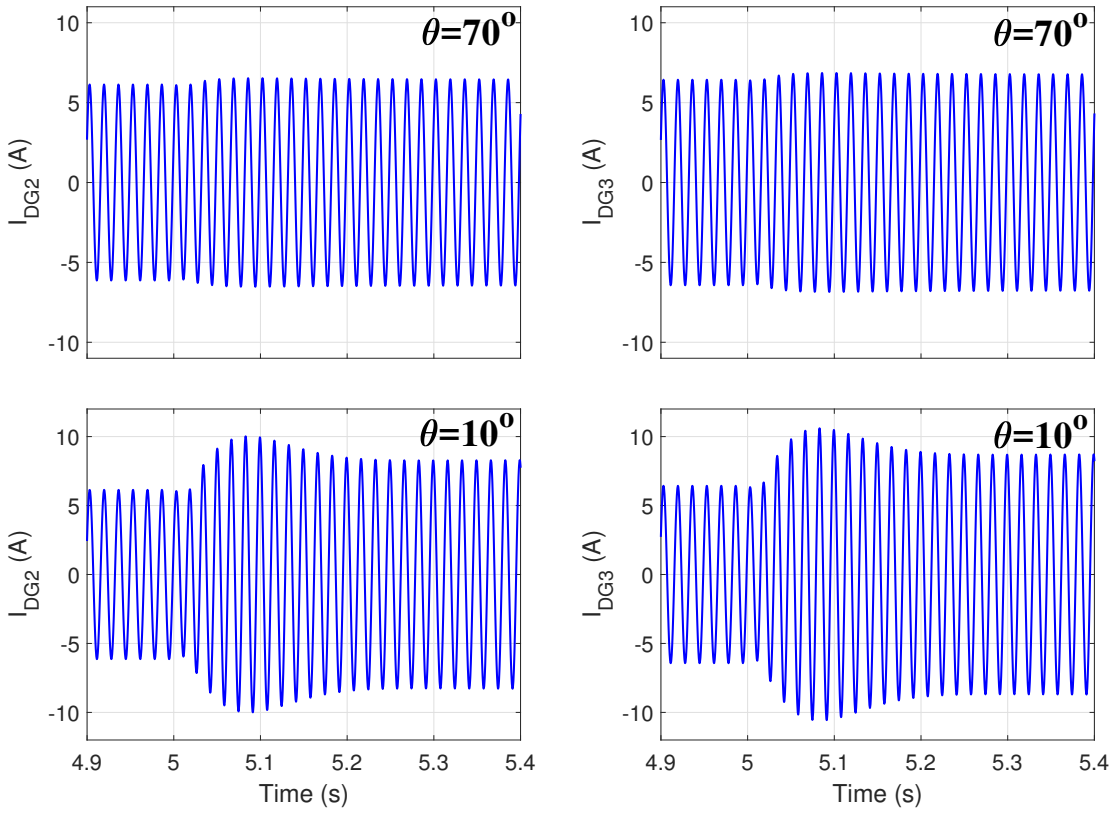

Figure 5.10: Output current of DG-2 and DG-3 (phase-A current) - Transition Mode

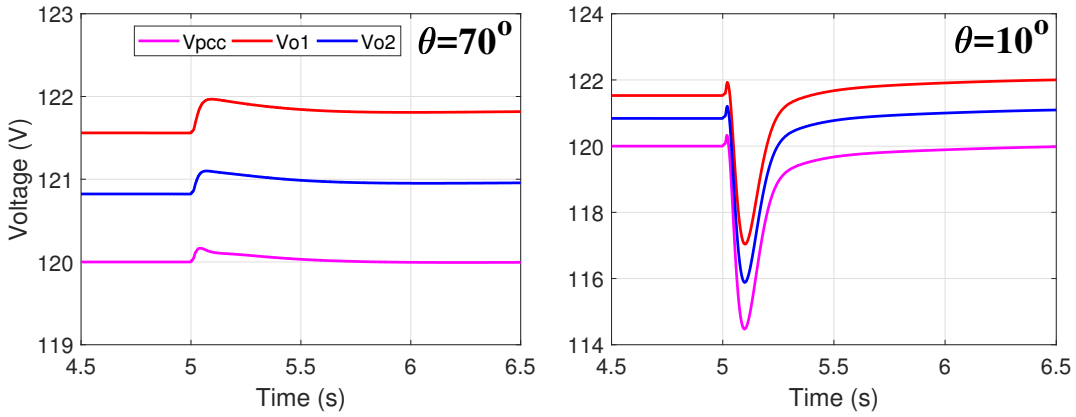

Figure 5.11: Voltage amplitudes - Transition Mode

The RTDS results show good agreement with the PSIM simulation results, shown in Figs. 5.9, 5.10, and 5.11, and they prove that a modest selection of cross-coupling terms guarantees a seamless transition.

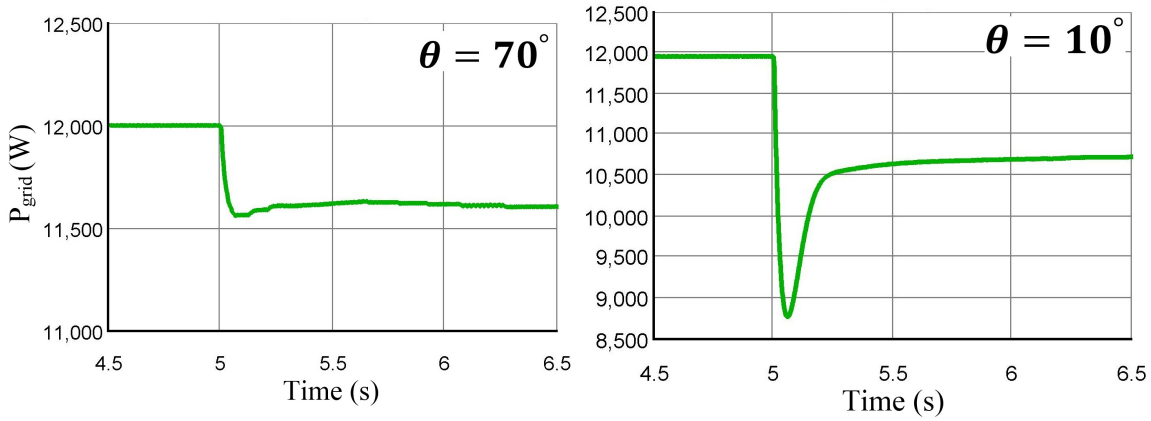

Figure 5.12: Real-time output power of the grid - Transition Mode

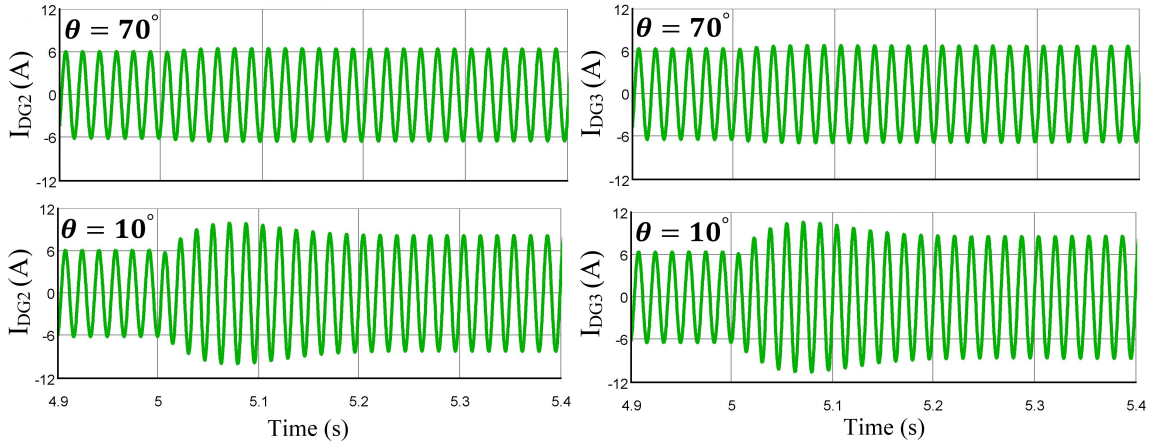

Figure 5.13: Real-time output current of DG-2 and DG-3 (phase-A current) - Transition Mode

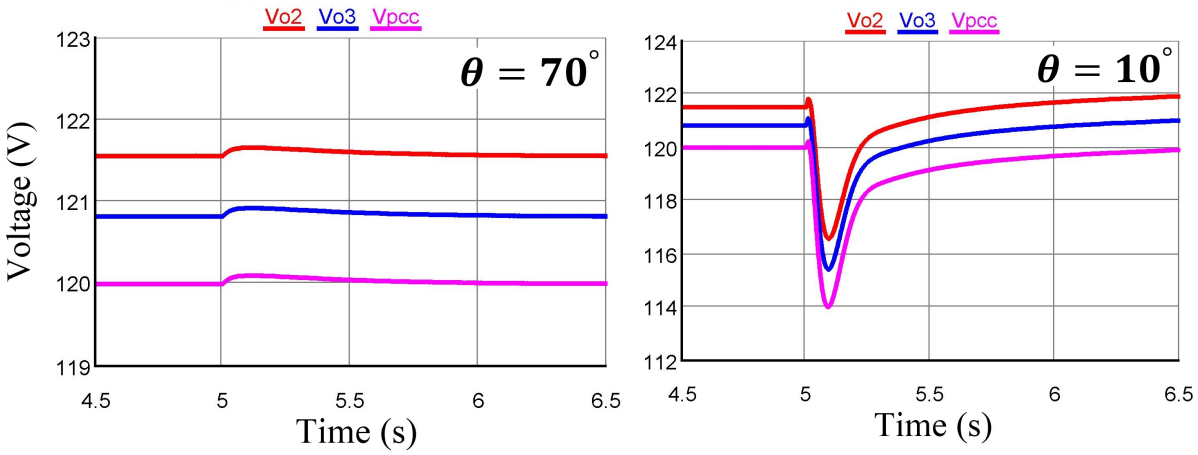

Figure 5.14: Real-time voltage amplitudes - Transition Mode

5.4 Experimental Results

Experiments are carried out on a 1.2 kVA three-phase inverter setup with 400 V dc link and 120 V (rms) line to neutral, 60 Hz grid voltage. Inverter in this setup is connected to the grid through a three-phase LC output filter with =5 mH and =2 F. The grid is emulated with a combination of three-phase Chroma ac source and loads. The controller is implemented on Texas Instrument TMS320F28335 DSP with sampling frequency of 20 kHz and the switching frequency of 10 kHz. The VSM parameters are the same as those used in the simulations. A photograph of the experimental setup is shown in Fig. 5.15.

The emulated grid using the Chroma source and the load shows a rather weak grid with large impedance and some dynamics which are caused by the internal circuitry of the ac source. In the following, the transformation angle is changed in three steps, i.e. 90 , 75 , and 60 . The inverter currents in response to two power commands (increase from 250 W to 750 W followed by decrease to 250 W) are shown in Fig. 5.16, Fig. 5.17, and Fig. 5.18, respectively.

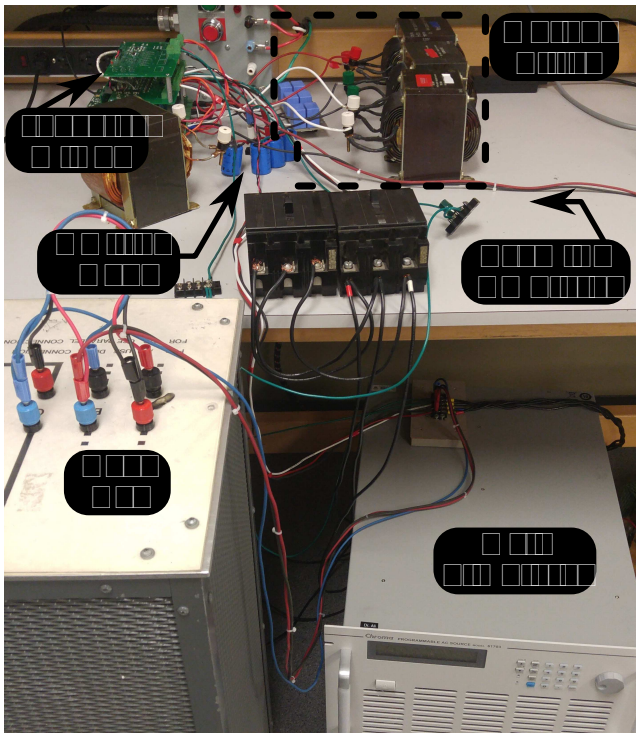

Figure 5.15: A photograph of the experimental setup.

It is clearly observed that the inverter responses become more damped as decreases. This confirms the theoretical developments because the ac source behaves similar to a voltage source which does not follow the conventional grid characteristics. Therefore, the implemented system behaves like a two-machine MG where one of them (i.e. the ac source) is fixed but the other one (i.e. the inverter) is adjusted at different transformation angles.

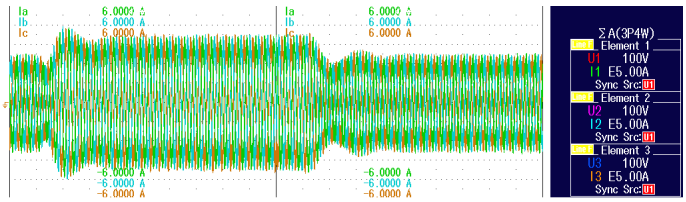

Figure 5.16: Inverter response to real power commands when .

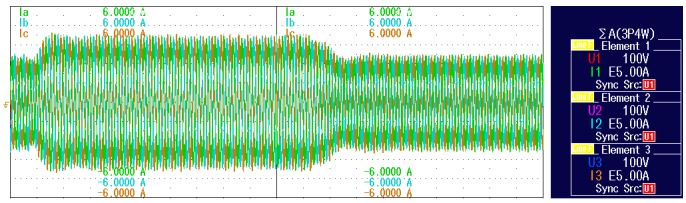

Figure 5.17: Inverter response to real power commands when .

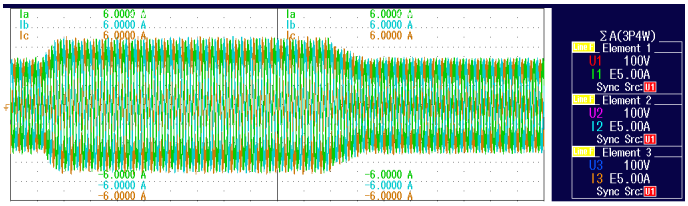

Figure 5.18: Inverter response to real power commands when .

5.5 IEEE 13-Bus System Case Study

The effectiveness of the proposed scheme and the study results are further verified by simulating a modified IEEE 13-bus system in both operational modes. The test system is shown in Fig. 5.19 and the complete line and load parameters of that system are given in tables A.1 and A.2. The autonomous 208 V/60 Hz three-phase MG shown in Fig. 5.19 comprises four inverters with ratings of kVA and kVA.

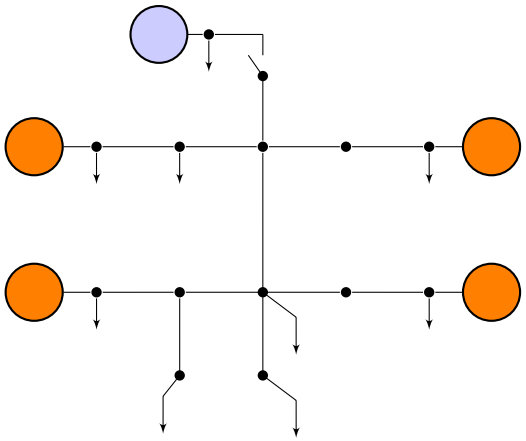

Figure 5.19: Modified IEEE 13-bus distribution system

The inverters' filter and control parameters are the same as used in Section 4.1 except for the droop coefficients which are selected based on the new ratings of the DG units as

–

, ,

–

, .

5.5.1 Scenario I: Standalone Mode

The VREI versus is shown in Fig. 5.20 where the output voltages of all inverters and the load voltages are considered. It can be noted that the voltage profile of the system is not strongly affected by the amount of cross coupling despite the slight improvement for small values of . The plots of PLII and PSEI/QSEI in percentage versus are illustrated in Fig. 5.20. It can be observed that the system efficiency improves as the angle decreases all the way to about 50 and the power sharing indices are similar to those of the standalone MG considered in Section 4.1. .

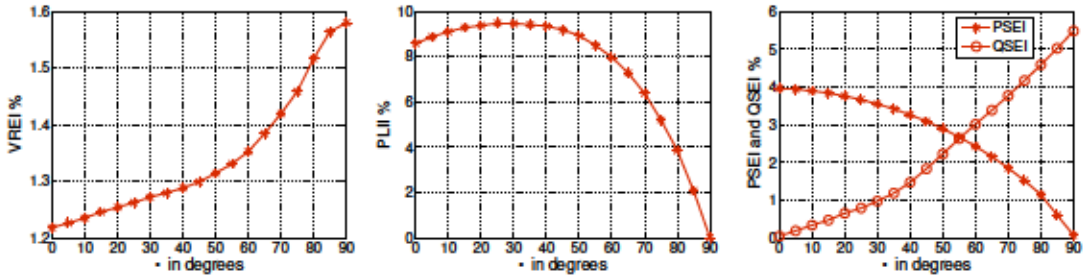

Figure 5.20: VREI, PLII and (PSEI, QSEI) - Standalone Mode

Simulation is performed in PSIM software to examine the impacts of cross coupling on system transient response when DG3 together with load 611 connect at $t = 3$ s and when load 692 connects at $t = 4.5$ s. The output apparent powers of DG2 and DG3 are illustrated in Fig. 5.21. It is observed that the system damping is significantly improved when $\theta = 0°$ which agrees with the result obtained for the simple case system.

5.5.2 Scenario II: Grid-Connected Mode

This section aims to evaluate the performance of the test system shown in Fig. 5.19 when it operates in grid-connected mode. The SG modeling the main grid is rated at $S = 50$ kVA and its control parameters are the same as used in Section 4.2 except for the droop coefficients which are selected based on the new rating of the grid as $k_f = S/\Delta f = 50000/2 = 25 \times 10^3$, $k_v = S/\Delta V = 50000/12\sqrt{2} = 2946$. The transformation angle of the inverters is equal and varied from 0° to 90°.

The plot of VREI as a function of θ is depicted in Fig. 5.22 for the entire load bus voltages. As can be seen, the system voltage profile is not significantly influenced by θ in the range $(60° - 90°)$ and it shows degradation as θ decreases to 0°.

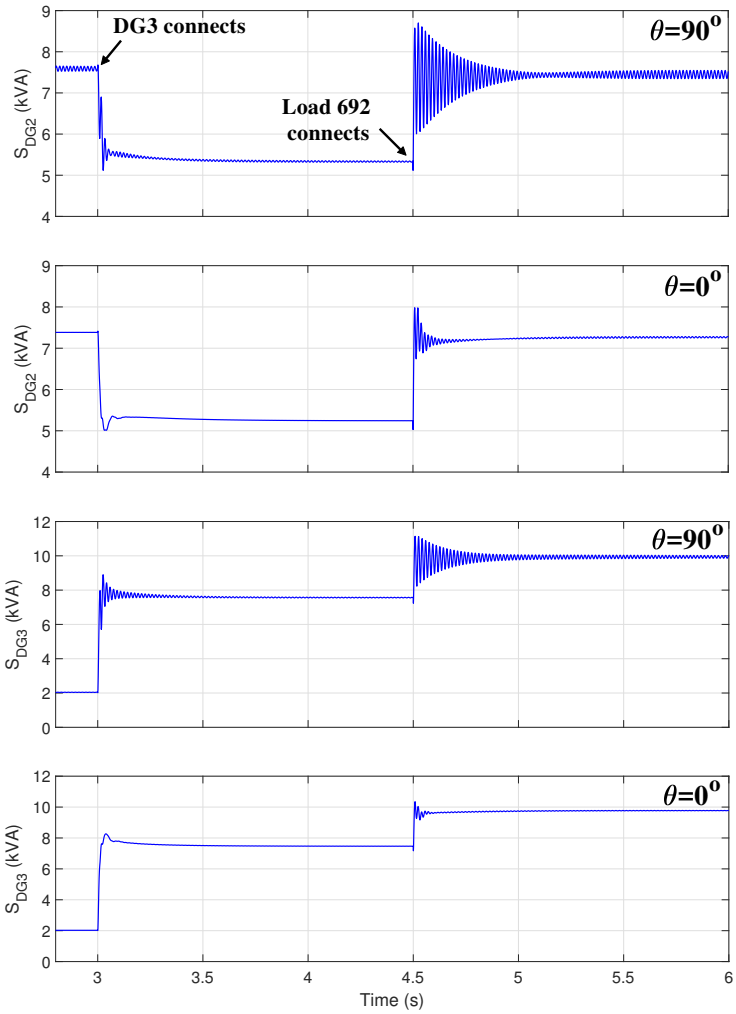

Figure 5.21: Output apparent power of DG2 and DG3 - Standalone Mode

The graphs of PLII and PSEI/QSEI versus are shown in Fig. 5.22. It can be observed that the PLII increases up to about 30% when decreases from 90 to 70 degrees. It then decreases to zero when is further decreased to about 45 degrees. For smaller than 45 degrees, the PLII keeps decreasing to negative numbers which indicates that the amount of transmission losses increases. When the MG operates based on the reverse droop principle, the transmission losses are maximum value at around four times the amount of losses when

it operates at conventional droop angle of 90 degrees. It can be noted from PSEI/QSEI curve that similar observations as those of the sharing indices of the grid-connected MG in Section 4.2 are obtained.

In another simulation, the grid connects at $t = 5$ s, and the load connected at bus 634 is increased from 2 kW, 3 kVar to 7 kW, 6 kVar at $t = 8$ s. The voltage magnitudes of some buses when the DG units operate at $\theta = (90°, 45°, 0°)$ are illustrated in Fig. 5.23. It is noted that the voltage magnitudes at $\theta = (45°, 0°)$ are further apart from the nominal value compared to those at $\theta = 90°$. It can also be seen that the transition from standalone to grid-connected mode is done more smoothly when $\theta = 90°$. In addition, the system transient response when the load changes is significantly improved which is consistent with the previous analysis .

5.5.3 Scenario III: Transition Mode

The transition performance of the test system for the selection of large and small amounts of cross-coupling is studied here. Two transformation angles of $\theta = 70°$ (modest coupling) and $\theta = 10°$ (large coupling) are considered.

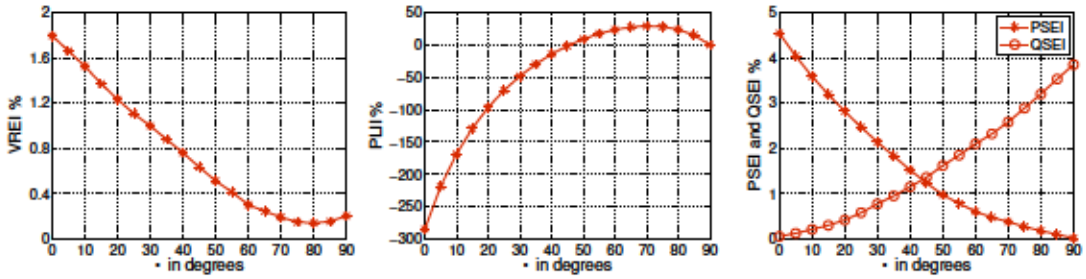

Figure 5.22: VREI, PLII and (PSEI, QSEI) - Grid-connected Mode

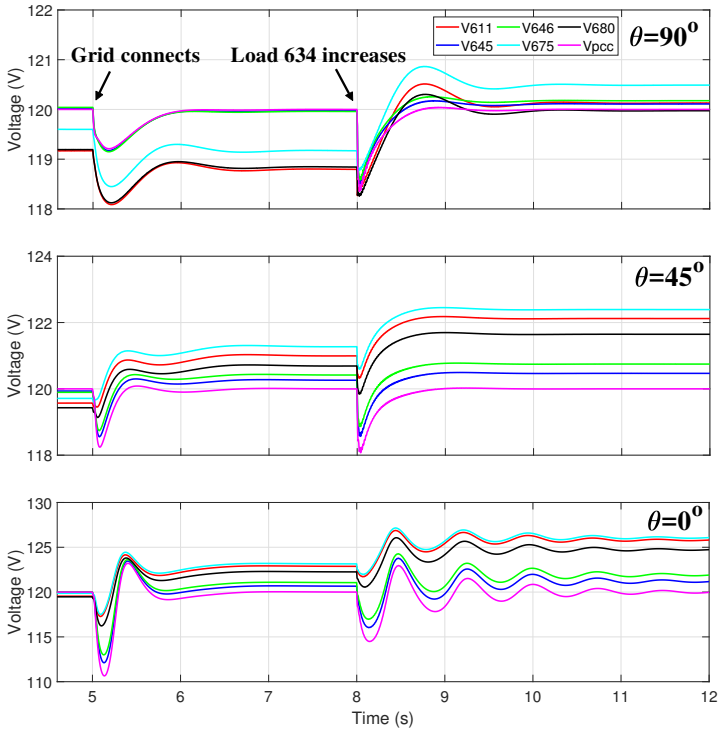

Figure 5.23: Voltage amplitude - Grid-connected Mode

The output currents of DG-2 and DG-3 and the voltage amplitudes of some buses for both values of when the grid connects at s are depicted in Figs. 5.24 and 5.25, respectively. It is observed and confirmed that the transition from standalone to grid-connected mode is done more smoothly when smaller amount of cross-coupling is added.

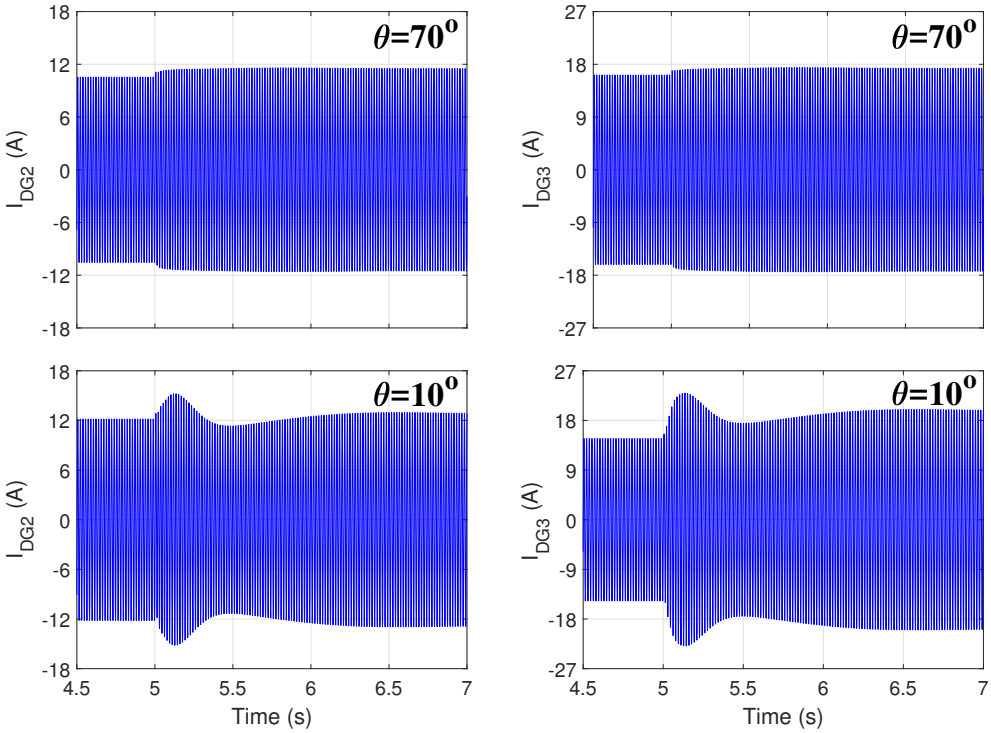

Figure 5.24: Output current of DG-2 and DG-3 (phase-A current) - Transition Mode

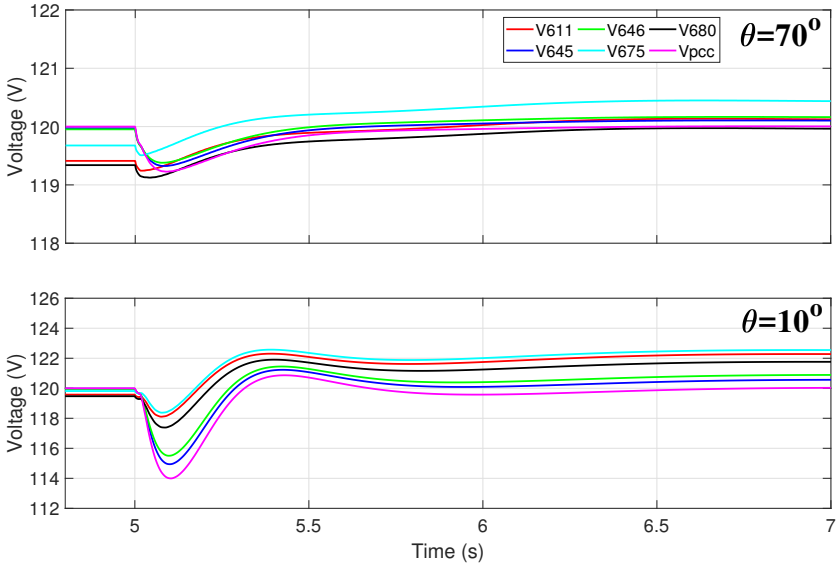

Figure 5.25: Voltage amplitude - Transition Mode

5.6 Summary

In this chapter, the MG system under consideration is simulated in both modes of operation and during transition between them as well. Results obtained from different platforms that include computer simulations, real-time simulations, and experimental results are presented. It can be concluded that these detailed results validate the derivations given in the previous chapter. In addition, real-time simulation results show perfect agreement with the results obtained from PSIM software. The study conclusions are further verified by simulating a realistic test system. For this purpose, a modified IEEE 13-bus system is simulated in PSIM for a broader range of system disturbances. The system responses in all modes of operation are very consistent with the previous derivations.

CHAPTER VI

OPTIMIZATION OF CROSS-COUPLING DROOP TERMS

For the sake of simplicity of analysis, identical amounts of cross-coupling have been assumed for all DERs in the MG in our study of previous chapters. In general, the trade-offs can be further optimized by allowing different DERs to have different levels of cross-coupling droop terms. This will entail a multi-variable nonlinear problem which needs to combine several cost functions. Our approach will be to define an overall cost function which includes a weighted sum of the performance indices. Particle swarm optimization (PSO) will be used to obtain the optimum parameters. Attempts will be made to derive general guidelines as how to set different levels of cross-coupling terms in the study MG system.

6.1 Overview of Particle Swarm Optimization

Particle swarm optimization is a population-based stochastic optimization algorithm proposed by Kennedy and Eberhart [27] in 1995. The PSO was inspired by the social behavior associated with birds flocking or fish schooling [51]. The PSO works with a population (swarm) of potential solutions (particles). Every particle moves in the search space with a direction that is determined by its own best known position in the search space as well as the entire group's best known position. In PSO, the system is initialized

with a population of random solutions and every candidate solution is assigned a random velocity. The particles are then flown through the problem space. The velocity of each particle is dynamically updated based on the flying experiences of its own and those of its neighbors [23]. Mathematically, assume a population of particles, each particle is an -dimensional real-valued vector, where represents the number of optimized parameters. Every particle is associated with a position vector which is a potential solution for the problem. Let the best previous position found by particle in the search space be denotaed by , and the best position that the particles in the neighborhood of particle have ever found is . At every iteration step ( ), the velocity vector of the th particle is updated using the following equation

(6.1)

where is the inertia weight used to control global exploration and local exploitation of the particles, and are two random numbers which are uniformly distributed in the interval [0, 1], and and are positive constants representing the particle's confidence in itself (cognition) and in the swarm (social behavior), respectively. Therefore, the second term represents the cognitive part of the PSO algorithm where the particle modifies its velocity based on its own thinking and experience, and the third term represents the social part of PSO where the particle changes its velocity based on the adaptation of the social-psychological knowledge. The position vector associated with the th particle changes based on the updated velocity vector as follows

(6.2)

This iterative process will continue until a stop criterion like the maximum number of iterations or a sufficiently good cost funcion value is reached. PSO has been applied to different power system problems because of its reliability and simplicity, and it has very few parameters to adjust [7, 11, 35, 52].

6.2 Definition of Objective Function

The autonomous and grid-connected MGs studied in Sections 4.1 and 4.2, respectively, are considered. The optimized parameters in both operation modes are the transformation angles which specify the amount of cross-coupling in the iVSM controllers of the DG units. The objective function is composed of a weighted sum of the normalized performance indices and is given as

(6.3)

The problem constrains are as follows

(6.4)

(6.5)

(6.6)

(6.7)

where and are the minimum and maximum allowable voltage magnitudes.

The overall optimization problem can be formulated as

Subject to

Constraints given in (6.4)-(6.7).

In this study, PSO is used to solve this optimization problem by obtaining the optimal levels of cross-coupling which are determined by the controller parameter . General guidelines as how to set different levels of cross-coupling terms in the studied MG are derived. Five different scenarios in both modes of operation are considered as follows.

6.3 Standalone Mode

The islanded MG in Section 4.1 is considered under the following scenarios for this study.

6.3.1 Scenario I: Change length of one line

In this scenario, the two DG units are assumed to have the same capacity of 2 kVA and identical local loads of 0.4 kW and 0.3 kVar. The length of line 2 is fixed at 1 km while the length of line 1 is increased from 0.1 km to 4.3 km. The optimal values of and are provided in Table 6.1 below. It is observed that as line 1 length increases, the optimal solution tends toward smaller angle values.

6.3.2 Scenario II: Change length of all lines

The two DG units are assumed to have the same rating of 2 kVA and identical local loads of 0.4 kW and 0.3 kVar. The lengths of line 1 and line 2 are increased equally from 0.1 km to 4.3 km. The optimal values of and are provided in Table 6.2. It can be noted that as the lengths of lines increase, the optimal values of and decrease.

Table 6.1: Change of line 1 length

Line 1 **(km)**	**(deg)**
0.1	27, 24
0.7	22, 23
1.3	19, 18
1.9	13, 15
2.5	9, 10
3.1	6, 7
3.7	4, 4
4.3	3, 2

6.3.3 Scenario III: Change R/X ratio of all lines

The impact of lines R/X-ratio on optimum amounts of cross-coupling is also investigated. The two lines have the same length of 1 km, and the DG units have ratings and local loads that are identical to those in the two previous scenarios. The lines R/X-ratio is decreased equally from 10 to 0.1. The optimized parameters and for every case are given in Table 6.3.

Table 6.2: Change of line 1 and line 2 lengths

Line 1 and 2 **(km)**	**(deg)**
0.1	21, 21
0.7	17, 17
1.3	14, 15
1.9	9, 9
2.5	6, 5
3.1	3, 4
3.7	1, 1
4.3	0, 0

It can be seen that the optimal level of cross coupling is fixed under the same operating conditions regardless of the lines R/X ratio as long as the lines are resistive (R/X 1). However, inductive lines (R/X 1) require higher level of cross coupling (smaller angles) compared to resistive lines.

6.3.4 Scenario IV: Change ratings of all DG units

The impact of DG units capacity on the optimal level of cross-coupling is investigated. Identical lines with R/X=7.7 and 1 km-length are considered. The ratings of DG1 and DG2 are increased equally from 1 kVA to 10 kVA, and the local loads are also increased in proportion to the DGs ratings. The optimal solutions are given in Table 6.4. It is noticed that the optimized parameters and increase as the size of the DG units increases.

Table 6.3: Change of lines R/X-ratio

Lines R/X-ratio	**(deg)**
10	18, 18
7.7	18, 18
6	18, 18
4	18, 18
2	18, 18
0.85	15, 15
0.1	8, 7

Table 6.4: Change of ratings of both DG units

(kVA)	Local loads	**(deg)**
1	0.4, 0.3	3, 3
2	0.8, 0.6	8, 8
4	1.6, 1.2	23, 23
6	2.4, 1.8	29, 29
8	3.2, 2.4	35, 35
10	4.0, 3.0	39, 39

6.3.5 Scenario V: Change rating of one DG unit

This scenario is similar to the previous one. However, only the size of DG1 is increased from 1 kVA to 10 kVA. In addition, its local load is increased proportionally. The rating of

DG2 is fixed at 2 kVA, and its local load remains unchanged (0.8 kW and 0.6 kVar). The effect of varying DG1 capacity on the optimal amount of cross-coupling is investigated. The optimal solutions are summarized in Table 6.5. It is seen that the optimized parameters and increase as the size of DG1 increases.

Table 6.5: Change of rating of DG1

(kVA)	Local load 1	**(deg)**
1	0.4, 0.3	1, 2
2	0.8, 0.6	8, 8
4	1.6, 1.2	11, 17
6	2.4, 1.8	14, 23
8	3.2, 2.4	24, 32
10	4.0, 3.0	29, 39

6.3.6 Summary of Results for Standalone Case

According to the results obtained in scenarios I-V, the following conclusion for the standalone MG under study can be derived

1. If the lengths of lines increase, the MG becomes weaker. Therefore, the optimal angle values decrease to improve the system stability (tables 6.1 and 6.2).

2. For resistive lines (R/X), the optimal level of cross coupling is not affected by the lines R/X-ratio. However, if the lines become more inductive (R/X 1), the required level of cross coupling should be increased (angles decrease) for stability issues (table 6.3).

3. As the DG units capacity goes down, it is recommended to increase the level of cross coupling by using smaller values of the transformation angles in order to improve system stability. Low level of cross-coupling (larger angles) should be adopted for systems with large DG units (tables 6.4 and 6.5). This will improve system efficiency without causing a noticeable degradation in stability.

6.4 Grid-Connected Mode

The grid-connected MG in Section 4.2 is studied under the same five scenarios considered in Section 6.3 for the islanded MG. In a similar way, we consider three generators where one of them is selected to model the main grid while the other two are selected to operate as inverter-based DERs to represent a grid-connected MG with two sources. DG1 is selected to emulate the main grid by modifying its controller parameters and setting its

transformation angle to 90 in this study. The rating of the main grid (20 kVA) and the length of line 1 (2 km) that connects the MG to the main grid remain unchanged in all scenarios.

6.4.1 Scenario I: Change length of one line

In this scenario, the influence of changing the length of line 2 on the optimum amount of cross coupling is examined. the two DG units are assumed to have the same capacity of 2 kVA and identical local loads of 0.4 kW and 0.3 kVar. The length of line 2 which connects DG2 to the PCC is increased from 0.1 km to 4.3 km while the length of line 3 remains fixed at 1 km. The optimal values of and (transformation angles of DG2 and DG3, respectively) are given in Table 6.6.

Table 6.6: Change of line 2 length

Line 2 **(km)**	**(deg)**
0.1	73, 69
0.7	74, 75
1.3	74, 76
1.9	75, 79
2.5	75, 80
3.1	75, 82
3.7	76, 84
4.3	76, 86

It is seen that the optimal solution moves toward larger values as line 2 length increases.

6.4.2 Scenario II: Change length of all lines

The two DG units are assumed to have the same capacity of 2 kVA and identical local loads of 0.4 kW and 0.3 kVar. The optimal solutions when the lengths of line 2 and line 3 are increased equally from 0.1 km to 4.3 km are provided in Table 6.7. It can be noted that as the lengths of lines increase, the optimal values of and also increase.

Table 6.7: Change of line 1 and line 2 lengths

Line 1 and 2 **(km)**	**(deg)**
0.1	72, 72
0.7	74, 74
1.3	76, 76
1.9	77, 77
2.5	79, 79
3.1	80, 80
3.7	83, 83
4.3	85, 85

6.4.3 Scenario III: Change R/X ratio of all lines

In this scenario, the two lines have the same length of 1 km, and the DG units have ratings and local loads that are similar to those in the two previous scenarios. The lines R/X-ratio is decreased equally from 10 to 0.1. The optimized parameters and for every case are summarized in Table 6.8.

It can be concluded that the optimal level of cross coupling is fixed under the same operating conditions regardless of the lines R/X ratio as long as the lines have high R/X-ratio. However, as the lines R/X-ratio approaches 1, the optimal amount of cross coupling decreases (angles increase). Moreover, as the lines become more inductive (R/X 1), the optimal values of and keep increasing and tend toward ninety degrees.

Table 6.8: Change of lines R/X-ratio

Lines R/X-ratio	**(deg)**
10	75, 75
7.7	75, 75
6	75, 75
4	75, 75
2	77, 77
0.85	82, 82
0.1	86, 86

6.4.4 Scenario IV: Change ratings of all DG units

The impact of the MG size on the optimal level of cross-coupling is investigated. The ratings of DG2 and DG3 are increased equally from 1 kVA to 10 kVA, and their local loads are also increased in proportion to the DGs ratings. The optimal solutions are provided in Table 6.9. It is noted that the values of the optimized parameters increase as the size of the DG units increases.

6.4.5 Scenario V: Change rating of one DG unit

This scenario is similar to the previous one. However, only the size of DG2 is increased from 1 kVA to 10 kVA. Its local load is increased proportionally as well. The capacity of DG3 is fixed at 2 kVA, and its local load remains unchanged (0.8 kW and 0.6 kVar). The optimal solutions when the capacity of DG2 is varied are summarized in Table 6.10. It can be noticed that the optimized parameters and increase as the size of DG2 increases.

Table 6.9: Change of ratings of both DG units

(kVA)	Local loads	**(deg)**
1	0.4, 0.3	67, 67
2	0.8, 0.6	73, 73
4	1.6, 1.2	77, 77
6	2.4, 1.8	81, 81
8	3.2, 2.4	83, 83
10	4.0, 3.0	86, 86

Table 6.10: Change of rating of DG2

(kVA)	Local load 2	**(deg)**
1	0.4, 0.3	72, 69
2	0.8, 0.6	73, 73
4	1.6, 1.2	75, 78
6	2.4, 1.8	77, 82
8	3.2, 2.4	78, 84
10	4.0, 3.0	80, 86

6.4.6 Summary of Results for Grid-Connected Case

Based on the results obtained in scenarios I-V, the following guidelines for the grid-connected MG under consideration can be derived

1. If the lengths of lines increase, the main grid becomes weaker. As a result, the values of the optimal angles increase in order to improve the system stability (tables 6.6 and 6.7).

2. For resistive lines, the optimal level of cross coupling is not affected by the lines R/X-ratio. Nevertheless, if this ratio decreases and approaches 1, the optimized angles will increase. This fact is more emphasized as the lines become more inductive (R/X 1) (table 6.8).

3. As the DG units capacity goes down, it is recommended to increase the level of cross coupling by using smaller values of the transformation angles in order to reduce line

losses without compromising stability. Low level of cross-coupling (larger angles) must be adopted for systems with large DG units in order to improve the system stability (tables 6.9 and 6.10).

6.5 Summary

In this chapter, general guidelines that can be used to specify the optimal amounts of cross-coupling droop terms in the study MG system are derived. PSO algorithm is used to obtain the optimum control parameters. The cost function is defined by combining several performance indices which results in a multi-variable nonlinear problem. Impacts of variations in the study MG size and lines characteristics (R/X-ratio and length) on the optimal level of cross coupling have been investigated. Table 6.11 provides a summary of the general rules that can be applied to the double-inverter MG system considered in this dissertation for both modes of operation.

Table 6.11: Impacts of lines characteristics and MG size on optimal parameters ( )

Scenario	$_i$ **(Standalone)**	$_i$ **(Grid-connected)**
Increase length of line between the DG and the PCC (one or two of them)	Both decrease	Both increase while the one whose line length is increased changes less
Decrease lines R/X-ratio	Both unaffected for resistive lines (R/X 1) and they both decrease for inductive lines (R/X 1)	Both unaffected for resistive lines (R/X 1) and they both increase for inductive lines (R/X 1)
Increase rating of both DG units	Both increase	Both increase
Increase rating of one DG	Both increase while of the other DG being more affected	Both increase while of the other DG being more affected

CHAPTER VII

SUMMARY AND CONCLUSION, AND FUTURE WORK

7.1 Summary and Conclusion

This dissertation presents a comprehensive study of the impacts of adding cross-coupling droop terms on performance of power system with DERs. Different performance aspects including stability, stability robustness, transmission power loss, voltage profile, and power sharing in both modes of operation of an MG are investigated. The conclusions of this study are as follows.

1. Adopting the conventional droop characteristics without cross-coupling terms, i.e. and , by the DG units in a grid-connected MG guarantees the highest level of stability.

2. In a grid-connected MG, adding a small amount of cross-coupling terms can improve the system efficiency (i.e. reduce the transmission losses) significantly (30%-60% in our studies systems) without causing a noticeable degradation in stability.

3. In an isolated MG, adding a large portion of cross-coupling terms up to the extreme point ( ) will both improve system stability and efficiency.

If seamless and efficient operation in both standalone and grid-connected are desired, it is recommended to include a mild amount of cross-coupling, i.e. . This

will offer a desirable trade-off between system stability (in both modes of operation) and efficiency. For a continued operation in islanded MG or for a permanently isolated MG, smaller values of can be selected to improve both the stability and efficiency.

A study for further optimizing the trade-offs that are obtained is also presented. General guidelines to set different levels of cross-coupling terms in the study system are introduced. The conclusions of this study are as follows.

1. It is recommended to increase the amount of cross-coupling in the islanded MG and to decrease it in the grid-connected MG if longer distribution lines are used. This avoids stability issues.

2. The level of cross-coupling should be increased in the standalone MG and decreased in the grid-connected system if the lines are more inductive. This avoids stability issues.

3. It is recommended to decrease the amount of cross-coupling in the autonomous MG as the size of the DG units increases. This will improve system efficiency without compromising stability. However, in the grid-connected scenario, the level of cross-coupling needs to be reduced as the MG size increases to avoid stability issues.

7.2 Future Work

The future work to be completed is given as follows.

1. Simplify the mathematical model for islanded inverters. Develop a linear time-invariant (LTI) model of the system whose control parameters can be designed optimally.

   Motivation: Our existing model is efficient for stability and sensitivity analysis. However, due to large number of control and system parameters, it is desired to derive an LTI model that can be used for optimal design. Identifying and formulating simplifications to the existing Jacobian model to reduce the computational aspects in a large MG can be the topic for a future work.

2. Apply to renewable-based DERs.

   Motivation: In analyzing the impacts of cross-coupling droop terms on performance of power systems that contain inverter-based resources in this dissertation, an ideal (stiff) DC side is assumed for the inverters. In the renewable systems, two approaches may be considered to implement the droop characteristics: 1) without adding a battery energy storage (BES) and 2) with the aid of a BES. In the first case, the PV control system must be properly adjusted to implement the droop characteristics, which necessarily implies a certain level of deloading. In the second case, a deloading is not necessary or may be reduced. Establishing a trade-off between the BES size and the level of deloading is a particularly interesting topic for future research.

3. BES-based distribution system stabilizer

Motivation: Increased integration of renewable energy resources such as PV and wind energy can cause voltage and frequency fluctuations due to their intermittent nature. Consequently, power quality degrades specially in weak grid conditions such as an islanded microgrid. Battery energy storage (BES) systems are being considered as a promising solution to alleviate these challenges. A BES system equipped with the proposed droop characteristics can be used to improve the stability of an existing distribution system as it is proved in this dissertation. Detailed study of this subject is another topic of interest.

REFERENCES

[1] AFDC, *Laws and Incentives*, 2017, https://www.afdc.energy.gov/laws/key_legislation.

[2] J. C. Boemer, M. Gibescu, and W. L. Kling, "Dynamic models for transient stability analysis of transmission and distribution systems with distributed generation: an overview," *PowerTech, IEEE Bucharest*. IEEE, 2009, pp. 1–8.

[3] M. Bollen and F. Hassan, *Integration of Distributed Generation in the Power System*, Wiley, New Jersey, 2011.

[4] K. D. Brabandere, B. Bolsens, J. V. den Keybus, A. Woyte, J. Driesen, and R. Belmans, "A Voltage and Frequency Droop Control Method for Parallel Inverters," *IEEE Transactions on Power Electronics*, vol. 22, no. 4, July 2007, pp. 1107–1115.

[5] Y. Cao, Z. Li, Z. Lu, Z. Chen, and X. Liu, "A full-dq based adaptive virtual impedance compensation in virtual power frame for droop-controlled parallel inverters under unbalanced conditions," *IECON 2017 - 43rd Annual Conference of the IEEE Industrial Electronics Society*, Oct 2017, pp. 8710–8715.

[6] S. J. Chapman, *Electric Machinery and Power System Fundamentals*, McGraw-Hill, New York, 2002.

[7] C. Chen, L. Xiao, S. Duan, and J. Chen, "Cooperative Optimization of Electric Vehicles in Microgrids Considering Across-Time-and-Space Energy Transmission," *IEEE Transactions on Industrial Electronics*, vol. 66, no. 2, Feb 2019, pp. 1532–1542.

[8] Y. Chen, J. M. Guerrero, Z. Shuai, Z. Chen, L. Zhou, and A. Luo, "Fast Reactive Power Sharing, Circulating Current and Resonance Suppression for Parallel Inverters Using Resistive-Capacitive Output Impedance," *IEEE Transactions on Power Electronics*, vol. 31, no. 8, Aug 2016, pp. 5524–5537.

[9] E. Coelho, P. Cortizo, and P. Garcia, "Small-signal stability for parallel-connected inverters in stand-alone AC supply systems," *IEEE Transactions on Industry Applications*, vol. 38, no. 2, 2002, pp. 533–542.

[10] EIA, *Energy Explained*, 2017, https://www.eia.gov/energyexplained/index.cfm?page=electricity_environment.

[11] A. Elgammal and M. El-Naggar, "Energy management in smart grids for the integration of hybrid wind–PV–FC–battery renewable energy resources using multi-objective particle swarm optimisation (MOPSO)," *The Journal of Engineering*, vol. 2018, no. 11, 2018, pp. 1806–1816.

[12] EPA, *About the U.S. Electricity System and its Impact on the Environment*, 2017, https://www.epa.gov/energy/about-us-electricity-system-and-its-impact-environment.

[13] W. R. E. M. T. Force, WECC PV *power plant dynamic modeling guide*, 2014, https://www.wecc.biz/Reliability/WECC%20Solar%20Plant%20Dynamic%20Modeling%20Guidelines.pdf.

[14] J. D. Glover, M. S. Sarma, and T. Overbye, *Power System Analysis & Design, SI Version*, Cengage Learning, 2012.

[15] J. M. Guerrero, L. G. De Vicuna, J. Matas, M. Castilla, and J. Miret, "A wireless controller to enhance dynamic performance of parallel inverters in distributed generation systems," *IEEE Transactions on power electronics*, vol. 19, no. 5, 2004, pp. 1205–1213.

[16] J. M. Guerrero, L. G. de Vicuna, J. Matas, M. Castilla, and J. Miret, "Output impedance design of parallel-connected UPS inverters with wireless load-sharing control," *IEEE Transactions on Industrial Electronics*, vol. 52, no. 4, Aug 2005, pp. 1126–1135.

[17] J. M. Guerrero, J. Matas, L. G. de Vicuna, M. Castilla, and J. Miret, "Decentralized Control for Parallel Operation of Distributed Generation Inverters Using Resistive Output Impedance," *IEEE Transactions on Industrial Electronics*, vol. 54, no. 2, April 2007, pp. 994–1004.

[18] M. Hassan and M. Abido, "Optimal design of microgrids in autonomous and grid-connected modes using particle swarm optimization," *IEEE Transactions on Power Electronics*, vol. 26, no. 3, 2011, p. 755.

[19] N. Hatziargyriou, "Microgrids [guest editorial]," *IEEE Power and Energy Magazine*, vol. 6, no. 3, 2008, pp. 26–29.

[20] N. Hatziargyriou, H. Asano, R. Iravani, and C. Marnay, "Microgrids," *IEEE Power and Energy Magazine*, vol. 5, no. 4, July 2007, pp. 78–94.

[21] N. Hatziargyriou, N. Jenkins, G. Strbac, J. P. Lopes, J. Ruela, A. Engler, J. Oyarzabal, G. Kariniotakis, A. Amorim, et al., "Microgrids–large scale integration of microgeneration to low voltage grids," *CIGRE C6-309*, 2006.

[22] J. He, Y. W. Li, J. M. Guerrero, F. Blaabjerg, and J. C. Vasquez, "An Islanding Microgrid Power Sharing Approach Using Enhanced Virtual Impedance Control Scheme," *IEEE Transactions on Power Electronics*, vol. 28, no. 11, Nov 2013, pp. 5272–5282.

[23] S. L. Ho, S. Yang, G. Ni, E. W. C. Lo, and H. C. Wong, "A particle swarm optimization-based method for multiobjective design optimizations," *IEEE Transactions on Magnetics*, vol. 41, no. 5, May 2005, pp. 1756–1759.

[24] IEA, *Renewables 2017*, 2017, `https://www.iea.org/publications/renewables2017/`.

[25] IRENA, *Renewable Energy Integration in Power Grids*, 2015, `http://www.irena.org/-/media/Files/IRENA/Agency/Publication/2015/IRENA-ETSAP_Tech_Brief_Power_Grid_Integration_2015.pdf`.

[26] M. Karimi-Ghartemani, S. A. Khajehoddin, P. Piya, and M. Ebrahimi, "Universal Controller for Three-Phase Inverters in a Microgrid," *IEEE Journal of Emerging and Selected Topics in Power Electronics*, vol. 4, no. 4, 2016, pp. 1342–1353.

[27] J. Kennedy and R. Eberhart, "Particle swarm optimization," *Proceedings of ICNN'95 - International Conference on Neural Networks*, Nov 1995, vol. 4, pp. 1942–1948.

[28] H. Khan, S. Dasouki, V. Sreeram, H. H. C. Iu, and Y. Mishra, "Universal active and reactive power control of electronically interfaced distributed generation sources in virtual power plants operating in gridconnected and islanding modes," *IET Generation, Transmission Distribution*, vol. 7, no. 8, Aug 2013, pp. 885–897.

[29] R. Kuffel, J. Giesbrecht, T. Maguire, R. P. Wierckx, and P. McLaren, "RTDS-a fully digital power system simulator operating in real time," *Proceedings 1995 International Conference on Energy Management and Power Delivery EMPD '95*, Nov 1995, vol. 2, pp. 498–503.

[30] P. Kundur, *Power System Stability and Control*, McGraw-Hill, New York, 1994.

[31] R. H. Lasseter, "MicroGrids," *2002 IEEE Power Engineering Society Winter Meeting. Conference Proceedings (Cat. No.02CH37309)*, 2002, vol. 1, pp. 305–308.

[32] R. H. Lasseter, "Smart Distribution: Coupled Microgrids," *Proceedings of the IEEE*, vol. 99, no. 6, June 2011, pp. 1074–1082.

[33] S. Leitner, M. Yazdanian, A. Mehrizi-Sani, and A. Muetze, "Small-Signal Stability Analysis of an Inverter-Based Microgrid With Internal Model-Based Controllers," *IEEE Transactions on Smart Grid*, vol. 9, no. 5, Sep. 2018, pp. 5393–5402.

[34] C. Li, S. K. Chaudhary, M. Savaghebi, J. C. Vasquez, and J. M. Guerrero, "Power Flow Analysis for Low-Voltage AC and DC Microgrids Considering Droop Control and Virtual Impedance," *IEEE Transactions on Smart Grid*, vol. 8, no. 6, Nov 2017, pp. 2754–2764.

[35] H. Li, D. Yang, W. Su, J. Lü, and X. Yu, "An Overall Distribution Particle Swarm Optimization MPPT Algorithm for Photovoltaic System Under Partial Shading," *IEEE Transactions on Industrial Electronics*, vol. 66, no. 1, Jan 2019, pp. 265–275.

[36] Y. Li and Y. W. Li, "Decoupled power control for an inverter based low voltage microgrid in autonomous operation," *2009 IEEE 6th International Power Electronics and Motion Control Conference*, May 2009, pp. 2490–2496.

[37] Y. Li and Y. W. Li, "Power Management of Inverter Interfaced Autonomous Microgrid Based on Virtual Frequency-Voltage Frame," *IEEE Transactions on Smart Grid*, vol. 2, no. 1, March 2011, pp. 30–40.

[38] J. A. P. Lopes, C. L. Moreira, and A. G. Madureira, "Defining control strategies for MicroGrids islanded operation," *IEEE Transactions on Power Systems*, vol. 21, no. 2, May 2006, pp. 916–924.

[39] J. Matas, M. Castilla, L. G. d. Vicuña, J. Miret, and J. C. Vasquez, "Virtual Impedance Loop for Droop-Controlled Single-Phase Parallel Inverters Using a Second-Order General-Integrator Scheme," *IEEE Transactions on Power Electronics*, vol. 25, no. 12, Dec 2010, pp. 2993–3002.

[40] B. Mather and F. Ding, "Distribution-connected PV's response to voltage sags at transmission-scale," *43rd Photovoltaic Specialists Conference (PVSC)*. IEEE, 2016, pp. 2030–2035.

[41] N. Mithulananthan, C. A. Canizares, J. Reeve, and G. J. Rogers, "Comparison of PSS, SVC, and STATCOM controllers for damping power system oscillations," *IEEE Transactions on Power Systems*, vol. 18, no. 2, May 2003, pp. 786–792.

[42] Y. A.-R. I. Mohamed and E. F. El-Saadany, "Adaptive decentralized droop controller to preserve power sharing stability of paralleled inverters in distributed generation microgrids," *IEEE Transactions on Power Electronics*, vol. 23, no. 6, 2008, pp. 2806–2816.

[43] F. D. Mohammadi, H. K. Vanashi, and A. Feliachi, "State-Space Modeling, Analysis, and Distributed Secondary Frequency Control of Isolated Microgrids," *IEEE Transactions on Energy Conversion*, vol. 33, no. 1, March 2018, pp. 155–165.

[44] D. E. Olivares et al., "Trends in Microgrid Control," *IEEE Transactions on Smart Grid*, vol. 5, no. 4, July 2014, pp. 1905–1919.

[45] G. A. Pagani and M. Aiello, "Towards Decentralization: A Topological Investigation of the Medium and Low Voltage Grids," *IEEE Transactions on Smart Grid*, vol. 2, no. 3, Sept 2011, pp. 538–547.

[46] N. Pogaku, M. Prodanovic, and T. C. Green, "Modeling, analysis and testing of autonomous operation of an inverter-based microgrid," *IEEE Transactions on power electronics*, vol. 22, no. 2, 2007, pp. 613–625.

[47] PSIM, *Software by Powersim Technologies, Professional Version*, Rockville, MD, USA, Rockville, MD, USA, 1994.

[48] M. Rasheduzzaman, J. A. Mueller, and J. W. Kimball, "An Accurate Small-Signal Model of Inverter- Dominated Islanded Microgrids Using Reference Frame," *IEEE Journal of Emerging and Selected Topics in Power Electronics*, vol. 2, no. 4, Dec 2014, pp. 1070–1080.

[49] M. Rasheduzzaman, J. A. Mueller, and J. W. Kimball, "Reduced-Order Small-Signal Model of Microgrid Systems," *IEEE Transactions on Sustainable Energy*, vol. 6, no. 4, Oct 2015, pp. 1292–1305.

[50] C. N. Rowe, T. J. Summers, R. E. Betz, D. J. Cornforth, and T. G. Moore, "Arctan Power-Frequency Droop for Improved Microgrid Stability," *IEEE Transactions on Power Electronics*, vol. 28, no. 8, Aug 2013, pp. 3747–3759.

[51] J.-H. Seo, C.-H. Im, C.-G. Heo, J.-K. Kim, H.-K. Jung, and C.-G. Lee, "Multimodal function optimization based on particle swarm optimization," *IEEE Transactions on Magnetics*, vol. 42, no. 4, April 2006, pp. 1095–1098.

[52] X. Sui, Y. Tang, H. He, and J. Wen, "Energy-Storage-Based Low-Frequency Oscillation Damping Control Using Particle Swarm Optimization and Heuristic Dynamic Programming," *IEEE Transactions on Power Systems*, vol. 29, no. 5, Sep. 2014, pp. 2539–2548.

[53] X. Sun, Y. Tian, and Z. Chen, "Adaptive decoupled power control method for inverter connected DG," *IET Renewable Power Generation*, vol. 8, no. 2, March 2014, pp. 171–182.

[54] NERC Distributed Energy Task Force Report, *Distributed Energy Resources Connection Modeling and Reliability Considerations*, February 2017, `https://www.nerc.com/comm/Other/essntlrlbltysrvcstskfrcDL/Distributed_Energy_Resources_Report.pdf`.

[55] US-FERC, *Federal Statutes*, 2017, `https://ferc.gov/legal/fed-sta.asp`.

[56] J. C. Vasquez, J. M. Guerrero, A. Luna, P. Rodriguez, and R. Teodorescu, "Adaptive Droop Control Applied to Voltage-Source Inverters Operating in Grid-Connected and Islanded Modes," *IEEE Transactions on Industrial Electronics*, vol. 56, no. 10, Oct 2009, pp. 4088–4096.

[57] X. Wang, Y. W. Li, F. Blaabjerg, and P. C. Loh, "Virtual-Impedance-Based Control for Voltage-Source and Current-Source Converters," *IEEE Transactions on Power Electronics*, vol. 30, no. 12, Dec 2015, pp. 7019–7037.

[58] T. Wu, Z. Liu, J. Liu, S. Wang, and Z. You, "A Unified Virtual Power Decoupling Method for Droop-Controlled Parallel Inverters in Microgrids," *IEEE Trans. Power Electronics*, vol. 31, no. 8, Aug 2016, pp. 5587–5603.

[59] A. Yaghooti, M. O. Buygi, and M. H. M. Shanechi, "Designing Coordinated Power System Stabilizers: A Reference Model Based Controller Design," *IEEE Trans. Power Systems*, vol. 31, no. 4, July 2016, pp. 2914–24.

[60] W. Yao, M. Chen, J. Matas, J. M. Guerrero, and Z. M. Qian, "Design and Analysis of the Droop Control Method for Parallel Inverters Considering the Impact of the Complex Impedance on the Power Sharing," *IEEE Transactions on Industrial Electronics*, vol. 58, no. 2, Feb 2011, pp. 576–588.

[61] A. Yazdani and R. Iravani, *Voltage-sourced converters in power systems : modeling, control, and application*, Wiley, New Jersey, 2010.

[62] Y. Zhang, Z. Jiang, and X. Yu, "Small-signal modeling and analysis of parallel-connected voltage source inverters," *Power Electronics and Motion Control Conference, 2009. IPEMC'09. IEEE 6th International*. IEEE, 2009, pp. 377–383.

[63] Q. C. Zhong, "Harmonic Droop Controller to Reduce the Voltage Harmonics of Inverters," *IEEE Transactions on Industrial Electronics*, vol. 60, no. 3, March 2013, pp. 936–945.

[64] Q. C. Zhong, "Power-Electronics-Enabled Autonomous Power Systems: Architecture and Technical Routes," *IEEE Transactions on Industrial Electronics*, vol. 64, no. 7, July 2017, pp. 5907–5918.

[65] Q. C. Zhong, W. L. Ming, and Y. Zeng, "Self-Synchronized Universal Droop Controller," *IEEE Access*, vol. 4, 2016, pp. 7145–7153.

[66] Q.-C. Zhong and G. Weiss, "Synchronverters: Inverters that mimic synchronous generators," *IEEE Transactions on Industrial Electronics*, vol. 58, no. 4, 2011, pp. 1259–1267.

[67] Q. C. Zhong and Y. Zeng, "Parallel operation of inverters with different types of output impedance," *IECON 2013 - 39th Annual Conference of the IEEE Industrial Electronics Society*, Nov 2013, pp. 1398–1403.

[68] Q. C. Zhong and Y. Zeng, "Universal Droop Control of Inverters With Different Types of Output Impedance," *IEEE Access*, vol. 4, 2016, pp. 702–712.

APPENDIX A

SYSTEM DIAGRAMS AND SPECIFICATIONS

A.1 Matlab Code

The m-file script that includes the parameters and dynamics of a two-DG MG is given below.

```
function F = root2d(x)
R1=1; R2=1;% the virtual resistance
%---------------------------
Lf1=0.005; Lf2=0.005;% the L filter parameters
%---------------------------
% the local loads 1 and 2 and common load parameters
Rload1=108;Cload1=52e-6;Lload1=100e-3;
Rload2=108;Cload2=52e-6;Lload2=100e-3;
Rpcc=24;Cpcc=64e-6;Lpcc=50e-3;
%---------------------------
% the transmission lines 1 and 2 parameters
Rl1=2*0.642;Ll1=2*0.083/(2*pi*60);Rl2=0.642;Ll2=0.083/(2*pi*60);
%---------------------------
% the controller parameters (iVSM)
Vg=120*sqrt(2);S=2000;DeltaV=0.1*Vg;Deltaf=2;
fnl=62;vnl=132*sqrt(2);kf=S/Deltaf;kv=S/DeltaV;L=0.005;alpha=100;
R=2*alpha*L;w=2*pi*60;X=L*w;Z=sqrt(R^2+X^2);wc=2*pi*100;k=(1/3)*(R*Z/L);
zeta=1;kw=k^2/(8*zeta^2*Vg^2);kq=k/Vg;kp=k/Vg^2;theta=45*pi/180;
%--------------------------------
%Defining the state variables
iod1=x(1);ioq1=x(2);ild1=x(3);ilq1=x(4);vod1=x(5);voq1=x(6);
iline1d=x(7);iline1q=x(8);vd1=x(9);w1=x(10);Pref1=x(11);delta1=x(12);
iod2=x(13);ioq2=x(14);ild2=x(15);ilq2=x(16);vod2=x(17);voq2=x(18);
iline2d=x(19);iline2q=x(20);vd2=x(21);w2=x(22);Pref2=x(23);
delta2=x(24);ildpcc=x(25);ilqpcc=x(26);vpccd=x(27);vpccq=x(28);
%-----------------------------------------------------------------
%Defining vq1 and vq2 in common frame
vq1=0; vq2=-vd2*tan(delta2);
%-----------------------------------------------------------------
%Defining the derivatives of phi1 and phi2
pphi1=w1+kp*(Pref1-1.5*(sin(theta)*(iod1*vd1+ioq1*vq1)-cos(theta)*...
    (iod1*vq1-ioq1*vd1)));
```

```
pphi2=w2+kp*(Pref2-1.5*(sin(theta)*(iod2*vd2+ioq2*vq2)-cos(theta)*...
    (iod2*vq2-ioq2*vd2)));
%-------------------------------------------------------------------
%The dynamics of Inverter 1
F(1)=1/Lf1*(vd1-vod1)-R1/Lf1*iod1+pphi1*ioq1;
F(2)=1/Lf1*(vq1-voq1)-R1/Lf1*ioq1-pphi1*iod1;
F(3)=1/Lload1*vod1+pphi1*ilq1;F(4)=1/Lload1*voq1-pphi1*ild1;
F(5)=1/Cload1*(iod1-iline1d-ild1)-1/(Cload1*Rload1)*vod1+pphi1*voq1;
F(6)=1/Cload1*(ioq1-iline1q-ilq1)-1/(Cload1*Rload1)*voq1-pphi1*vod1;
F(7)=1/Ll1*(vod1-vpccd)-Rl1/Ll1*iline1d+pphi1*iline1q;
F(8)=1/Ll1*(voq1-vpccq)-Rl1/Ll1*iline1q-pphi1*iline1d;
F(9)=kq*(kv*(vnl-sqrt(vod1^2+voq1^2))-1.5*(cos(theta)*...
    (iod1*vd1+ioq1*vq1)+sin(theta)*(iod1*vq1-ioq1*vd1)));
F(10)=kw*(Pref1-1.5*(sin(theta)*(iod1*vd1+ioq1*vq1)-cos(theta)*...
    (iod1*vq1-ioq1*vd1)));
F(11)=wc*(kf*(fnl-w1/(2*pi))-Pref1);F(12)=0;
%-------------------------------------------------------------------
%The dynamics of Inverter 2
F(13)=1/Lf2*(vd2-vod2)-R2/Lf2*iod2+pphi1*ioq2;
F(14)=1/Lf2*(vq2-voq2)-R2/Lf2*ioq2-pphi1*iod2;
F(15)=1/Lload2*vod2+pphi1*ilq2;F(16)=1/Lload2*voq2-pphi1*ild2;
F(17)=1/Cload2*(iod2-ild2-iline2d)-1/(Cload2*Rload2)*vod2+pphi1*voq2;
F(18)=1/Cload2*(ioq2-ilq2-iline2q)-1/(Cload2*Rload2)*voq2-pphi1*vod2;
F(19)=1/Ll2*(vod2-vpccd)-Rl2/Ll2*iline2d+pphi1*iline2q;
F(20)=1/Ll2*(voq2-vpccq)-Rl2/Ll2*iline2q-pphi1*iline2d;
F(21)=kq*(kv*(vnl-sqrt(vod2^2+voq2^2))-1.5*(cos(theta)*...
    (iod2*vd2+ioq2*vq2)+sin(theta)*(iod2*vq2-ioq2*vd2)));
F(22)=kw*(Pref2-1.5*(sin(theta)*(iod2*vd2+ioq2*vq2)-cos(theta)*...
    (iod2*vq2-ioq2*vd2)));
F(23)=wc*(kf*(fnl-w2/(2*pi))-Pref2);F(24)=pphi1-pphi2;
%-------------------------------------------------------------------
%The common load dynamics
F(25)=1/Lpcc*vpccd+pphi1*ilqpcc;F(26)=1/Lpcc*vpccq-pphi1*ildpcc;
F(27)=1/Cpcc*(iline1d+iline2d-ildpcc)-1/(Cpcc*Rpcc)*vpccd+pphi1*vpccq;
F(28)=1/Cpcc*(iline1q+iline2q-ilqpcc)-1/(Cpcc*Rpcc)*vpccq-pphi1*vpccd;
end
```

The script of the Matlab function *fsolve* that finds the equilibrium point of the system is given below.

```
fun = @(x)root2d(x);%call the function
x0 = [7,-6,0.05,-5,170,1,2.5,2,177,390,270,0,6,-5,0.05,-4,170,1,3,2, ...
    177,377,350,0.1,0.1,5,170,5];%initial values of states
[x fval] = fsolve(fun,x0,options)%solve for equilibrium point x
```

A.2 Study System Diagrams in RTDS and PSIM

The grid-connected MG schematic diagram and the iVSM controller block diagram in RSCAD/Draft module are shown in Figs. A.1 and A.2, respectively. Real-time simulation plots in RSCAD/RunTime module are illustrated in Fig. A.3.

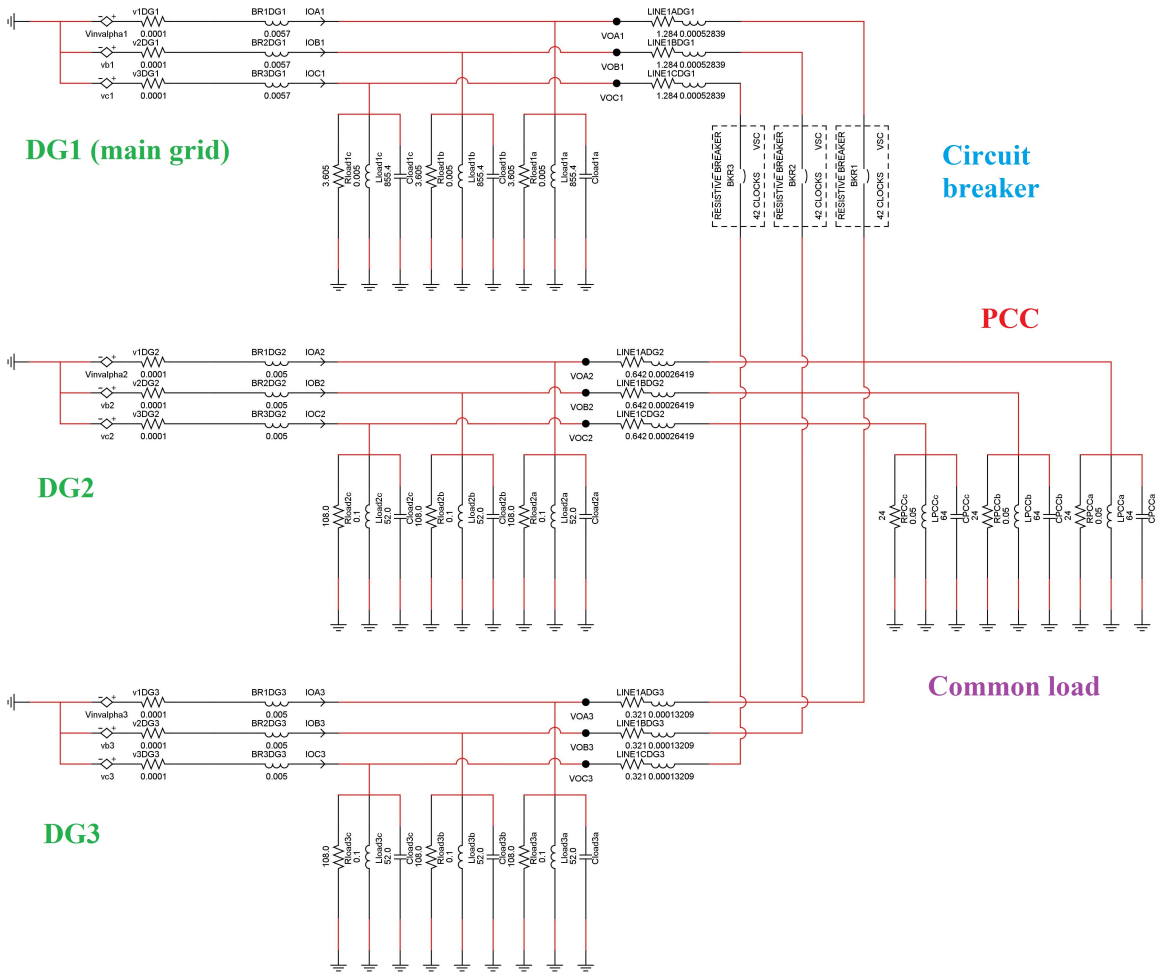

Figure A.1: Circuit schematic of two-DG units MG in RSCAD - Grid-connected Mode

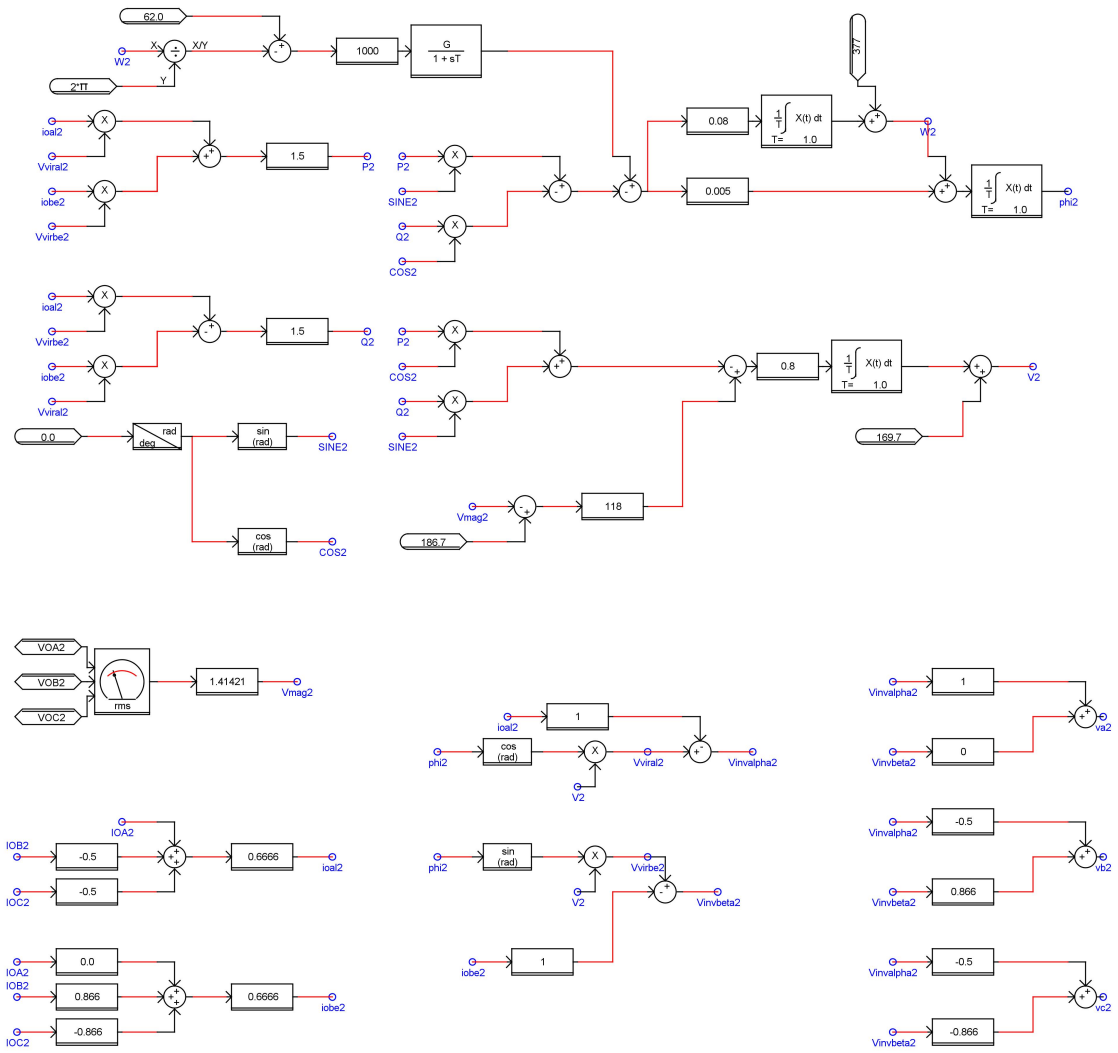

Figure A.2: iVSM controller block diagram in RSCAD/Draft module

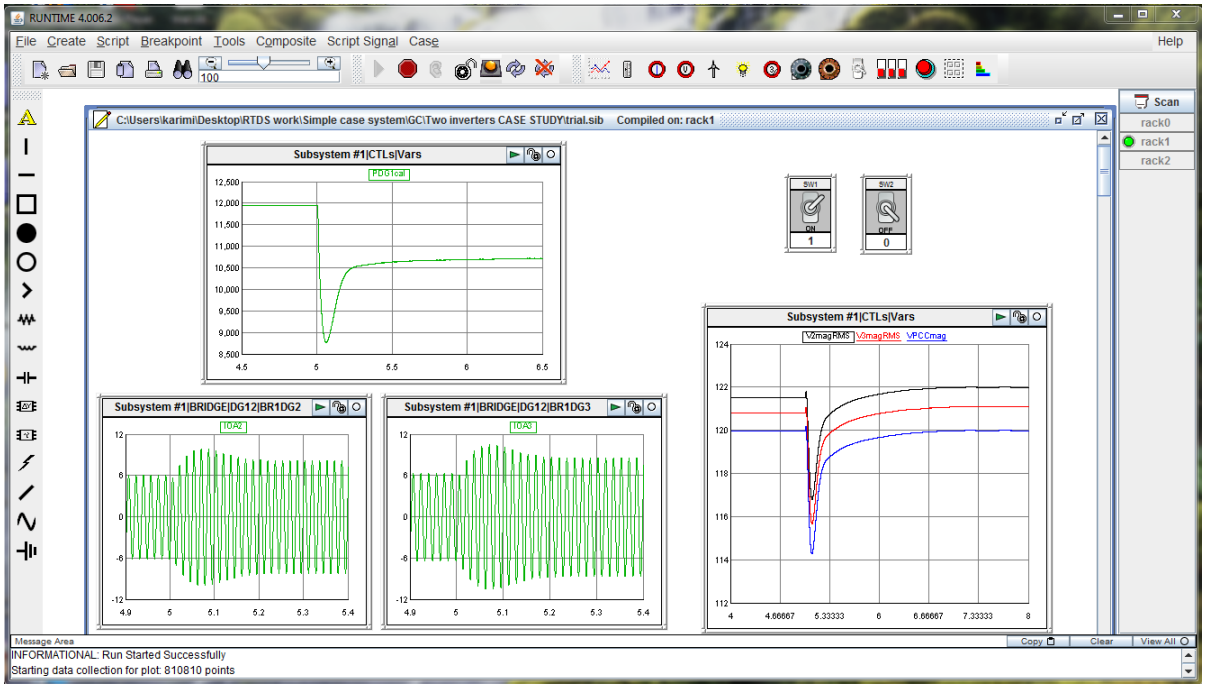

Figure A.3: Simulation plots in RSCAD/RunTime module

The islanded MG circuit diagram and the iVSM controller block diagram in PSIM software are shown in Figs. A.4 and A.5, respectively.

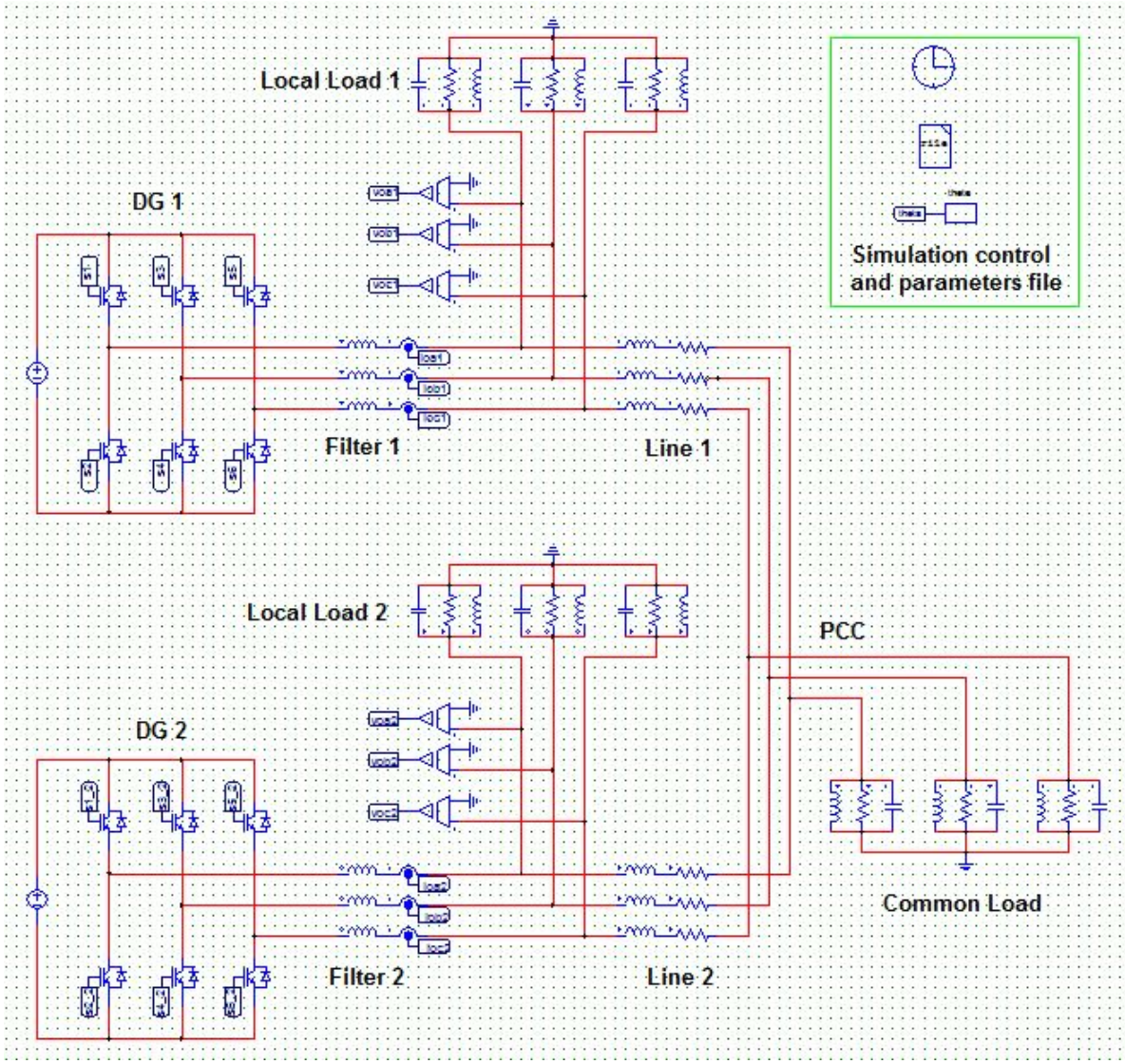

Figure A.4: Circuit schematic of two-DG units MG in PSIM - Standalone Mode

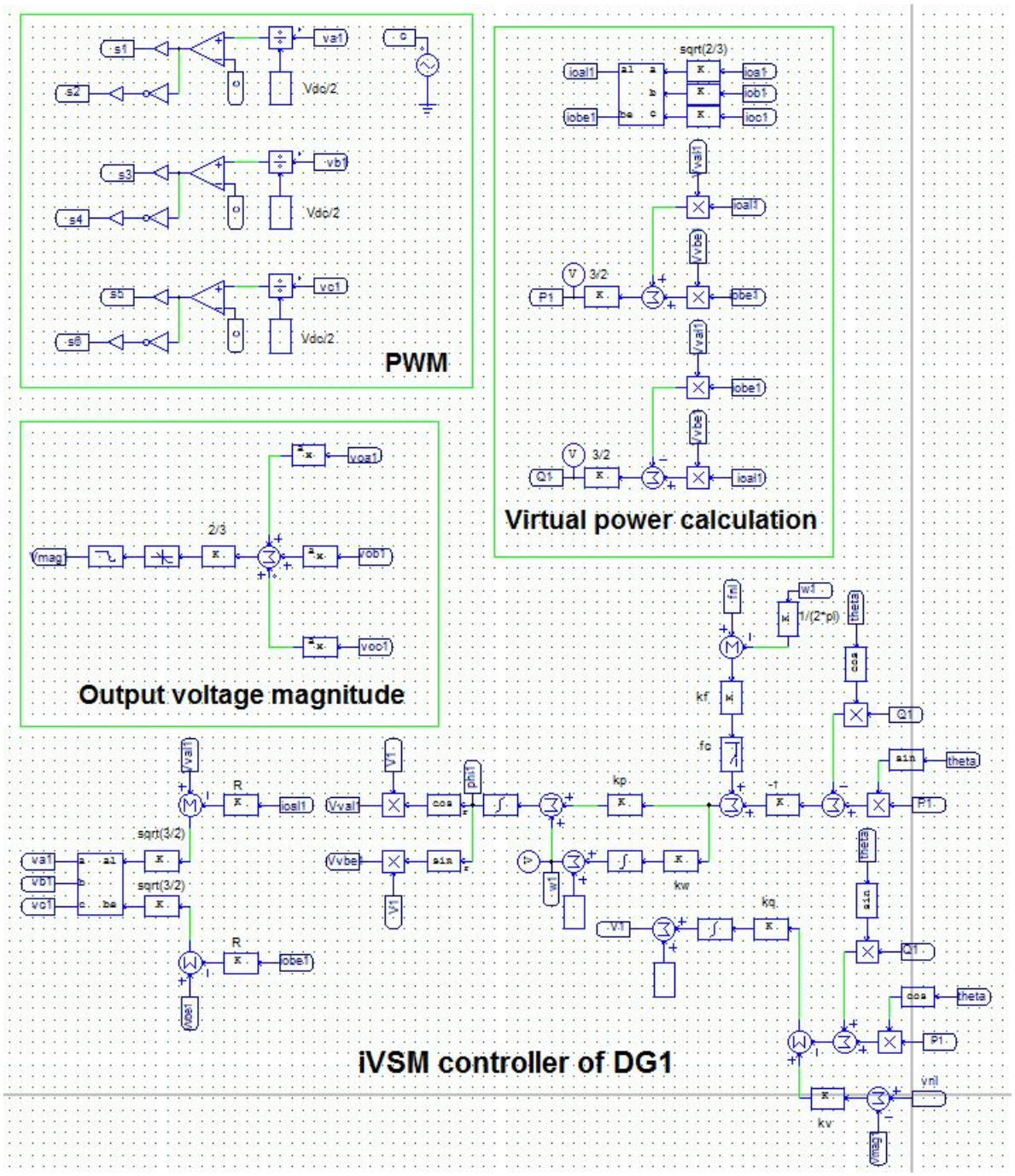

Figure A.5: iVSM controller block diagram in PSIM

A.3 IEEE 13-Bus System

The complete line parameters of the IEEE 13-bus case study system are given below.

Table A.1: Line parameters

Line	From	To	Length (km)	R ( )	L (mH)
L1	646	645	0.09144	0.0587	0.0201
L2	645	632	0.1524	0.0978	0.0336
L3	632	650	0.1524	0.0978	0.0336
L4	632	633	0.1524	0.0978	0.0336
L5	633	634	0.04572	0.0293	0.01
L6	632	671	0.6096	0.3913	0.1342
L7	611	684	0.09144	0.0587	0.0201
L8	684	652	0.24384	0.1565	0.0536
L9	684	671	0.09144	0.0587	0.0201
L10	671	680	0.3048	0.1956	0.0671
L11	671	692	0.09144	0.0587	0.0201
L12	692	675	0.1524	0.0978	0.0336

The load details of the IEEE 13-bus case study system are provided below.

Table A.2: Load details

Node	P (kW)	Q (kVar)	Node	P (kW)	Q (kVar)
646	2	1.5	652	3	2
645	3.5	2	680	4	3
634	2	3	675	1.25	1
671	2.5	1.5	650	10	8
611	1.5	1	692	6	5